Master's degree in Automotive Engineering

Enhancing composite material structures simulation with multi-scale approach

Tutors

Prof. Giovanni Belingardi

Prof. Davide Paolino

Ing. Mauro Olivero

Candidate

Claudio Verga

TABLE OF CONTENTS

ACKNOWLEDGEMENTS

ABSTRACT

Global automotive industry is strongly driven by innovation necessities to comply with fuel economy regulations, emissions, performance and recyclability, so that the interest and utilization of composite materials is very high due to their unique mix of characteristics.

This opportunity is taken in many parts of the car to ensure low weight, corrosion resistance, good energy absorption, complex shape molding and vibration absorption; given these advantages, there are also drawbacks related to manufacturing cost optimization and process complexity which, by the way, largely affects also the mechanical properties of the component: fiber orientation, presence of weld lines and defects play a major role in the final strength of the part and in damage onset.

This latest aspect is of paramount importance considering that at present day numerical simulation accuracy is mandatory to optimize structural performances to reach targets and that classical numerical models should be enhanced and refined to comply with composite materials peculiarities with respect to classical ones.

This treatment aims precisely to verify the improvement in finite element analysis representativeness of the component by exploiting the so called "multi-scale" approach, which means considering and implementing properties belonging to micro-material level up to full component level.

Describing the complete microstructural evolution is not a viable path due to computational cost, instead homogenization techniques have increasingly gained importance to couple the micro scale to the macro output and for such reason several algorithms and commercial software doing this job are on the market.

In order to verify the improvement in FEA by using multi-scale approach at first a test campaign on experimental specimens, all made of thermoplastic glass fiber reinforced Polypropylene, is done to fine tune the ability to model the composite material in a proficient

way in a multi-scale methodology chain and to verify correlation between the new advanced finite element coupled analysis and experimental results.

As a further step, multi-scale approach is used on a more complex structure like an omega beam, where the variability on fiber orientations and inputs coming from the manufacturing process is greater, in order to appreciate the representativeness improvement of the model over the standard method.

Chapter 1

COMPOSITE MATERIALS

1.1 DEFINITION AND CLASSIFICATION

A material is defined as "composite" when it is made of different constituents (materials or phases) and the global physical and chemical properties are effectively divergent from the single counterparts, which have a distinct macroscale interface separation; moreover they do not mix or dissolve into each other.

By this definition impurities, alloying elements, additives, lubricants, fillers would be eligible as candidates to define a composite but generally they are not considerate in this regard since they do not imply significant property change and are present in small fractions.

The fiber composite materials treated in this thesis are characterized by a continuous phase named matrix and a stronger discontinuous one named reinforcement, which affects the mechanical properties in a conspicuous way, according to its concentration, geometry, distribution, shape and interfacial area.

To control these attributes, it's important to focus on the manufacturing process, in order to avoid nonuniformity and defects, which result in part weakness and to predict the fibers arrangement which determines the isotropic or anisotropic behavior.

Composites can be classified following different criteria, mainly based on the strengthening mechanism or the type of matrix.

Classification based on matrix type includes, at first level, Polymeric Matrix Composites

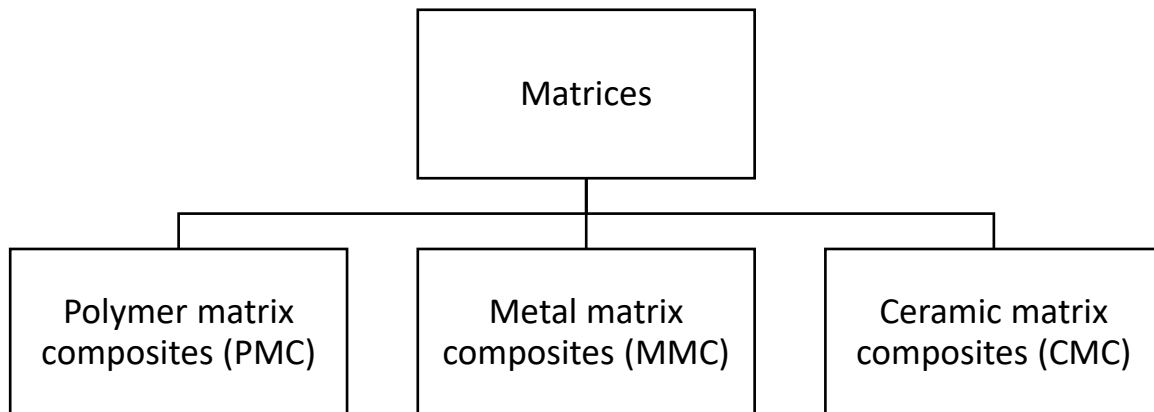(PMCs), Metal Matrix Composites (MMCs) and Ceramic Matrix Composites (CMCs).

```
                    ┌─────────────────────┐
                    │                     │
                    │      Matrices       │
                    │                     │
                    └─────────────────────┘
          ┌───────────────────┼───────────────────┐
┌─────────────────┐ ┌─────────────────┐ ┌─────────────────┐
│  Polymer matrix │ │   Metal matrix  │ │  Ceramic matrix │
│ composites (PMC)│ │ composites (MMC)│ │ composites (CMC)│
└─────────────────┘ └─────────────────┘ └─────────────────┘
```

Fig. 1.1 Matrix classification

Polymer matrix composites will be treated in detail after, metal matrix composites typically contain silicon carbide (SiC), aluminum oxide (Al_2O_3) or other ceramic particles or short fibers in a light alloy, such as aluminum, magnesium and titanium to ensure high thermal conductivity, high strength and stiffness, high strength-to-density ratio, low coefficient of thermal expansion and corrosion resistance.

Ceramic matrix composites consist of a ceramic matrix combined with a dispersed phase (carbides, oxides). CMCs are tougher than conventional ceramics due to the desired configuration of the fiber matrix interface, which arrests and deflects cracks in the matrix, preventing failure of the fibrous reinforcement; nonetheless they exhibit limited plasticity and the tendency to cause catastrophic failure. For these reasons CMCs are used in extreme conditions, at temperatures above 1000 °C where creep and wear resistance are of primary importance like in jet engines, turbines, combustion chambers and so on.

A second classification can be made according to the reinforcement that gives the mechanical properties improvement and its geometry.
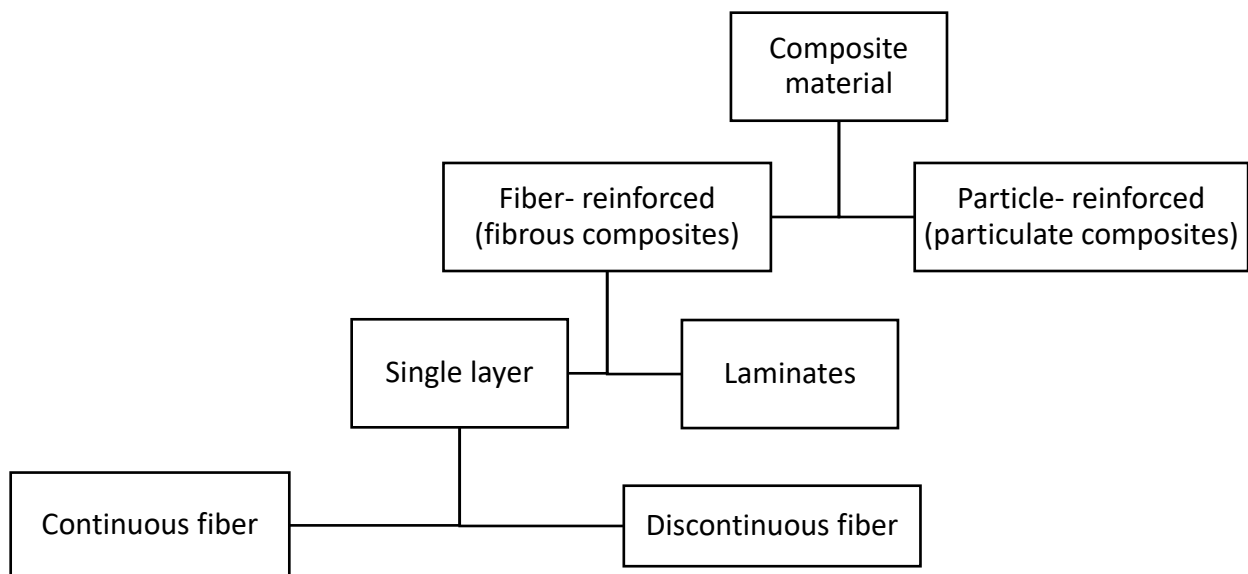
Fig. 1.2 Reinforcement classification

Concerning this hierarchy graph, the first distinction distinguishes between fibers and particles: a particle is nonfibrous, with an irregular equiaxed shape, whereas a fiber has one dimension much greater than its cross section.

Particle-reinforced composites are recurrently referred to as particulate composite; the first aspect that contributes to the total composite property is the dimension of the particle, which constrains the plastic deformation of the matrix material and share part of the load.

The load shared, however, is way smaller than what fiber reinforcements are capable to sustain, that is the reason why particles are effective in improving the stiffness, but they don't offer room for much strengthening. They are also not good in assuring fracture resistance, in general.

Particle fillers are exploited to increase the thermal and electrical conductivities, performance at high temperatures, reduce friction, improve manufacturability, increase surface hardness, and reduce shrinkage. In many cases they are used simply for cost reduction.

1.2 FIBER REINFORCED COMPOSITES

To increase material performances the use of reinforcing fibers is very common since they minimize imperfections and flaws impact on strength. High mechanical properties are achieved through orientation of the molecular structure in polymeric materials, through improved orientation of the atomic links in graphite and aramid fibers and in glass fibers as result of a defect free surface.

Fibers can't be used directly, they are embedded, protected and bonded together in the matrix, which also transfers the load, especially in discontinuous fibers composites.

From a macro scale point of view these composites are classified as single-layer or multilayer ones: "single layer" means that even if actually the composite structure is layered, they all have the same orientation and properties, whereas "multilayer" indicates that each "lamina" has different orientation and characteristics according to design intentions.

Laminas are typically 0.1 mm thick and when they are stacked one above the other, maintaining the same material they are called "laminates", otherwise if there is a combination of materials they are called "hybrid laminates".

The length of the reinforcing fiber with respect to overall dimensions is variable: composites with short fibers are named discontinuous-fiber-reinforced composites, and those with long fibers, continuous-fiber-reinforced composites. In the latter, load is sustained principally by the fibers, especially when they have high module and concentration. Failure mode depends a lot by the fibers.

Continuous fibers can be used to make "prepregs", a single layer unidirectional composites, with high alignment, strong in fiber direction but weak perpendicular to it. For this reason, they are stacked with different angles to form laminates. From the fabrication point of view, they are made depositing the fibers and impregnating them with resinous materials.

Discontinuous fibers instead can't be positioned as pleased in a composite material, in fact they generally are randomly orientated, especially when they are sprayed all together with a resin matrix against a mold or deposited and impregnated after, resulting in a isotropic global behavior; however producing with injection or compression molding determines strong flow of the melt and orientation of the fibers

1.3 GLASS FIBERS

The attention is now shifted on glass fiber reinforced composites because it's the kind of material that will be used in the experimental part of the thesis.

Their utilization is very common because of the low cost-high strength properties, though attention must be taken in presence of humidity that hinders the adhesion with the matrix. To solve this issue, they are treated successfully with coupling agents to reinforce polyester, epoxy and phenolic resins.

Their modulus is lower with respect to Kevlar, carbon and others so the modulus-to-weight ratio is only moderate, that is the reason why aeronautical industry was driven towards other fibers (boron, carbon etc.). Moreover, fiber glass is subjected to static fatigue, due to crack growth after constant and long-time load bearing.

Density ($g \ cm^{-3}$)	Tensile strength (MPa)	Young's modulus (GPa)	Coefficient of thermal expansion ($10^{-6} \ K^{-1}$)
2.55	1750	70	4.7

Fig. 1.3 Typical properties of E glass fibers

On the market there are different chemical composition of glass fibers available: in general they are silica based plus minor fraction of other oxides of calcium, sodium, aluminum, iron, boron. A letter in the name is useful to indicate the utilization, like E for electrical glass, for its insulating properties; C for corrosion; S for high silica content (high temperature resistance)

Composition	E glass	C glass	S glass
SiO_2	55.2	65.0	65.0
Al_2O_3	8.0	4.0	25.0
CaO	18.7	14.0	–
MgO	4.6	3.0	10.0
Na_2O	0.3	8.5	0.3
K_2O	0.2	–	–
B_2O_3	7.3	5.0	–

Fig. 1.4 Approximate chemical composition of some glass fibers

Pure crystalline silica melts at 1800 °C whereas silica-based glass is amorphous and needs the addition of metal oxides to break some Si-O bonds and lower the glass transition temperature. Fig. 1.5 shows the oxygen-silicon atom bonding before and after adding sodium, which becomes linked ionically with oxygen but without joining the network directly. Also, the quantity of Na_2O should not exceed a certain value to avoid problem in the glassy structure formation. The presence of other metal oxides affects the network shape and so the properties.

Remarkably the structure looks isotropic and so are, more or less, the properties of glass fibers, which is not true for other kind of fiber reinforcements which are anisotropic.
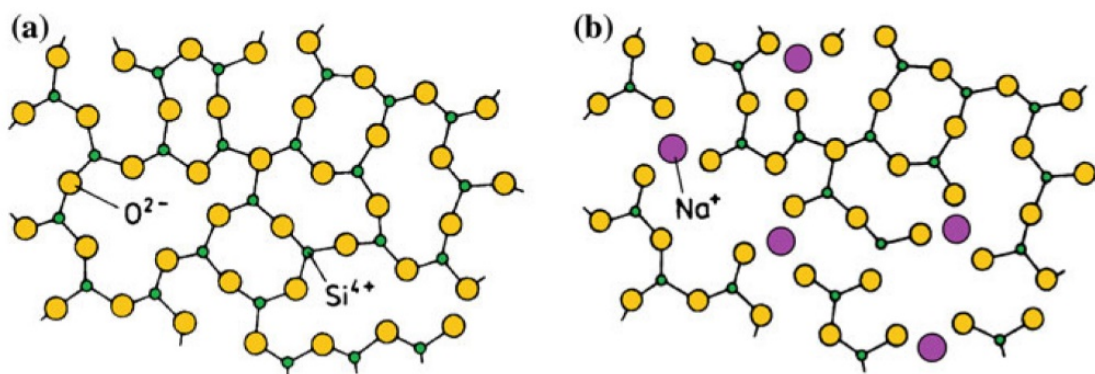

Fig. 1.5 amorphous structure of glass: a) 2-D silica glass network, b) modified network after Na_2O addition

1.4 PRODUCTION OF GLASS FIBERS

The typical manufacturing process for glass fibers (mainly E fibers) comprise a hopper where the raw material is fed and melted, then it flows into electrically heated platinum bushings with several holes.
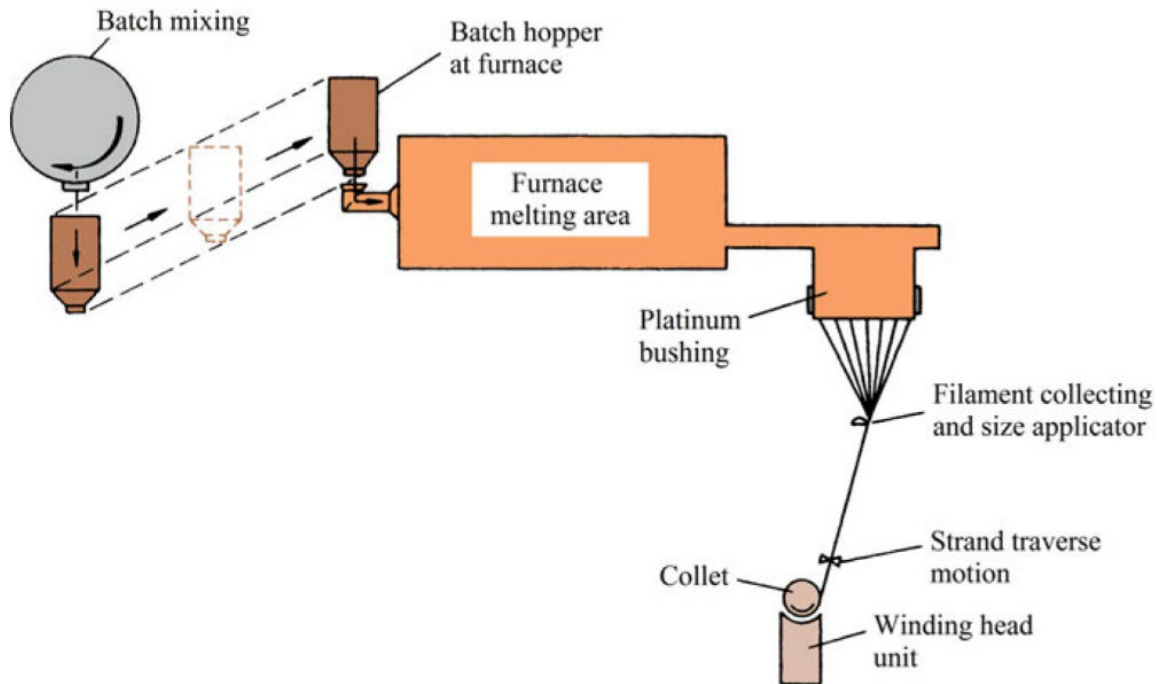
Fig. 1.6: glass fiber manufacturing process

By gravity some continuous filaments are formed and then gathered into a strand and a size is set before it is wound on a drum. The final fiber diameter is dependent on the bushing orifice diameter, viscosity, which is a function of composition and temperature and the head of glass in the hopper. In old production facilities molten glass is first turned into marbles, which after inspection are melted in the bushings. In present day plants the preferred method is direct drawing.

The difficulties to overcome in this process are the management of melt high temperature, desired composition, immiscibility of components in liquid state and crystallization during cooling.

Some final forms in which glass fiber is sold on the market are chopped strand, continuous yarn, roving and fabric.
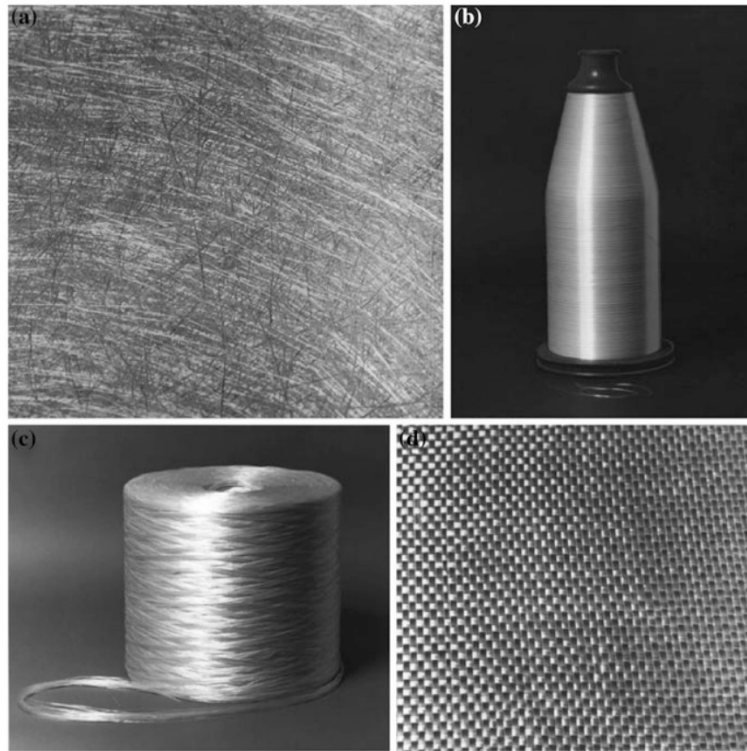
Fig. 1.7 glass fiber available forms: a) chopper strand, b) continuous yard, c) roving, d) fabric (Morrison Molded Fiber Glass Company)

Another production technique is the sol-gel one, taking its name from the sol, a colloidal suspension of small particles and from gel, a suspension in which the liquid is very viscous.

The sol–gel process involves a transformation of fibrous gels, drawn from a cold solution, into glass fibers at hot temperature but still lower than in conventional glass fiber manufactures. The process consists of preparing an appropriate homogeneous solution, changing the solution to a sol, gelling the sol, and converting the gel to glass or ceramic by heating. At the end the filament is coated to prevent damage originated from surface defects.

Glass fiber reinforced resins are used widely in the building and construction industry (window frames, tanks, bathroom units), in the chemical business and in the transportation sector (rail, road and aerospace).

1.5 CARBON AND GRAPHITE FIBERS

Amongst the high strength, high modulus types of reinforcement, the spotlight is taken by carbon and graphite fibers. Their employment has risen since the 90's due to their greater availability and pricing on the market and it extended from high end aerospace applications to automotive and many other consumer products. Carbon is a light element with a density equal to 2.268 g/cm^3 that can present different crystalline structure: the diamond structure where atoms are arranged in a 3D way with little structural flexibility, Buckminster fullerene and the so-called graphitic structure where the atoms take the shape of a hexagonal layers with dense packing in the layer planes. The lattice structure (with only lattice planes) is shown in Fig 1.8. The high strength bond between carbon atoms in the layer plane results in an extremely high modulus while the weak van der Waals-type bond between the neighboring layers results in a lower modulus in the c-direction.
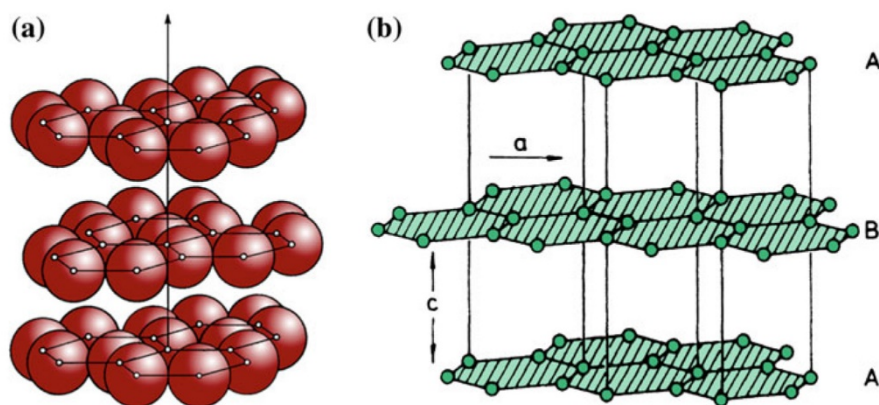
Fig. 1.8 a) graphitic structure, b) hexagonal lattice structure of graphite

In Theory a Young's modulus as high as 1000 Gpa is achievable in the layer plane, while along the c-axis it is only 35 Gpa. Production should further a very high degree of orientation of hexagonal planes along the fiber axis by various kinds of thermal and stretching treatments involving rather rigorous controls.

Strictly speaking there is no true graphite in the fibers, the term refers to fibers that have more than 99% carbon content, whereas "carbon fiber" are in the range 80-95%.

Carbon fibers of extremely high modulus can be made by thermal decomposition (pyrolysis) of organic precursor fibers followed by graphitization at high temperatures. The organic precursor fiber (the raw material for carbon fiber), is generally a special textile polymeric fiber that can be carbonized without melting and consists of long-chain molecules arranged in a random manner, like any polymeric fiber. Such polymeric fibers generally have poor mechanical properties and typically show rather large deformations at low stresses mainly because the polymeric chains are not organized. Currently available carbon fibers are made using one of these precursor materials: polyacrylonitrile (PAN), rayon and the ones obtained from pitches, polyvinyl alcohol, polyimides, and phenolics.

Proposed organic materials for pyrolysis into carbon fibers should meet four criteria. First, the precursor should possess strength and handling characteristics needed "to keep the fibers together" the carbon conversion process. Second, the precursor should not melt during any stage of the conversion process. Third, the precursor material must not volatilize completely during the pyrolysis process. Furthermore, as previously stated in order to obtain optimal properties, the carbon atoms should tend to array themselves in an aligned graphite structure during pyrolysis.

The production process starting from PAN is described like this:

- Spinning the PAN into a precursor fiber.
- Stretching it.
- Stabilization by holding under tension the polymer at a temperature of 205-240°C for up to a day in air.
- Carbonization at approximately 1500°C in an inert atmosphere to eliminate most noncarbon elements of the precursor fibers until they are essentially transformed into carbon fibers. At this point the high mechanical properties found in most commercially available carbon fibers are developed.
- Graphitization (heat treatment) at approximately 2500°C in inert atmosphere in order to improve the tensile modulus of elasticity of the fiber by promoting the crystallite structure formation and preferred orientation of the graphite-like crystallite within each individual fiber.
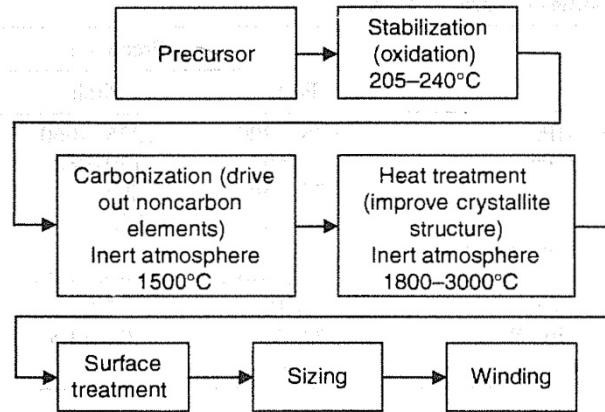
Fig. 1.9 converting PAN to carbon fibers

The PAN-based carbon fibers are not too expensive and hence widespread in structural applications.

Rayon is a thermosetting polymer. The manufacturing process (Fig. 1.10) used for its conversion into carbon fiber involves the same stages: fiberization, stabilization in a reactive atmosphere, carbonization (<1500 °C), and graphitization (>2500 °C). Various reactions occur during the first stage, causing extensive decomposition and evolution of H_2O, CO, CO_2 and tar. The stabilization is carried out in a reactive atmosphere to inhibit tar formation and improve yield (Bacon 1973). The carbonization treatment involves heating to about 1000 °C in nitrogen. Graphitization is carried out at 2800 °C under stress, resulting in plastic deformation via operation of slip on multiple systems and diffusion. The carbon fibers yield from rayon is between 15 and 30% by weight, compared to a yield of about 50% in the case of PAN precursors and are not used for structural applications, but more as insulators and ablative applications due to their low thermal conductivity.
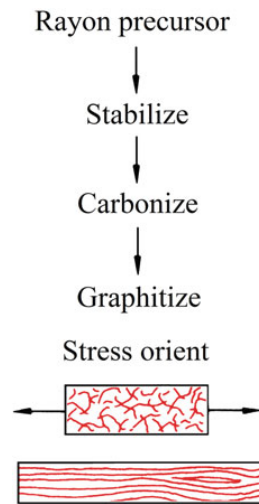
Fig. 1.10 rayon-based carbon fiber production schematics

Commercial pitches are aggregates of different organic compounds, being polyvinyl chloride (PVC), petroleum asphalt, and coal tar the main sources.

Pitch-based carbon fibers are interesting because of the low-cost raw material, high yield of the finished fiber, and easily obtainable orientation.

Production process is again similar also for the pitch precursor: starting from an isotropic but aromatic pitch subjected to melt spinning at very high strain rates and quenched to give a highly oriented, pitch precursor fiber is then oxidized to form a crosslinked structure. This is followed by carbonization and graphitization.

Pitch-based carbon fibers generally have higher stiffness and thermal conductivities. In the following table some typical property ranges are reported for different kind of carbon fibers. Variability can be also affected batch by batch because the structure is sensible to manufacturing process manipulation.

a)

Precursor	Density ($g\ cm^{-3}$)	Young's modulus (GPa)	Electrical resistivity ($10^{-4}\ \Omega\ cm$)
Rayon[a]	1.66	390	10
Polyacrylonitrile[b] (PAN)	1.74	230	18
Pitch (Kureha)			
LT[c]	1.6	41	100
HT[d]	1.6	41	50
Mesophase pitch[e]			
LT	2.1	340	9
HT	2.2	690	1.8
Single crystal graphite[f]	2.25	1000	0.40

[a]Union Carbide, Thornel 50
[b]Union Carbide, Thornel 300
[c]LT, low-temperature heat-treated
[d]HT, high-temperature heat-treated
[e]Union Carbide-type P fibers
[f]Modulus and resistivity are in-plane values

b)

Fig. 1.11 a) different carbon fibers properties, (source Singer), b) carbon fiber and graphite yarns

1.6 ARAMID FIBERS

Various types of polymer fibers (e.g., nylon, polyester, rayon) have been in use for many years as reinforcements in automobile tires, large balloons and dirigibles, body armor, and rubber-coated fabrics.

Aramid fiber is a generic term for a class of synthetic organic fibers called aromatic polyamide fibers. By definition an aramid fiber is "a manufactured fiber in which the forming substance is a long-chain synthetic polyamide in which at least 85% of the amide linkages are attached directly to two aromatic rings" (US Federal Trade Commission).

Well-known commercial names of aramid fibers include Kevlar and Nomex (DuPont) and Twaron (Teijin Aramid), whereas Nylon is a generic name for any long-chain polyamide.

Aramid fibers such as Nomex or Kevlar or Twaron, however, are ring compounds based on the structure of benzene as opposed to the linear compounds used to make nylon. Kevlar is a polyamide, in which all the amide groups are separated by para-phenylene groups, that is, the amide groups attach to the phenyl rings opposite to each other, at carbons 1 and 4. Nomex, on the other hand, has meta-phenylene groups, that is, the amide groups are attached to the phenyl ring at the 1 and 3 positions as shown in Fig 1.12.
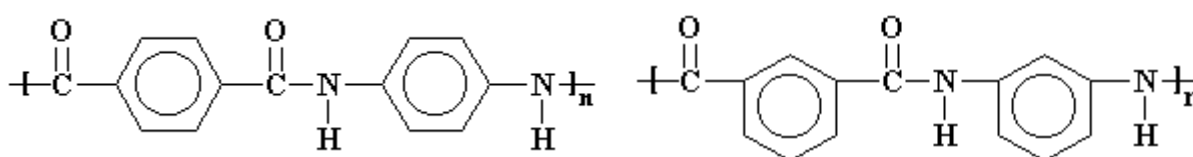

Fig. 1.12: Kevlar molecular structure left. Nomex molecular structure right

The basic chemical structure of aramid fibers consists of oriented para-substituted aromatic units, which makes them rigid rod-like polymers resulting in a high glass transition temperature and poor solubility, which makes fabrication of these polymers, by conventional drawing techniques, difficult.

Processing of aramid fibers involves solution polycondensation of diamines and diacid halides at low temperatures; the starting spinnable solutions that give high strength and high modulus fibers must have liquid crystalline order.

Fig. 1.13a shows two-dimensional, linear, flexible chain polymers in solution called "random coils". If the polymer chains can be made rod-like, we can depict them as random array of rods (Fig. 1.13b).

Increasing concentration of rod-like molecules you can form regions of greater order with parallel array, a state named " liquid crystalline " (Fig. 1.13c); When the rod-like chains become approximately arranged parallel to their long axes, but their centers remain unorganized or randomly distributed, we have what is called a nematic liquid crystal (Fig. 1.13d).
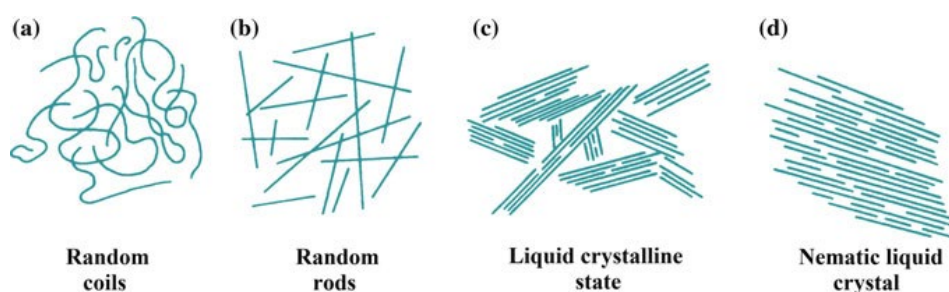

| (a) | (b) | (c) | (d) |
| Random coils | Random rods | Liquid crystalline state | Nematic liquid crystal |

Fig. 1.13: Various states of polymer in solution: a) random coils, b) random array of rods, c) partially ordered liquid crystalline state, and d) nematic liquid crystal state

Thus, starting from liquid crystalline spinning solutions containing highly ordered arrays of extended polymer chains, we can spin fibers directly into an extremely oriented, chain-extended form with high strength.

One would like to have, for any spinning process, a high molecular weight in order to have improved mechanical properties, a low viscosity to easily spin the fiber, and a high polymer concentration for high yield.

The production process used for aramid fibers is the dry-jet wet spinning one. The process is illustrated in Fig. 1.14. Solution polycondensation of diamines and diacid halides at low temperatures (near 0 °C) gives the aramid forming polyamides. The resulting polymer is pulverized, washed, and dried; mixed with concentrated H_2SO_4; and extruded through a spinneret at about 100 °C. The jets from the orifices pass through about 1 cm of air layer

before entering a cold water (0–4 °C) bath. The fiber solidifies in the air gap, and the acid is removed in the coagulation bath. The spinneret capillary and air gap cause rotation and alignment of the domains, resulting in highly crystalline and oriented as-spun fibers.

The higher temperature allows a more concentrated spinning solution to be used, and higher spinning rates are possible (rates of several hundred meters per minute are not unusual). The oriented chain structure, together with molecular extension, is achieved with dry-jet wet spinning.

The as-spun aramid fibers are washed in water, wound on a bobbin, and dried. Fiber properties are modified using appropriate solvent additives, by changing the spinning conditions, and by means of some post-spinning heat treatments, if necessary.
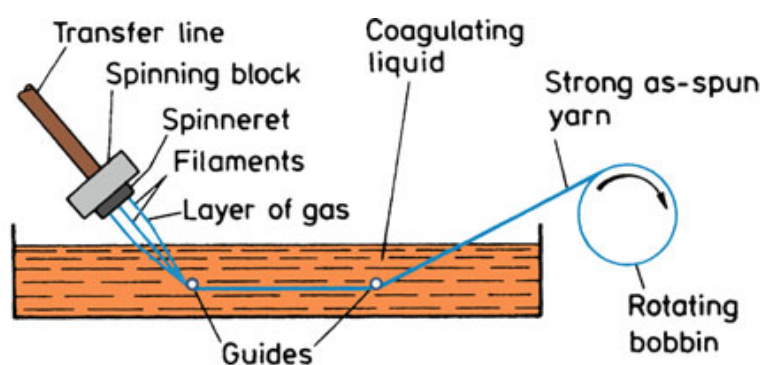

Fig. 1.14 The dry-jet wet spinning process

Kevlar aramid fiber is the most known of all: it is a polycondensation product of terephthaloyl chloride and p-phenylene diamine. The aromatic rings impart the rigid rod-like chain structure of aramid. These chains are highly oriented and extended along the fiber axis, with the resultant high modulus. In fact, tensile strength and modulus are substantially higher than for other organic fibers but elongation is significantly lower. Moreover, Kevlar fibers have poor characteristics in compression, with compressive strength being only one-eighth the tensile strength. This results from their anisotropic structure, which permits rather easy local yielding, buckling, and kinking of the fiber in compression. They are not as brittle as glass or graphite fibers and can be readily woven on conventional fabric looms. Some representative properties are given in Tab 1.15.

Property	K 29	K 49	K 119	K 129	K 149
Density $(g\ cm^{-3})$	1.44	1.45	1.44	1.45	1.47
Diameter (μm)	12	12	12	12	12
Tensile strength (GPa)	2.8	2.8	3.0	3.4	2.4
Tensile strain-to-fracture (%)	3.5–4.0	2.8	4.4	3.3	1.5–1.9
Tensile modulus (GPa)	65	125	55	100	147
Moisture regain (%) at 25 °C, 65% RH	6	4.3	–	–	1.5
Coefficient of expansion $(10^{-6}\ K^{-1})$	−4.0	−4.9	–	–	–

[a]All data from DuPont brochures. Indicative values only. 25-cm yarn length was used in tests (ASTM D-885). *K* stands for Kevlar, a trademark of DuPont

Tab 1.15 Kevlar aramid fiber yarns properties

1.7 BORON FIBERS

Boron filaments are produced by chemical vapor deposition (CVD) from the reduction of boron trichloride (BC13) with hydrogen on a tungsten or carbon monofilament substrate, so that practically it is itself a composite fiber. To realize this CVD process, high temperatures are required, so the choice of the substrate material in the core of the fiber is limited. Usually the choice falls on tungsten wire or carbon fiber.

The tensile strength of boron-tungsten filaments has improved steadily over the past decade from an average of under 2750 MPa to over 3445 MPa.

This value can be increased trough etching of the external part of the filament which is in state of compression (residual stress).

The interest in the use of boron fibers for aeronautical and structural purposes has always been discontinuous and faded out in favor of stiffer composites.

1.8 OTHER FIBERS

Basalt is a rock found in several locations worldwide and its fibers are obtained in similar way to glass fiber, sharing also other similarities like density and Young's module. Tensile strength instead, is higher.

The ceramic fibers combine high strength with high-temperature and general corrosion resistance.

An example of ceramic fibers are alumina fibers, marketed by Du Pont (E.I. Du Pont de Nemours & Co.) with the trade name "Fiber FP", which are a continuous alumina yarn with a 98% theoretical density. These fibers are made by spinning of an aqueous slurry and a two-step firing. As-produced Fiber FP surface is very rough; by coating with thin silica, tensile strength is increased by 50%; properties are in Fig 1.16a.

Silicon carbide (SiC) fibers are produced by a chemical vapor deposition, as well as by controlled pyrolysis of a polymeric precursor (Nippon Carbon Co.-Nicalon fibers).

Properties of SiC fibers are also given in Fig 1.16a.

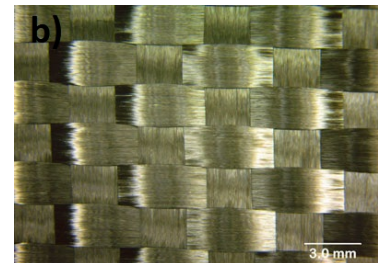| a) Property, units	Fiber		
	Alumina (Fiber FP)	SiC (CVD)	SiC (Pyrolysis)
Diameter, μm	20 ± 5	140	10–20
Density, g/cm³	3.95	3.3	2.6
Tensile strength, MPa	1380	3500	2000
Tensile modulus, GPa	379	430	180

Fig. 1.16 other fibers: a) ceramic properties, b) a woven fabric made of basalt fiber

Silicon carbide fibers' strength is maintained well above 650°C. Alumina and SiC fibers are suitable for reinforcing metal matrices, where carbon and boron fibers are not advisable. In addition, alumina has an inherent resistance to oxidation that is desirable in applications such as gas-turbine blades.

Another high modulus fiber can be produced starting from ultra-high-molecular-weight polyethylene (UHMW-PE), by dissolving in a solvent, spinning through a spinneret and cooled. The resultant product, named High-Performance Polyethylene (HPPE) Fibers, has interesting properties given by very long molecular chains, oriented and crystallized in the fiber direction. HPPE fibers have a density of only 0.97 g/cm³, their modulus and strength are slightly lower than those of Kevlar fibers but on a per-unit-weight basis, HPPE fibers have 30-40% higher strength and modulus than Kevlar fibers. High-energy absorption of HPPE fibers makes them

suitable for use in ballistic protection applications since PE fibers are strain rate sensitive: the higher the strain rate the higher the stiffness increase.

1.9 MATRIX MATERIALS

Fibers have small cross-sectional dimensions so they cannot be loaded directly nor share loads from one to the other. This severely limits their direct use in load bearing engineering applications, so they must be embedded in a matrix material to form a composite. The matrix binds the fiber together, transfers loads between them, and protects them against environmental attack and damage due to handling. It also has a strong influence on several mechanical properties of the composite, such as transverse modulus and strength, shear and compression properties, temperature behavior.

Physical and chemical characteristics of the matrix, such as melting or curing temperatures, viscosity, and reactivity with fibers, must be taken in account to choose the fabrication process.

1.9.1 POLYMERS

Polymers (commonly called plastics) are the most widely used matrix material for fiber composites due to their price and ease of production even though they are structurally much more complex than metals or ceramics.

On the other hand, polymers have lower strength and modulus, lower temperature use limits, weakness against prolonged exposure to ultraviolet light and some solvents.

Because of predominantly covalent bonding, polymers are generally poor conductors of heat and electricity. Polymers, however, are generally more resistant to chemicals than metals. Structurally, polymers are giant chain-like molecules (hence the name macromolecules) with covalently bonded carbon atoms forming the backbone of the chain. The process of forming large molecules from small ones (monomers) is called polymerization and can be done by addition or condensation.

According to the different chain molecules configuration we can structurally divide polymers in (Fig 1.17):

- Linear polymers. This type of polymer consists of a long chain of atoms with lateral groups. Examples include polyethylene, polyvinyl chloride, and polymethyl methacrylate. The chain tends to bend and warp.
- Branched polymers. Polymer branching can occur with linear, crosslinked, or any other type of polymer. An example is low density polyethylene (LDPE).
- Crosslinked polymers. In this case chains tend to crosslink and create a three-dimensional network. Crosslinking hinders sliding of molecules past one another, thus such polymers are strong and rigid. Examples are cross-Linked polyethylene or ethylene-vinyl-acetate.
- Ladder polymers. If we have two linear polymers linked in a regular manner, i.e., at regular distances we get a ladder shape similar to DNA molecule. Aromatic polyamides or aramids are other examples. Not unexpectedly, ladder polymers are more rigid and thermally more stable than linear polymers.
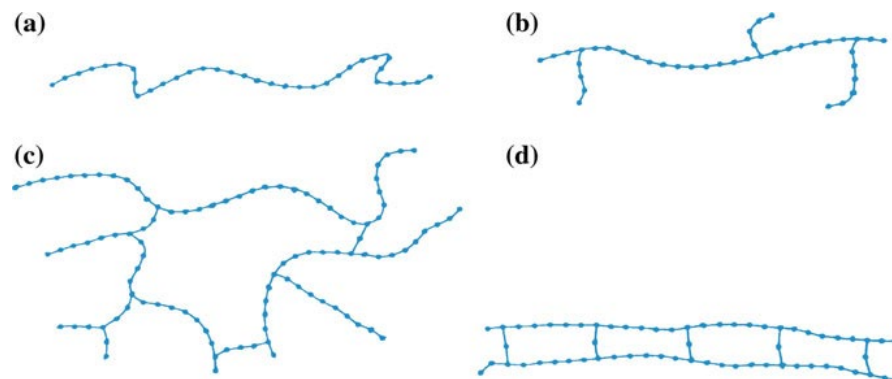
Fig. 1.17 molecular chain configuration: a) linear, b) branched, c) crosslinked, d) ladder

There is another type of classification of polymers based on the type of repeating unit: when we have one type of repeating unit forming the polymer chain, we call it a homopolymer; when the chain is composed of two different monomers we call it a copolymer. In addition, if the monomers are distributed randomly along the chain, we have a regular, or random,

copolymer, otherwise if one monomer is followed by a long sequence of another monomer, we have a block copolymer.

Speaking about molecular characteristics polymers show a "glass transition temperature", in fact when cooled, a liquid polymer contracts because of reduced thermal molecular vibration, up to the T_m (melting temperature) where a phase transformation occurs in which the polymer assumes an ordered crystalline structure. In the case of a semi crystalline one, that consists of a crystalline and an amorphous phase, the crystalline part undergoes this transformation. T_m can't be defined in the case of amorphous polymers since the liquid continues to contract, below what would be the melting point for the crystalline phase. It does so down to a lower undefined temperature called the glass transition temperature T_g, where it becomes a supercooled liquid polymer that is quite rigid and viscous. Such a phenomenon is also observed in silica-based inorganic glasses, although their T_g is several hundred degrees Celsius higher than that of polymers.

The glass transition temperature does not represent a thermodynamic phase transformation; it is in many ways akin to the melting point for the crystalline solids, when many physical properties (e.g., viscosity, heat capacity, elastic modulus, and thermal expansion coefficient) change quite rapidly. An influence given by the type of polymer backbone structure seen before is also reported. Polymers thermal stability is nonetheless lower than that of inorganic glasses because they have mainly covalent and van der Waals bonding and a lesser amount of crosslinking. A schematic is found in Fig 1.18.
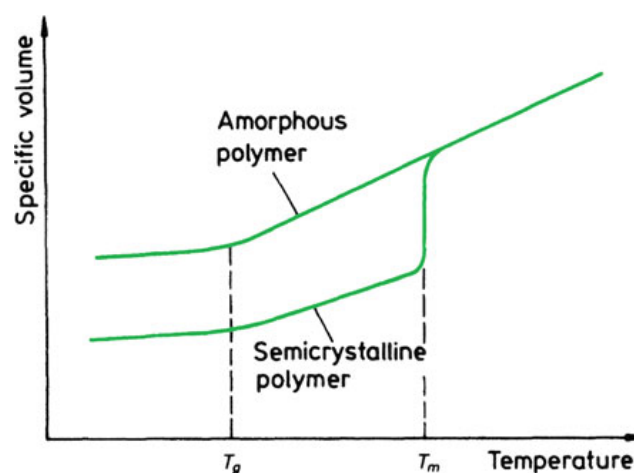

Fig. 1.18 Specific volume versus temperature for an amorphous and a semi crystalline polymer

1.9.2 THERMOPLASTICS AND THERMOSETS

Coming back to molecular structure (shape, size, mass, amount and type of bond, covalent or van der Waals) we can expect two main behavior differences: thermosetting or thermoplastic. Thermosets undergo a curing reaction that involves crosslinking of polymeric chains, hardening them. The curing reaction can be initiated by appropriate chemical agents or by application of heat and pressure, or by exposing the monomer to an electron beam. Thermoplastics are polymers that flow under the application of heat and pressure, i.e., they soften or become plastic on heating; cooling to room temperature hardens thermoplastics, which is the reason why they are suitable for liquid flow forming; in addition melting and solidification are reversible so they can be reshaped by a new application of heat and pressure. Examples include polyethylene, polypropylene, polystyrene, and polymethyl methacrylate (PMMA).

When the structure is amorphous, there is no global order among the molecules and the chains are arranged casually; see Fig. 1.19a. Small, plate-like single crystalline regions called lamellae or crystallites can be obtained by precipitation of the polymer from a dilute solution. In the lamellae, long molecular chains are folded in a regular manner; see Fig. 1.19b. Many crystallites group together and form spherulites, much like grains in metals.
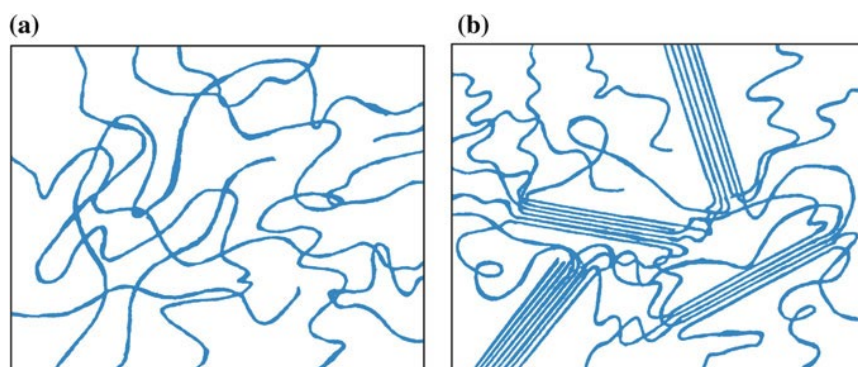

Fig. 1.19 polymer molecular arrangement: a) amorphous, b) semicrystalline

Thermoplastic polymers are used extensively for short-fiber reinforced composites in large-volume applications, where mass production can cut cost significatively and higher-strength and higher-stiffness replacements for plastics are needed.

When the molecules in a polymer are crosslinked in the form of a network, they do not soften on heating. We call such crosslinked polymers thermosetting polymers. Thermosetting polymers decompose on heating so they cannot be reshaped. Crosslinking makes sliding of molecules past one another difficult, giving strength and rigidity.

A typical example is that of rubber crosslinked with sulfur, that is, vulcanized rubber. Vulcanized rubber has ten times the strength of natural rubber. Common examples of thermosetting polymers include epoxy, phenolic, unsaturated polyester, and vinyl ester.

1.9.3 EXTERNAL VARIABLE INFLUENCES

Unlike metals and ceramics, polymers may be considerably influenced by external variables such as temperature, moisture and strain rate.

The processing temperature of thermoplastics is governed by either the melt temperature or glass transition temperature. For example, an amorphous thermoplastic must be molded well above its T_g in order to reduce its melt viscosity sufficiently.

An understanding of the effect of these temperatures on the mechanical behavior of polymers is best seen by the behavior of modulus of elasticity with temperature (Fig. 1.20). An amorphous thermoplastic (polystyrene, polycarbonate, or polymethylmethacrylate) has a significant change of mechanical properties at the glass transition temperature. Hence maximum use temperatures must be less than the glass transition temperatures. This phenomenon is reduced for thermosets (epoxy, polyester, or phenolic) because of high degree of cross-linking; nonetheless their maximum use temperatures should not exceed T_g.

Semicrystalline thermoplastics have a modest change in properties at the glass transition temperature owing to the presence of the crystalline regions. Their maximum use temperatures are more dictated by the melting points, as in the case of metals and ceramics.
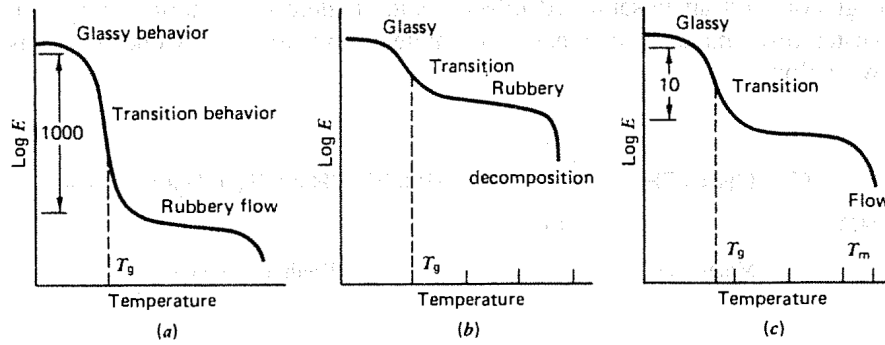
Fig. 1.20 elastic modulus variations: a) thermoplastics amorphous, b) thermoset highly cross linked, c) semicrystalline

For what concerns stress-strain curves for thermoplastics there is a general trend in Fig 1.21 both for crystalline and amorphous materials. Further, the rate of strain has a comparable effect, although much greater rate changes must occur to notice it substantially. Thermosets are not as affected by temperature and strain rate; the range of behavior being limited to approximately the higher three curves shown in Fig. 1.21.
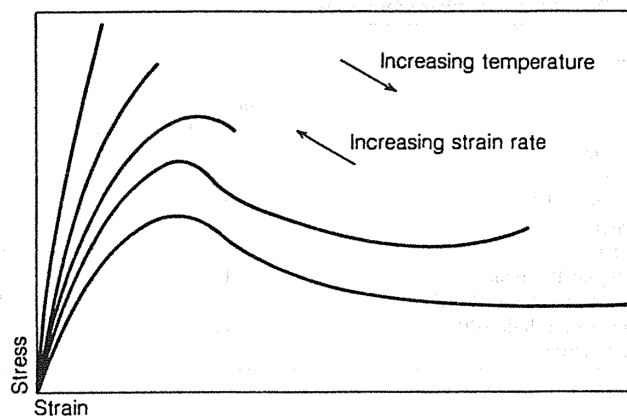

Fig. 1.21 Tensile stress-strain curves of a thermoplastic at different strain rates and temperatures

Moisture absorption also has an important effect on polymers, particularly relative to metals and ceramics. For example, epoxy or polyester resins can absorb up to 4-5% by weight of water if exposed to l00% relative humidity or immersed in water.

Another relevant external variable is also deterioration as a result of exposure to ultraviolet radiation. All these effects must be properly taken into consideration when the matrix is selected for a composite.

1.9.4 FILLERS

Fillers are used widely in polymeric composites primarily to reduce cost with some sacrifice in desired performance. They also are used to reduce shrinkage, control viscosity, and improve part stiffness. Commonly used fillers include calcium carbonate, kaolin (china clay), silica (sand), feldspar, talc, and glass microspheres. Fillers are not as common in high end applications because they may adversely affect the fiber-resin load transfer and toughness. Glass-fiber-reinforced polyesters from sheet-molding compounds or bulk-molding compounds may contain substantial amounts of $CaCO_3$ (Calcium carbonate) to achieve high surface smoothness and eliminate sink marks.

Kaolin is used to increase resin viscosity to prevent fibers from extruding from molded surfaces. Natural silicas are used in thermoset resins for dimensional stability, good electrical insulation, and improved thermal conductivity. Talc, in the form of finely ground thin platelets, is added to resins to improve stiffness and creep resistance.

Some natural organic materials such as wood flour, shell fibers, cotton and vegetable fibers are also used as fillers.

Hollow microspheres made from glass or polymers can be used to reduce the density of the resin significantly. Additives used for fire resistance (e.g., antimony oxide), chemical thickening (e.g. magnesium oxide and calcium hydroxide), and for lowering shrinkage (fine-powdered polyethylene) are also common.

1.10 RHEOLOGY OF PLASTICS

The adopted strategy to elevate the accuracy of finite element analysis of composite structures is to include information coming from manufacturing process, particularly injection molding.

The first basic concept linked with injection molding is that molten polymers have a certain rheological behavior. Rheology is the science that deals with the way materials deform and

flow when forces are applied (under controlled conditions) to them: flow is a special case of deformation and deformation is a special case of flow.

Solid plastic products parts, whether injection-molded polycarbonate compact laser disks, high-strength fibers spun from Kevlar liquid crystalline polymer, or injection-molded car bumpers, are all processed in a fluid state, either molten or in solution. In this state, these polymers are viscoelastic complex fluids, whose rheological properties determine the feasibility and expense of processing and, to some extent, the final properties of the finished parts. For example, the pressure drop required for injection molding is affected by the melt viscosity. The attainable extrusion speed, as well as the shape of extruded parts, depends on elastic forces generated when the molecules are stretched out by the flow. "Molded-in" stresses can lead to warping of injection-molded parts or undesired residual birefringence properties.

A "rheometer" measures the rheological properties of a complex liquid as a function of rate or frequency of deformation. For liquids, the simplest devices impose a shearing flow on the liquid and measure the resulting stresses, or alternatively, impose a shearing stress and measure the resulting shearing rate.

Melting is a fundamental process for the transformation of thermoplastics and for their regular flow into runners and cavities; thus, the knowledge of the rheological behavior of thermoplastic materials is of extreme importance. The term rheological behavior addresses the variation of viscosity as a function of flow conditions and of temperature. In general

$$\eta = f(\tau, \dot{\gamma}, T) \tag{1.1}$$

where τ is the tangential stress, $\dot{\gamma}$ is the rate of deformation being γ the deformation and T is the temperature. Newtonian fluids have viscosity η constant, independently from shear rate. All materials show a behavior between two extremes: solid like (ideal solid) and liquid like (ideal liquid) as depicted in Fig 1.22.

- Solid extreme (elasticity): ''The power of any spring is in the same proportion with the tension thereof" (Hooke). We apply Hooke's Law:

$$\tau = G \, \gamma \qquad\qquad (1.2)$$

$$\sigma = E \varepsilon \qquad\qquad (1.3)$$

where G is the rigidity modulus.

- Liquid Extreme (viscosity) ''The resistance which arises from the lack of slipperiness of the parts of the liquid, other things being equal, is proportional to the velocity with which the parts of the liquid are separated from one another" (Newton).

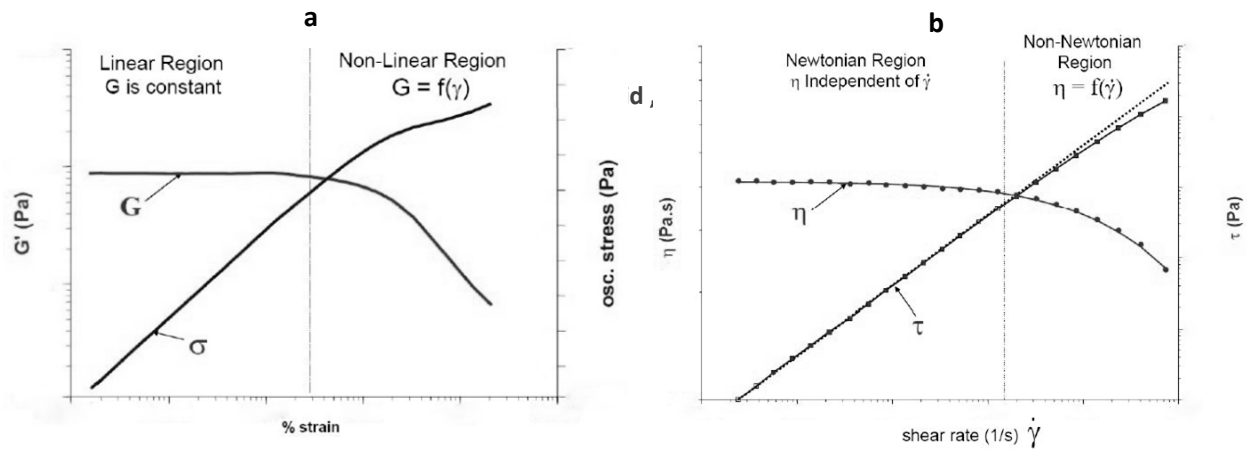$$\tau = \eta \, \dot{\gamma} \qquad\qquad (1.4)$$

where η is the coefficient of viscosity.

Fig. 1.22 a) behavior of solids, b) behavior of fluids

Consider a molten liquid polymer flowing between two plates of area A separated by distance h (Fig 1.23). One plate moves relatively to the other with velocity v. The movement is resisted by the viscous reaction in the fluid. Since the movement is in shear, the reaction is the shear viscosity.
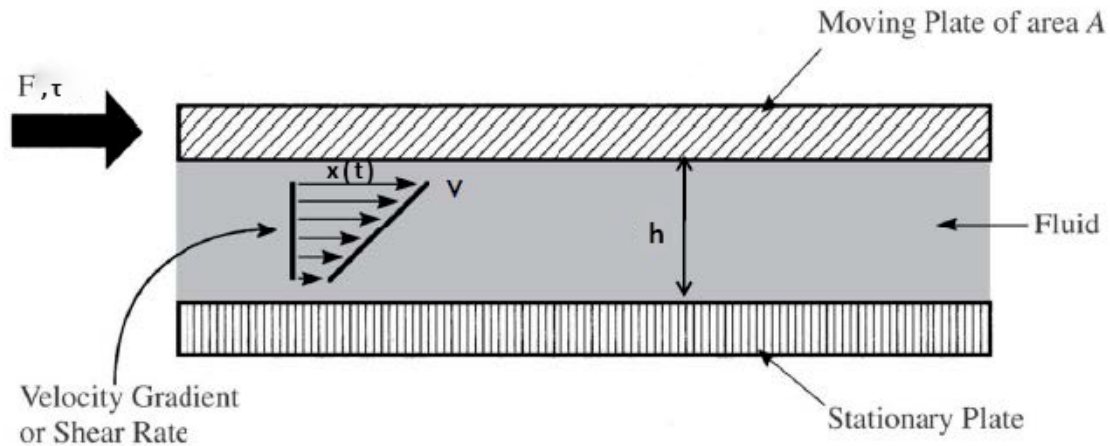
Fig. 1.23 sliding plate schematic

From the schematic shear stress is equal to τ = F/A, shear strain is γ = x(t)/h and strain rate $\dot{\gamma}$ = v/h. Applying eq. (1.2) and (1.4), viscosity and G (shear modulus) can be easily obtained. In addition, considering shear rate or strain rate, we can say that with respect to material being sheared, velocity gradient is the change dv in relative velocity v between parallel planes with respect to the change dh in perpendicular distance h throughout the depth of the material.

Velocity gradient has the same dimensions as rate of shear, which is reciprocal seconds.

All these rheological properties depend upon the rate of shear, the molecular weight and structure of the polymer, the concentration of various additives, as well as upon the temperature. The viscosity rapidly decreases as temperature increases; typical polymer melts have values of the order of 103 to 104 poise.

For thermoplastics a unique value of the viscosity is not enough to describe the rheological behavior of the material, since it changes with flow conditions, therefore thermoplastics are considered non-Newtonian fluids. Another point is that the rheological behavior of the molten polymer is affected also by temperature, so a curve that describes the variation of viscosity as a function of the shear rate for each temperature is needed.

Ability to flow for a molten material depends on the molecular chain mobility that hold molecule together. Low mobility with high degree of chain entanglement will influence the ability to flow and the process ability of polymeric materials.

Most polymer melts and rubber compound behave in a so called pseudoplastic way.

Pseudoplastics or shear thinning fluids have a lower apparent viscosity at higher shear rates.
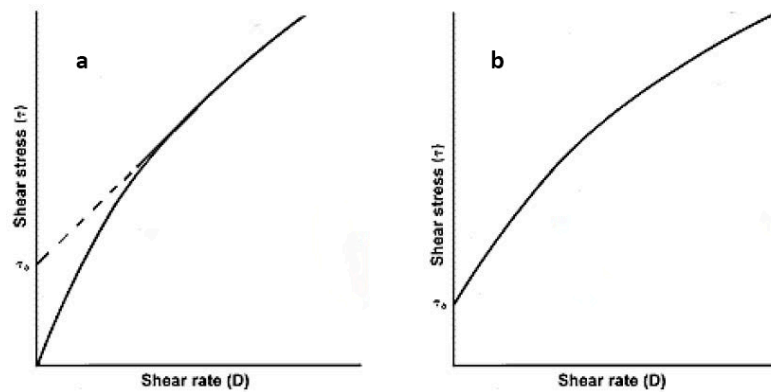

Fig. 1.24 pseudo-plastic material behavior: a) normal, b) with yield value

At very low rates of shear, the entanglements have time to slip and become disengaged before enough stress can develop in them to orient the molecules (Fig 1.25).
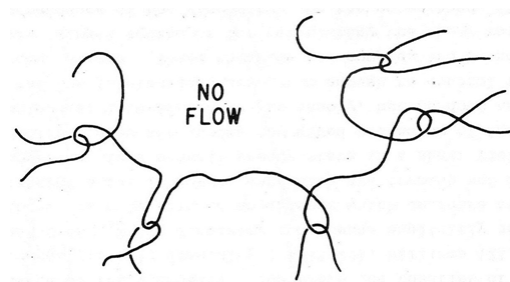

Fig. 1.25 low shear chain state

An outstanding characteristic of polymer melts is their non-Newtonian behavior whereby the apparent viscosity decreases as the rate of shear increases.

 At higher rates of shear instead, the segments between entanglements become oriented before the entanglements can disappear.

As a load-bearing entanglement disappears, there develops in the melt a steady state condition in which the rates of formation and destruction of entanglements become equal.
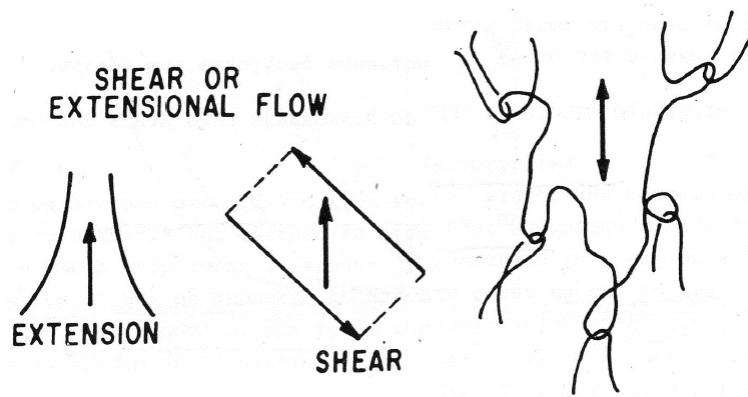
Fig. 1.26 high shear chain state

At very high rates of shear practically no entanglements can exist. The viscosity should reach a relatively small value which becomes independent of the shear rate. In other words, polymer melts may be expected to become Newtonian in behavior at very high rates of shear.

To conclude the paragraph some hints about the main parameters affecting the rheology of a polymer are given:

- Molecular weight is a considerable factor. The higher it is, the higher is viscosity.
- In some cases solvents, plasticizers and lubricants are added to plasticize the polymer, to improve its processability or to stabilize the polymer to processing conditions.
- Branched structure: If the branches are so long that they can participate in entanglements, the branched polymer may have a viscosity at low rates of shear greater than that of a linear polymer of the same molecular weight. On the contrary, at high rates of shear, branched polymers in nearly all cases have lower viscosity than linear ones of the same molecular weight. See an example of polyethylene rheology at 150° C in Fig 1.27.
- Temperature is the main factor. As it increases obviously the viscosity drops down. In Fig 1.28 there is a comparison between different polymers.
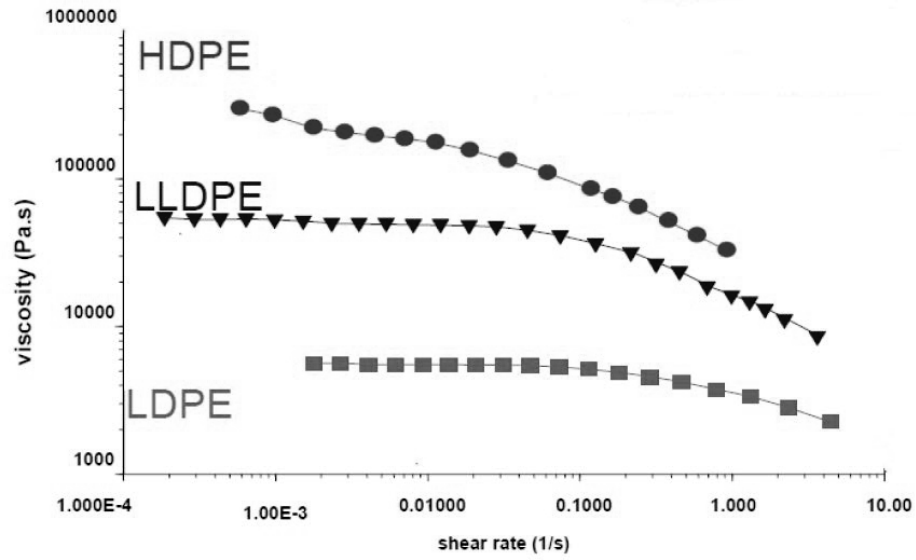
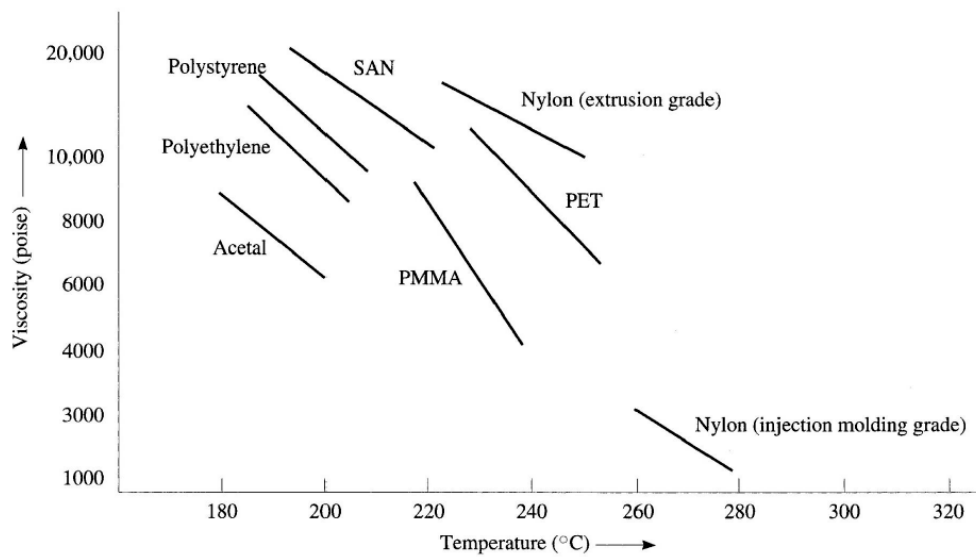Fig. 1.27 polyethylene rheology at 150° C

Fig. 1.28 temperature influence on various polymers

1.11 COMPOSITE MANUFACTURING

1.11.1 INTRODUCTION

In general, finished products are formed from materials such as plastics and metals by molding or shaping methods. The material is first created and then processed at a later stage by specialized facilities in forging, sheet forming, injection molding, etc. However, composites can also be realized in the same phase of material creation, in only one process. Such is the case when filament winding a pipe from a polymer and glass fiber strands. Regarding polymeric matrix composites, the processing methods for thermosetting materials typically involves material formation during final molding (e.g., hand lay-up, spray-up, and vacuum-bag molding). In some cases, material formation is accomplished separately from forming or shaping but because of the curing nature of thermosetting resins, final curing occurs during final formation. In thermoplastic matrix composites, it is more common to fabricate the composite first and form or mold a shape in a second operation. However, in this latter step, the composite properties still can be vastly influenced (e.g., fiber length reduction or fiber orientation during molding).

The material and production process used in this thesis will belong to this last category, which is the reason why also in this paragraph the focus is shifted more on injection molding than on thermosetting composites.

1.11.2 THERMOSETTINGS FABRICATION

Fabrication processes for thermosetting resin matrix composites can be broadly classified as wet-forming processes and processes using premixes or prepregs. In the wet-forming processes, the final product is formed while the resin is quite fluid, and then the curing process is usually completed by healing. The wet processes include hand lay-up, bag molding, filament winding, resin-transfer molding and pultrusion. In the processes using premixes, as the name suggests, material preparation is separated from lay-up or molding. Premixes such as bulk

molding compounds (BMCs) and sheet molding compounds (SMCs) are compounded from resin, fillers, and fibers and partially cured; their use makes manufacturing simpler and increases the possibility of automation. Prepregs are usually partially cured sheets of oriented fibers or fabric. High-fiber-volume fractions can be achieved with uniform fiber distribution. Hand layup and spray techniques are perhaps the simplest polymer processing techniques. Fibers can be laid onto a mold by hand and the resin (unsaturated polyester is one of the most common) is sprayed or brushed on. Frequently, resin and fibers (chopped) are sprayed together onto the mold surface. In both cases, the deposited layers are densified with rollers. Fig. 1.29 shows schematics of these processes. Accelerators and catalysts are frequently used. Curing may be done at room temperature or at a moderately high temperature in an oven.
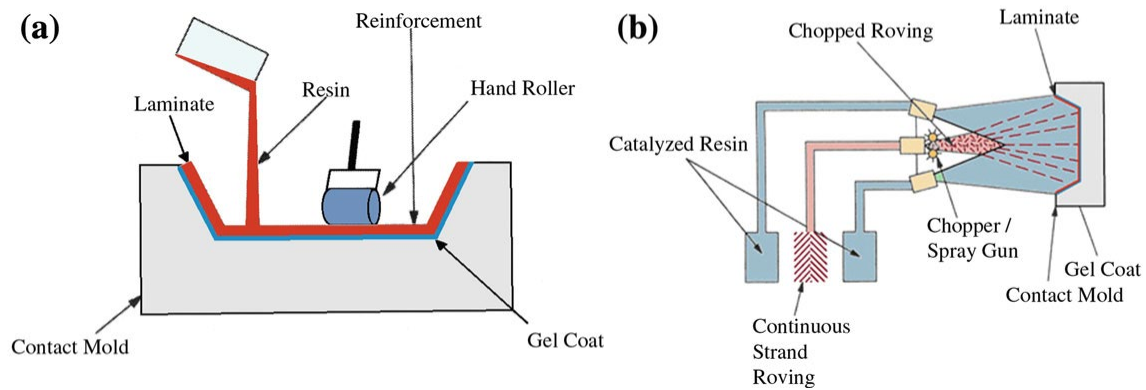

Fig. 1.29 a) In hand layup, fibers are laid onto a mold by hand, and the resin is sprayed or brushed, **b)** In spray-up, resin and fibers (chopped) are sprayed together onto the mold surface

Filament winding is another very versatile technique in which a continuous tow or roving is passed through a resin impregnation bath and wound over a rotating or stationary mandrel. A roving consists of thousands of individual filaments. Fig. 1.30 shows a schematic of this process. The winding of roving can be polar (hoop) or helical. In polar winding, the fiber tows do not cross over, while in the helical they do. The helix angle depends on the shape of the object to be made. Successive layers are laid on at a constant or varying angle until the desired thickness is attained. Curing of the thermosetting resin is done at an elevated temperature and the mandrel is removed. Very large cylindrical and spherical vessels are built by filament winding by using glass, carbon, and aramid with epoxy, polyester, and vinyl ester resins.
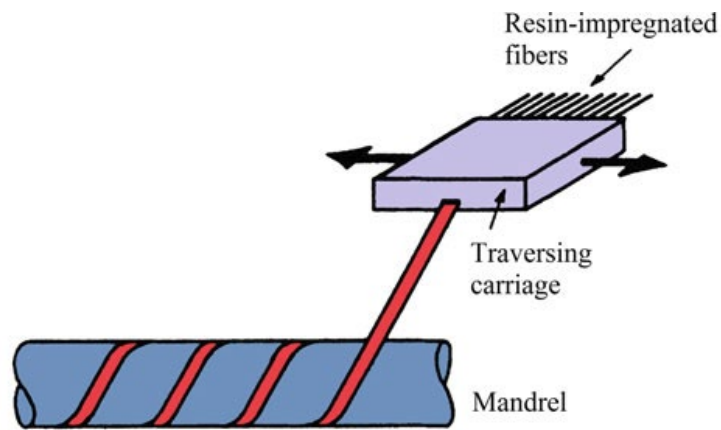
Fig. 1.30 filament winding process

Pultrusion is a process in which, continuous sections of polymer matrix composites with fibers oriented mainly axially are produced. Fig. 1.31a shows a schematic of this process. Continuous fiber tows come from various creels. Mat or biaxial fabric may be added to these to provide some transverse strength. These are passed through a resin bath containing a catalyst. After this, the resin impregnated fibers pass through a series of wipers to remove any excess polymer and then through a collimator before entering the heated die. Stripped excess resin is recirculated to the resin bath. The heated die has the shape of the finished component to be produced. The resin is cured in the die and the composite is pulled out. At the end of the line, the part is cut by a flying saw to a fixed length. An example of a product obtained by pultrusion is shown in Fig. 1.31b. The hollow trapezoidal-shaped product shown is a helicopter windshield post made of carbon fiber mat and tows in a high temperature vinyl ester resin matrix.

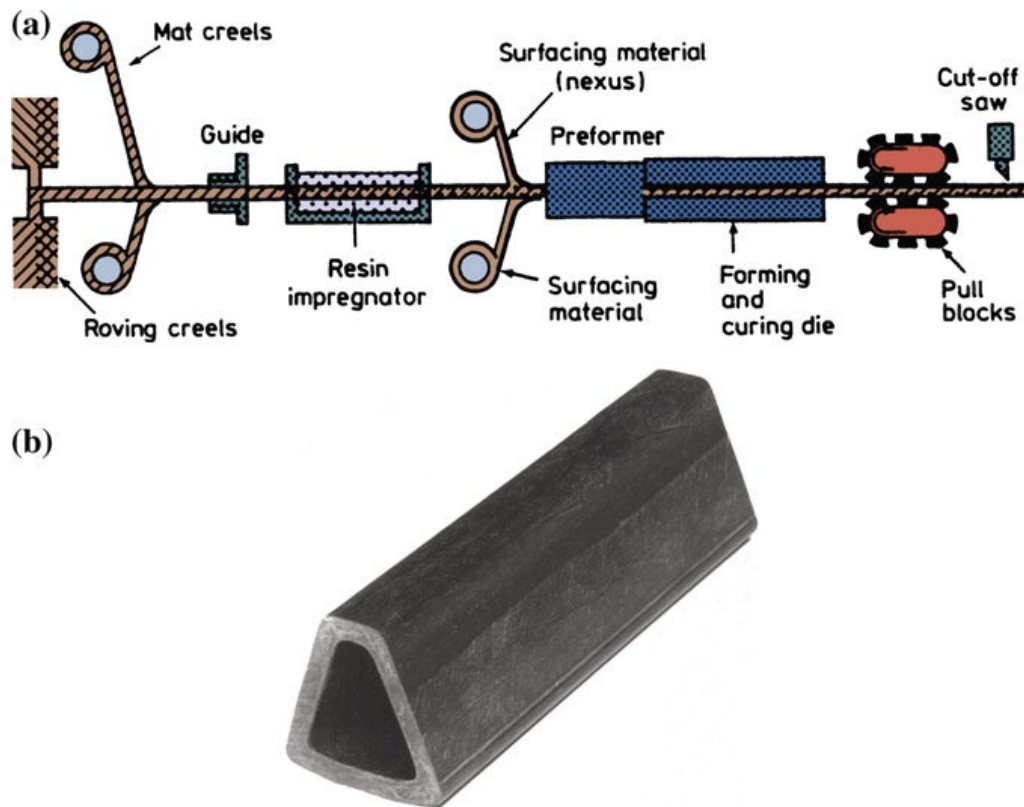Main advantages of the process are low labor cost and product consistency.

Fig. 1.31 a) Schematic of the pultrusion process, **b)** A helicopter windshield post made of carbon fibers/vinyl ester resin by pultrusion (Morrison Molded Fiber Glass Co.)

The Resin Transfer Molding (RTM) is a closed mold process which allows the creation of composite in different shapes, size and performance assuring good efficiency and low manufacturing costs. This process differs from other types of molding by the fact that the reinforcement and the resin are combined inside the mold. More precisely, it consists in the injection of a thermosetting polymer resin inside a mold in which a pre-assembled fibers preform has previously been disposed, starting from dry fibers, in different geometry and complexity fabrics; after that resin curing and piece removal from the mold are disposed.
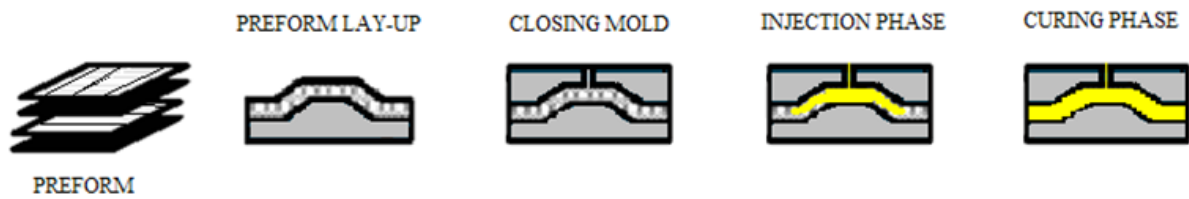A schematic is shown in Fig. 1.32

PREFORM   PREFORM LAY-UP   CLOSING MOLD   INJECTION PHASE   CURING PHASE

Fig. 1.32 RTM schematic

Sheet molding compound (SMC) refers to both a material and a process for producing glass fiber reinforced parts, compounded in sheet form, starting from a polyester resin matrix. The glass fiber is added to a resin mixture that is carried onto a plastic carrier film; after partial cure, the carrier films are removed. The sheet molding material is cut into lengths and placed onto matched metal dies under heat and pressure. Advantages of this process are high volume production, excellent part reproducibility, minimum material scrap and excellent design flexibility.
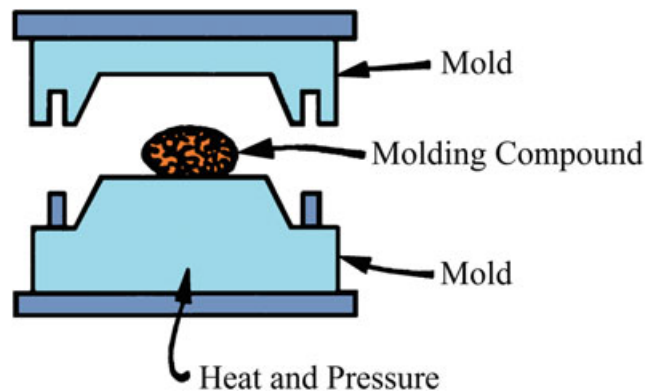

Fig. 1.33 SMC schematic

1.11.3 THERMOPLASTICS FABRICATION

Injection molding is the main manufacturing technology used to produce short fiber reinforced thermoplastic parts. The mold can be a classic mold and plunger one or a

reciprocating screw type machine.

The molding process is the same both for reinforced or unreinforced thermoplastics, but operating parameters, conditions, cycle times must be tuned accordingly since reinforced polymers show significantly different rheological and conductive properties.

Moreover, the properties of short-fiber-reinforced thermoplastic are very dependent on fiber length and orientation, which on their turn are influenced by manufacturing conditions.

An injection molding machine is composed by an injection unit, a mold system, a clamping system and controls as shown in Fig. 1.34
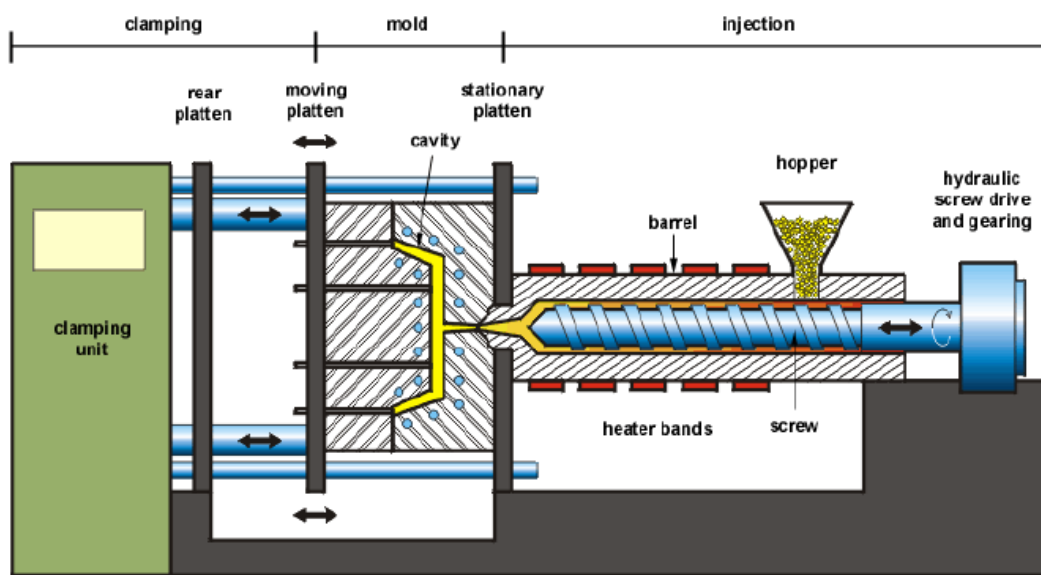

Fig. 1.34 injection molding machine

The purpose of the injection unit is to liquify the plastic materials and then inject the liquid into the mold. The resin is introduced through a single or multiple hopper (to feed filler, colorants, other additives) by gravity and it is further mixed by mechanical shear and thermal energy from heater during the forward motion phase in the reciprocating screw. The injection unit or sled can be also pushed back to facilitate purging and nozzle maintenance. The barrel is made of heavy steel cylinder to withstand the pressure and temperature involved in melting the resin.

Alternatively to the reciprocating screw system you can use a ram injector where plastic is

pre-melted in the hopper, fed into a chamber, and forced into the mold with a piston.

The injection unit of a mold machine is specified by its shot size i.e. the maximum amount of plastic that can be injected in one molding cycle, by its capacity and recovery rate (a measure of the amount of plastic that can be melted and homogenized per unit of time) and by maximum injection velocity and pressure.

The clamping unit is designed to open and close the mold, generate enough pressure to prevent flashing during mold filling and holding and maintain the right pressure when the polymer is injected.

The mold is the central point in an injection molding machine. Each mold can contain multiple cavities where the melted polymer is distributed, shaped, cooled by a dedicated circuit and finally ejected.

During injection molding, the material is subjected to large amount of shear forces during the cavity filling stage. The shear rate is proportional to the injection speed. If the shear rates are in the non-Newtonian region of the curve, then small variations in the shear rate will cause a large shift in the viscosity. This will make the mold filling inconsistent resulting in shot to shot inconsistency. It is therefore important to find the Newtonian region of the curve and set the injection speed (therefore shear rate) in this region.

The injection mold process can be divided into three different phases:

- Injection/filling phase. The time during which the screw translates to inject the material. At the end of it mold is in pressure and the 100% (whole volume of the cavity) of material has been injected.

- Packing/Holding phase. During this part of the process the axial screw speed is slow; another 15% of material is forced to flow into the cavity to compensate the thermal contraction of the material keeping the pressure constant. The holding pressure phase has an important influence on such features as weight, dimensional accuracy, and internal structure.

- Cooling phase. It begins simultaneously with injection because the melt starts to cool as it meets the cold mold walls; it continues also after part ejection.

When the material flows into the cavity it is subjected to flow and cooling processes; a distinction can be made between the velocity profile of areas behind the flow front and the one at the melt front. Behind the flow front, a cross section from wall to wall has a solidified or frozen layer next to the mold wall because of the cooling effect. No further flow is possible within this solidified layer whereas inside there is a hot core that still contains fluid material. The highest velocity gradient (shear rate) is in the proximity of the solidified layer. In this area the melt is subjected to especially strong shearing, which orients the material in the direction of flow. The different velocity gradient between flow front and "behind" determines a fountain flow effect at the melt front i.e. the flow is perpendicular to the wall like a fountain.
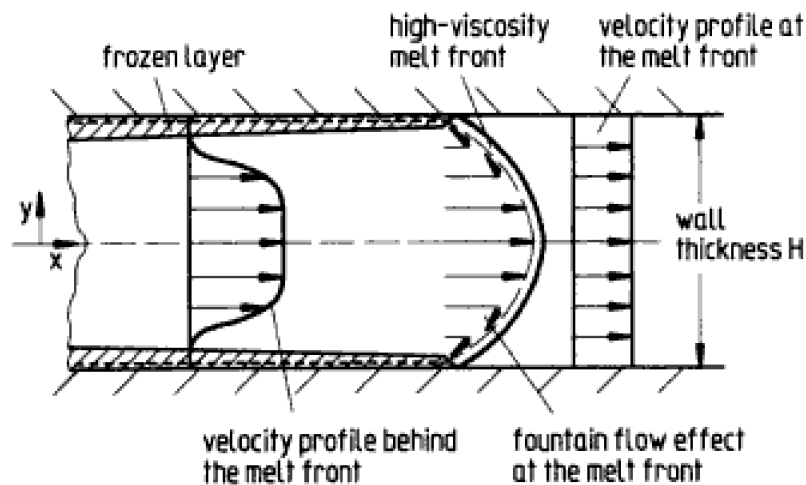

Fig. 1.35 flow velocity gradient

The frozen layer thickness depends on the thermal equilibrium:

$$Q_T = Q_M + Q_F \qquad\qquad 1.5)$$

Where Q_T is the heat transferred to the mold, Q_M is the heat introduced by the flow of new molten material and Q_F is the heat generated by shear friction on the frozen layer.

Since the mold filling phase lasts some seconds, the frozen layer soon reaches an equilibrium at the beginning of the filling phase. If the injection speed is reduced, less shear heating is generated and the heat transferred by new molten material is lower. As the heat exchange

through the mold does not change (the mold is cooled and conditioned), the frozen layer will then have a higher thickness. On the contrary, if the injection speed is increased, the frozen layer will be thinner.
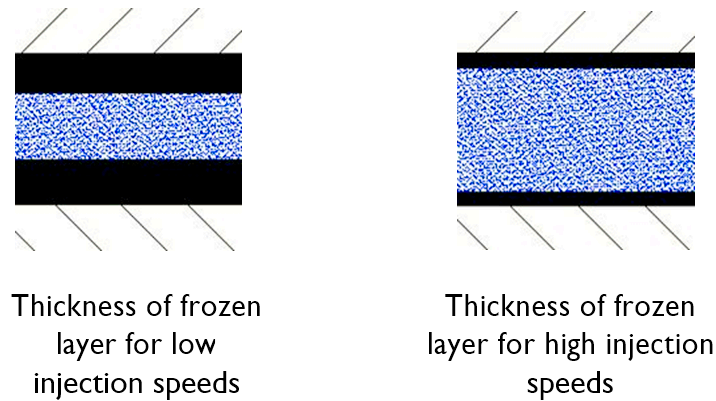

Thickness of frozen layer for low injection speeds

Thickness of frozen layer for high injection speeds

Fig. 1.36 thickness of frozen layer during filling

At the end of filling, the flow stops and the cooling of the material begins. If compared to what occurs for the frozen layer, molten plastic cooling is very slow and doesn't influence the orientation of the molecular chains.

Taking into consideration the effects of the orientation on the levels of stress, it can be stated that at the end:

- On the internal wall of the frozen layer the material is highly oriented and it will undergo a great shrinkage when solid.
- The shrinkage of the oriented material is contrasted by the inner layer that shows no particular molecular orientation.

The frozen layer will be subjected to a tensile state, while the inner material will be in a compression state resulting in possible unwanted deformations. During the packing phase, the material behavior is similar to the one of the filling phase. Since the flow velocity decreases as the pressure into the cavity raises, the frozen layer will thicken. The difference with respect to the filling phase lays in the increase of pressure on the material. In holding phase again

pressure decreases, we complete compensation of volume change.

To resume molded part quality is affected mainly by this process parameters: temperature of molten material, gradient of temperature dependent on cooling system design, injection/mold filling time, mold temperature.

Chapter 2

MULTI SCALE ANALYSIS

2.1 INTRODUCTION

Traditionally structural analysis contemplates nonlinearity given by material, boundary constraints and geometry plus anisotropy and composites layered structure, all of this at a macro level scale. The frontier is to take in account and relate these properties to the microstructure of the composite part, at micro scale, which is highly affected by manufacturing processes as described in previous chapters.

To realize this goal, the software suite offered by Ex-Stream Digimat is used.

On the microscopic scale Digimat-MF (in this thesis) and Digimat-FE (in general) are used in the context of direct engineering approach for understanding, predicting and screening composite material properties.

Multi-scale coupling is based on Digimat-MF material models stored in Digimat-MX, the materials database. Coupled analysis uses the power of Digimat-RP to interface manufacturing process and structural FEA software in combination with mapping (Digimat-MAP), visualization and post-processing technology.

Specifically Digimat MF is used to model the linear and nonlinear material behavior of glass-reinforced thermo-plastic injection molded parts taking into account the fiber orientation predicted by injection molding software and act as the micro-mechanical material model within the structural finite element analysis software. To achieve this goal it uses Eshelby-based semi-analytical mean-field homogenization approaches and an analytical description of

the material in order to compute the thermo-mechanical, thermal or electrical properties of a composite as a function of its microstructure morphology, i.e., inclusion shape, orientation, volume/mass fraction, and micro, i.e., per-phase, material behavior.

2.2 MEAN – FIELD HOMOGENIZATION

The objective of micromechanical modeling of heterogeneous materials, whose microstructure consists of a matrix material and multiple phases of so-called "inclusions", which can be short fibers, platelets, micro-cavities or micro-cracks (see Fig 2.1), is to predict the interaction between the microstructure and the macroscopic (or overall or effective) properties.
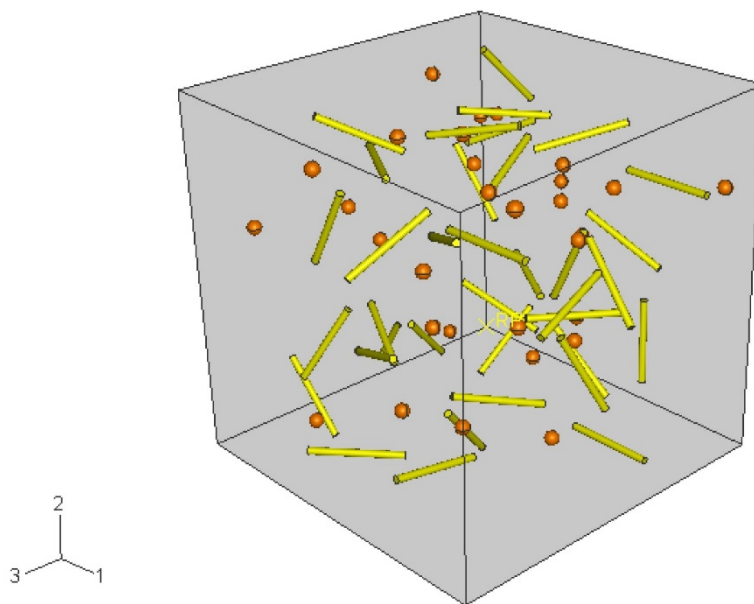

Fig. 2.1 Matrix material reinforced with multiple phases of inclusions

It would require a huge amount of computing power to solve the mechanical problem at the micro- scale level. To link micro-scale and macro-scale (where the solid can be seen as locally

homogeneous), the concept of RVE (representative volume element) is used.

At macro scale, each material point is supposed to be the center of an RVE, which should be sufficiently large to represent the underlying heterogeneous microstructure but small with respect to the size of the solid body (see Fig 2.2).
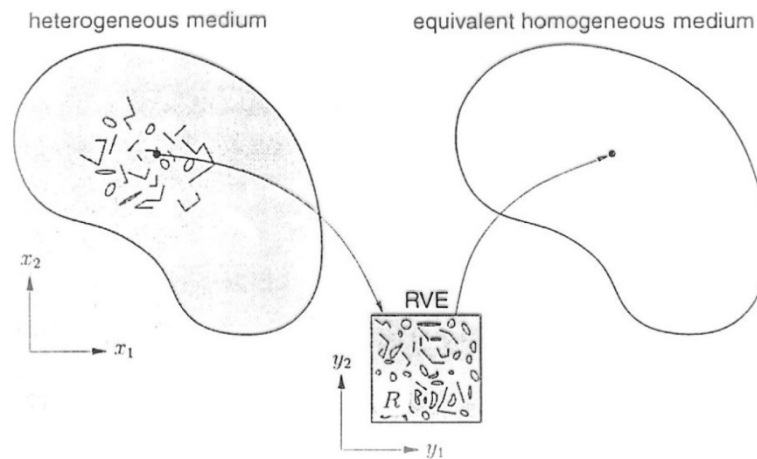

Fig. 2.2 Micro- Macro transition Upper left: microscopic scale, **upper right**: macroscopic scale, **bottom**: representative volume element (RVE). After Nemat-Nasser and Hori (1993).

A schematic approach which enables a transition between the two scales, both ways, is summarized in the following steps:

- Macro material point: center of a representative volume element (RVE).
- At micro scale: RVE contains a finite number of constituents.
- Need of a constitutive model for each of the constituents.
- Micro/macro transition: homogenization method to find the macro constitutive response of RVE.
- Continuum mechanics at macro scale with macro constitutive equation.
- To go in the opposite direction (macro to micro transition), At each time and at each macro material point, do a numerical zoom in order to see what happens at the micro level (e.g., stresses and strains in each phase).

The RVE problem solution is not trivial, so it is necessary to introduce averaging results.

At each macro point X, we know the macro strain $E(X)$ and need to compute the macro stress $\sigma(X)$ or vice-versa.

The average quantity over a RVE (domain ω, volume V) is defined by

$$\langle f(X,x) \rangle = \frac{1}{V} \int_{\omega} f(X,x) \, dV \tag{2.1}$$

where integration is performed with respect to micro coordinates, and $f(X,x)$ is the micro field inside the RVE. In the following, dependence on macro coordinates X will be omitted for simplicity. We consider two classical types of BCs: (1) linear displacements, and (2) uniform traction. The former corresponds to a given macro strain (or more accurately an imposed macro displacement gradient) and the latter to a known macro stress.

At micro level, the boundary $\partial\omega$ of the RVE is subjected to imposed linear displacements:

$$u_i(x) = G_{ij}x_j, \qquad x \in \partial\omega \tag{2.2}$$

Result: the average strain equals the macro strain, i.e., $\langle \varepsilon_{ij} \rangle = E_{ij}$. At micro level, imposed traction on:

$$F_i(x) = \sigma_{ij}n_j(x), \quad x \in \partial\omega \tag{2.3}$$

where n is the outward unit normal to $\partial\omega$. Result: the average stress equals the macro stress: $\langle \sigma_{ij} \rangle = \sigma_{ij}$.

To conclude for an RVE under classical BCs, the macro strains and stresses are equal to the volume averages over the RVE of the unknown micro strain and stress fields inside the RVE. Another useful result is given hereafter:

Consider any self-equilibrated micro stress field and micro strain field

$$\sigma_{ij}^* = \sigma_{ji}^*, \quad \frac{\partial \sigma_{ij}^*}{\partial x_j} = 0, \quad \forall x \in \omega \text{ and } \varepsilon_{ij}^* = \frac{1}{2}\left(\frac{\partial u_i^*}{\partial x_j} + \frac{\partial u_j^*}{\partial x_i}\right) \tag{2.4}$$

where u(X) is the micro displacement field associated with $\varepsilon^*(X)$.

Note that $\sigma^*(X)$ and $\varepsilon^*(X)$ are not necessarily related, and neither one is necessarily a solution to the micro problem.

If $\varepsilon^*(X)$ satisfies the linear displacement boundary condition previously described on $\partial\omega$ or $\sigma^*(X)$ satisfies uniform traction on $\partial\omega$ then

$$\langle \sigma^* : \varepsilon^* \rangle = \langle \sigma^* \rangle : \langle \varepsilon^* \rangle \qquad (2.5)$$

This is known as Hill's macro-homogeneity condition or Hill-Mandell condition, and is very useful for the derivation of homogenization models from variational formulations. In linear elasticity, the condition has a simple and powerful interpretation: if $\sigma^*(X)$ and $\varepsilon^*(X)$ are related, then the average of the micro energy equals the macro energy.

From a continuum mechanics viewpoint, the problem of homogenization can be stated as follows: at the macro scale, in each macro material point, if we know the macro strain, we need to compute the macro stress, and vice-versa. From the above results, we know that relating E and σ means also relating $\langle\sigma\rangle$ and $\langle\varepsilon\rangle$.

In linear elasticity, the problem can be stated in a simpler form: find the macro stiffness such that $\langle\sigma\rangle = \bar{C} : \langle\varepsilon\rangle$. This is illustrated in Fig. 2.3.
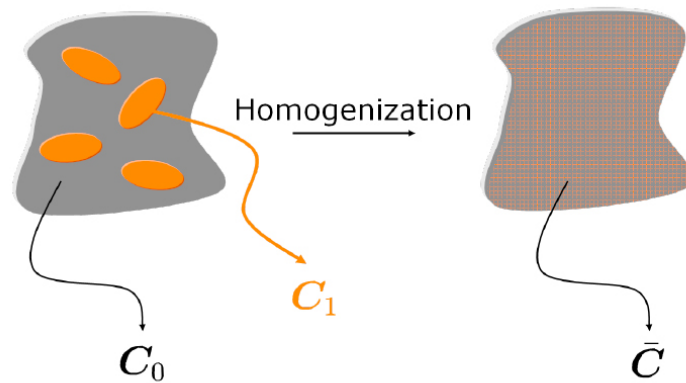

Fig. 2.3 The idea of homogenization in linear elasticity. Left: heterogeneous material under given boundary conditions (BCs). Right: equivalent homogeneous material having the same effective stiffness under the same BCs

This is the fundamental problem of homogenization in linear elasticity: find an equivalent homogeneous material which has the same effective macro stiffness as the real heterogeneous composite, under the same boundary conditions. The approaches used in Digimat are two: direct finite element analysis of RVE at micro scale and mean field homogenization.

The first is very accurate and detailed but it is very expensive in terms of numerical calculation cost and time, making it unpracticable especially in nonlinear regime.

Mean field homogenization instead is a semi analytical model, less taxing on the CPU, faster, but it only gives approximations to the volume averages of stresses and strains, either at the macro level or in each phase.

It is important to emphasize that MFH does not solve the RVE problem in detail, and therefore does not compute the detailed micro stress and strain fields in each phase.

The simplest two MFH models are due to Voigt and Reuss. Voigt model assumes that the strain field is uniform inside the RVE. Consequently, the macro stiffness is found to be the volume average of the micro stiffnesses. In the Reuss model, the stress field is assumed to be uniform in the RVE. Therefore, the macro compliance (the inverse of the stiffness) is found to be the volume average of the micro compliances. Voigt and Reuss models generalize the simple 1D models of bars in parallel, and in series, respectively. Both models are too simplistic.

To introduce some concept, let's study simple two-phase composites made of a matrix material reinforced with a number of identical inclusions (I), having all the same material, shape and orientation. We use subscripts 0 for the matrix and 1 for the inclusions phase. The volume fractions in the two phases are such that $v_1 + v_0 = 1$.

The volume averages of the strain field over the RVE, the matrix phase and the inclusion phase are related as follows:

$$\langle \varepsilon \rangle_\omega = v_0 \langle \varepsilon \rangle_{\omega 0} + v_1 \langle \varepsilon \rangle_{\omega 1} \qquad (2.5)$$

Actually, this identity holds for any micro field (e.g., stress field). Any MFH model can be defined by so-called strain concentration tensors such that:

$$\langle \varepsilon \rangle_{\omega 1} = B^\varepsilon : \langle \varepsilon \rangle_{\omega 0} \ , \ \langle \varepsilon \rangle_{\omega 1} = A^\varepsilon : \langle \varepsilon \rangle_\omega \tag{2.6}$$

The volume average of strain over all inclusions is related to the volume average of strain over the matrix phase via the first tensor, and to the volume average of strain over the entire RVE (macro strain) with the second tensor. The two strain concentration tensors are not independent. Indeed, the second one can be computed from the first one:

$$A^\varepsilon = B^\varepsilon : [v_1 B^\varepsilon + (1 - v_1)I]^{-1} \tag{2.7}$$

For any homogenization model defined by a strain concentration tensor, the macro stiffness (sub. 0 for matrix and 1 for inclusions) is:

$$\bar{C} = [v_1 C_1 : B^\varepsilon + (1 - v_1)C_0] : [v_1 B^\varepsilon + (1 - v_1)I]^{-1} \tag{2.8}$$

Reminding Voigt and Reuss estimates, the real composite's stiffness is bounded between the two. Sophisticated MFH models or bounds closer than the Voigt and Reuss estimates all use a fundamental solution due to Eshelby (1957): inside an infinite solid body of uniform stiffness C_0, an ellipsoidal volume (I) is cut out, undergoes a stress-free eigenstrain ε^* and is then welded back into the cavity it occupied. The result is that strain inside the ellipsoidal volume (I) is uniform and related to the eigenstrain as follows

$$\varepsilon(x) = \zeta(I, C_0) : \varepsilon^* \ \forall x \in (I) \tag{2.9}$$

Where $\zeta(I, C_0)$ is Eshelby's tensor. It depends on C_0 and the shape (not the size) and orientation of (I). If C_0 is isotropic and (I) is a spheroid (that is an ellipsoid of revolution), then the stiffness dependence is through Poisson's ratio only, and the shape dependence through the aspect ratio only. Eshelby's solution plays a fundamental role in MFH, as it enables to solve the single inclusion problem.
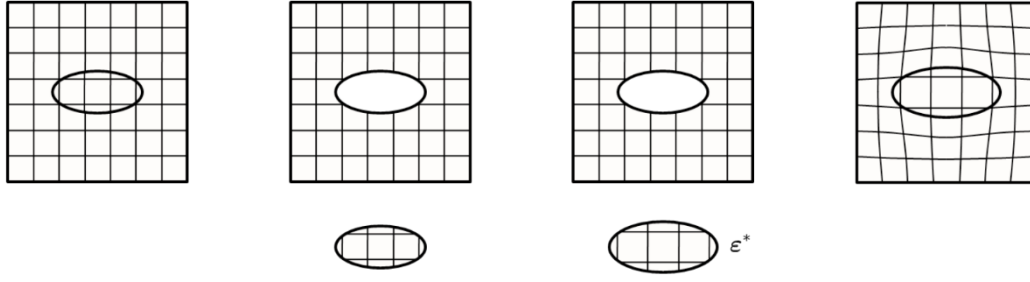
Fig. 2.4 Eshelby's problem: an ellipsoidal volume within an infinite solid body of uniform stiffness is cut out, undergoes an eigenstrain and is welded back into the body

An infinite solid body is subjected to linear displacements on its boundary corresponding to a uniform remote strain E. The body is made of a matrix phase of uniform stiffness C_0 in which is embedded a single ellipsoidal inclusion (I) of uniform stiffness C_1 as in Fig 2.5.

Using Eshelby's solution, this problem can be solved in closed form. It is found that the strain inside the inclusion (I) is uniform and related to the remote strain as follows:

$$\varepsilon(x) = H^\varepsilon(I, C_0, C_1) : E, \quad \forall x \in (I) \tag{2.10}$$

where H^ε is the single inclusion strain concentration tensor, defined as follows:

$$H^\varepsilon(I, C_0, C_1) = \left\{ I + \zeta(I, C_0) : C_0^{-1} : [C_1 - C_0] \right\}^{-1} \tag{2.11}$$

Another tensor which plays an important role is Hill's (polarization) tensor defined as:

$$P^\varepsilon(I, C_0) = \zeta(I, C_0) : C_0^{-1} \tag{2.12}$$

The solution of the single inclusion problem is the cornerstone of well-known and successful MFH models.
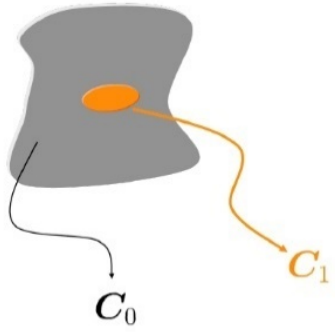
Fig. 2.5 Single inclusion embedded in an infinite body

We now go back to the case of a composite RVE made of a matrix phase of uniform stiffness reinforced C_0 with several inclusions of uniform stiffness C_1, supposed to be so far identical in terms of material, shape and orientation. Linear displacements corresponding to a remote strain E are imposed on the boundary. Unlike the single inclusion problem, this multi-inclusion problem does not have an analytical solution. Therefore, several MFH models exist based on different assumptions. They all use the solution of the single inclusion problem. We will concentrate on the Mori Tanaka model.

2.3 MORI- TANAKA MODEL

This model is derived on an approximate use of Eshelby's solution. It is found that the strain concentration tensor relating the volume average of strain over all inclusions to the mean matrix strain is given by:

$$B^{\varepsilon} = H^{\varepsilon}(I, C_0, C_1)$$ (2.13)

which is exactly the strain concentration tensor of the single inclusion problem. Each inclusion in the real RVE behaves as if it were isolated in the real matrix. The body is infinite and subjected to the average matrix strains in the real RVE as the far field (remote) strain. The M-T model is very successful in predicting the effective properties of two-phase composites. In theory, it is restricted to moderate volume fractions of inclusions (less than 25% say) but in practice it can give good predictions well beyond this range.

In fact Eshelby/Mori-Tanaka homogenization with direct mean field homogenization of an assembly of inclusions proved to provide adequate predictions [1] for the mechanical behavior of short and long wavy fibers reinforced composites for:

- Homogenized elastic properties.
- Stress-strain state of individual inclusions.
- Interface stresses and debonding defined by these stresses.
- Stress-strain curves for tension loading of random fiber reinforced composites.

2.4 FIBER ORIENTATION

In the previous treatment simple two-phase composite where all inclusions were identical and aligned were considered.

A typical injection molded part shows a particular fiber distribution in terms of orientation and length, so before homogenizing such a composite material, we first need to introduce some

tools in order to describe the fibers orientation. Actually, the following presentation is not restricted to fibers, it applies to spheroids (ellipsoids of revolution). The orientation of each individual inclusion is described by a unit vector p along its axis of revolution, which in turn can be determined in 3D with two spherical angles θ and φ (Fig 2.6).
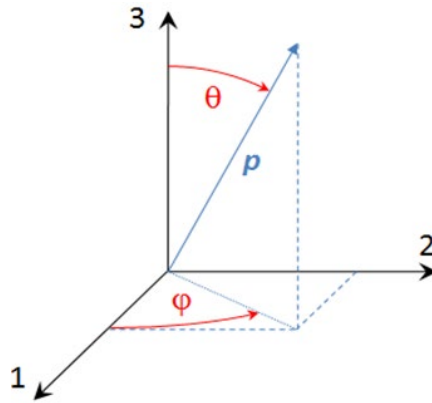

Fig. 2.6 orientation of a single inclusion

Since the axis vector p varies from one inclusion to another within the same RVE, the notion of orientation distribution function (ODF) $\psi(p)$ is introduced. By definition $\psi(p)dp$ is the probability to find fibers within the solid angles [p, p + dp].

We now consider a rather general case where a matrix material is reinforced with N families of inclusions, each one defined by the same stiffness, aspect ratio and ODF:

- Matrix phase (domain ω_0): volume fraction v_0 and stiffness C_0;
- N inclusion families (i): v_i, C_i, AR_i, ODF i(p).ω_0

Obviously, the volume fractions of matrix and inclusion families add up to 1:

$$v_0 + \sum_{i=1}^{N} v_i = 1 \qquad (2.14)$$

Each ODF obeys two conditions:

$$\psi_i(p) = \psi_i(-p), \qquad \oint \psi_i(p)dp = 1 \qquad (2.15)$$

The first equality simply means that two opposite axis vectors define indistinguishable inclusions, and the second identity is a normalization condition imposing that the sum of probabilities equals 1.

The homogenization of such composites in Digimat-MF is carried out in two steps which are illustrated in Fig. 2.7. The real composite RVE is replaced with a model RVE which is an aggregate of so-called pseudo-grains. Each pseudo-grain occupies a domain: $\omega_{i,p}$ and is a basic two-phase composite made of a matrix phase (in concentration v_0) reinforced with identical and aligned inclusions from family (i), of orientation between p and p+dp. The homogenization of the model RVE is performed in two steps. First, each pseudo-grain is homogenized using an MFH model appropriate for basic two-phase composites (e.g., Mori-Tanaka). Next, the effective response of the set of homogenized pseudo-grains is computed. In the current version of Digimat-MF, the Voigt model is used in this second step. Recall that Voigt is inappropriate for a real composite, but for an aggregate (step 2 in this procedure) our experience shows that it gives good and physically acceptable predictions, especially in the most common case of N = 1(that is one family of inclusions).
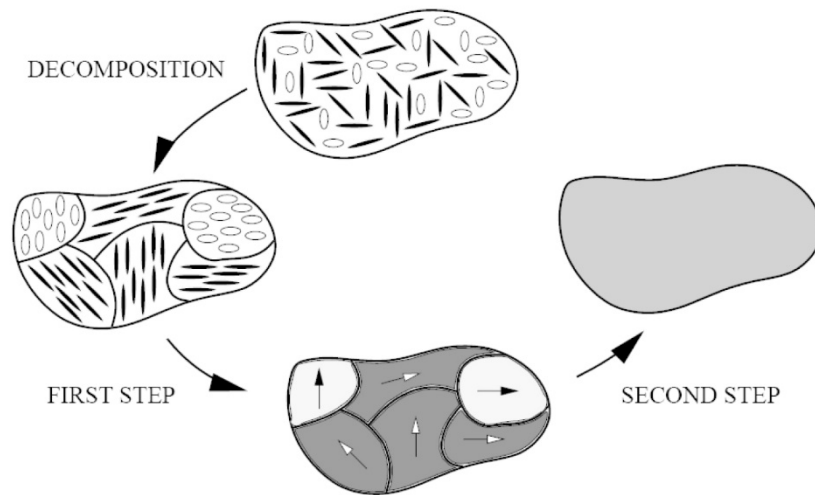

Fig. 2.7 Two-step homogenization procedure for a composite with misaligned inclusions. Top: real RVE. Middle left: decomposition into an aggregate of pseudo-grains. Bottom: homogenization of each pseudo-grain (first step). Middle right: homogenization of the aggregate of homogenized pseudo-grains (second step).

2.5 MATERIAL MODEL

Given the experimental vocation of this thesis the material it is important to define a basic material model to correlate data with laboratory analysis.

Material is referred to as elastic when its body recovers its original shape once the applied external loadings are removed, i.e., it shows a 'reversible' behavior and no residual strains remain. Both linear and nonlinear elastic behaviors are observed in laboratories and, as such, both linear and nonlinear models have been developed to represent their behavior.

Although most materials exhibit nonlinear stress/strain relationships when it comes to larger deformations, most of them also exhibit a linear regime for sufficiently small strain. Let's focus on linear elasticity.

The linear elasticity law, relating the material strains ε and stresses σ, also referred to as Hooke's law, reads

$$\sigma = C : \varepsilon \tag{2.16}$$

where C is called Hooke's operator and the: operator denotes the inner product over two indices. Hooke's operator is a fourth-order tensor which, due to symmetries, can be represented by 21 independent scalar components. As a consequence, Hooke's operator can be represented by a 6 × 6 symmetric matrix, called the stiffness matrix, yielding the matrix form of the linear elasticity law:

$$\begin{Bmatrix} \sigma_{11} \\ \sigma_{22} \\ \sigma_{33} \\ \sigma_{12} \\ \sigma_{23} \\ \sigma_{13} \end{Bmatrix} = \begin{bmatrix} C_{11}^{el} & C_{12}^{el} & C_{13}^{el} & C_{14}^{el} & C_{15}^{el} & C_{16}^{el} \\ & C_{22}^{el} & C_{23}^{el} & C_{24}^{el} & C_{25}^{el} & C_{26}^{el} \\ & & C_{33}^{el} & C_{34}^{el} & C_{35}^{el} & C_{36}^{el} \\ & & & C_{44}^{el} & C_{45}^{el} & C_{46}^{el} \\ & sym. & & & C_{55}^{el} & C_{56}^{el} \\ & & & & & C_{66}^{el} \end{bmatrix} \begin{Bmatrix} \varepsilon_{11} \\ \varepsilon_{22} \\ \varepsilon_{33} \\ 2\varepsilon_{12} \\ 2\varepsilon_{23} \\ 2\varepsilon_{13} \end{Bmatrix}. \tag{2.17}$$

This relation can be inverted to express the strain field components as a function of the stress field components. The inverse of the stiffness matrix is also known as the compliance matrix. It reads

$$
\begin{Bmatrix}
\varepsilon_{11} \\
\varepsilon_{22} \\
\varepsilon_{33} \\
2\varepsilon_{12} \\
2\varepsilon_{23} \\
2\varepsilon_{13}
\end{Bmatrix}
=
\begin{bmatrix}
S_{11}^{el} & S_{12}^{el} & S_{13}^{el} & S_{14}^{el} & S_{15}^{el} & S_{16}^{el} \\
 & S_{22}^{el} & S_{23}^{el} & S_{24}^{el} & S_{25}^{el} & S_{26}^{el} \\
 & & S_{33}^{el} & S_{34}^{el} & S_{35}^{el} & S_{36}^{el} \\
 & & & S_{44}^{el} & S_{45}^{el} & S_{46}^{el} \\
 & sym. & & & S_{55}^{el} & S_{56}^{el} \\
 & & & & & S_{66}^{el}
\end{bmatrix}
\begin{Bmatrix}
\sigma_{11} \\
\sigma_{22} \\
\sigma_{33} \\
\sigma_{12} \\
\sigma_{23} \\
\sigma_{13}
\end{Bmatrix} .
\qquad (2.18)
$$

Depending on the symmetries the material exhibits, the stiffness and compliance matrices degenerate into simpler forms, decreasing the number of independent components needed to describe the material linear elastic behavior. Shear strains are taken as the engineering shear strains, i.e., $\gamma_{ij} = 2\varepsilon_{ij}$ for $i \neq j$.

An elastic material is said to be isotropic when its material properties are independent of the considered loading direction. For such a material, the characterization of Hooke's operator requires two independent parameters only, being the isotropic Young's modulus and Poisson's ratio. These parameters are also referred to as engineering constant in software environment. For isotropic materials, the compliance matrix degenerates into

$$
S^{el} = \frac{1}{E}
\begin{bmatrix}
1 & -\nu & -\nu & 0 & 0 & 0 \\
 & 1 & -\nu & 0 & 0 & 0 \\
 & & 1 & 0 & 0 & 0 \\
 & & & 2(1+\nu) & 0 & 0 \\
 & sym. & & & 2(1+\nu) & 0 \\
 & & & & & 2(1+\nu)
\end{bmatrix} .
\qquad (2.19)
$$

Note that the shear and bulk moduli can be deduced from the Young's modulus and the Poisson's ratio and are defined as follows

$$G = \frac{E}{2(1+\nu)} \quad \text{and} \quad K = \frac{E}{3(1-2\nu)}.$$
(2.20)

The Young's modulus is a positive scalar while the Poisson's ratio ranges from −1 to 0.5, the latter bound being synonymous of incompressibility.

An elastic material is said to be orthotropic if it presents three orthogonal planes within which the material properties are independent of the loading direction. Describing such a material requires nine independent parameters to populate the stiffness (compliance) matrix.

The compliance matrix for orthotropic materials reads

$$S^{el} = \begin{bmatrix} \frac{1}{E_1} & -\frac{\nu_{21}}{E_2} & -\frac{\nu_{31}}{E_3} & 0 & 0 & 0 \\ -\frac{\nu_{12}}{E_1} & \frac{1}{E_2} & -\frac{\nu_{32}}{E_3} & 0 & 0 & 0 \\ -\frac{\nu_{13}}{E_1} & -\frac{\nu_{23}}{E_2} & \frac{1}{E_3} & 0 & 0 & 0 \\ & & & \frac{1}{G_{12}} & 0 & 0 \\ & sym. & & & \frac{1}{G_{23}} & 0 \\ & & & & & \frac{1}{G_{13}} \end{bmatrix}$$
(2.21)

For symmetry reasons, the following equivalence $\nu_{ij} E_i = \nu_{ji} E_j$ (no summation) stands. The Poisson's ratio are defined as follows: for a tension test in the 1-direction, $\nu_{12} = -\varepsilon_{22}/\varepsilon_{11}$ Similar definitions hold for the other ratios.

Positive definiteness of the compliance (stiffness) matrix requires its components to verify the following constraint equations:

- $E_1, E_2, E_3, G_{12}, G_{13}, G_{23} > 0$
- $|\nu_{12}| < (E_1/E_2)^{0.5}$
- $|\nu_{13}| < (E_1/E_3)^{0.5}$
- $|\nu_{23}| < (E_2/E_3)^{0.5}$
- $1 - \nu_{12}\nu_{21} - \nu_{23}\nu_{32} - \nu_{13}\nu_{31} - 2\nu_{21}\nu_{32}\nu_{13} > 0$

Finally an elastic material is said to be transversely isotropic if it is an orthotropic material

which present uniform material properties in one plane and different properties in the direction normal to this plane. To describe such a material, five independent parameters are required. Typical examples of such materials are carbon fibers and a unidirectional composite ply; that is a fiber-reinforced composite where all the fibers are aligned in a fixed given direction. The compliance matrix takes the following form:

$$
S^{el} = \begin{bmatrix}
\frac{1}{E_t} & -\frac{\nu_{pt}}{E_p} & -\frac{\nu_{pt}}{E_p} & 0 & 0 & 0 \\
-\frac{\nu_{tp}}{E_t} & \frac{1}{E_p} & -\frac{\nu_p}{E_p} & 0 & 0 & 0 \\
-\frac{\nu_{tp}}{E_t} & -\frac{\nu_p}{E_p} & \frac{1}{E_p} & 0 & 0 & 0 \\
& & & \frac{1}{G_{tp}} & 0 & 0 \\
& sym. & & & \frac{2(1+\nu_p)}{E_p} & 0 \\
& & & & & \frac{1}{G_{tp}}
\end{bmatrix}
\tag{2.22}
$$

with, as in the orthotropic case, the following equivalence $\nu_{pt}\,E_p = \nu_{tp}E_t$. Several constraints apply to the material parameters:

- $E_p, E_t,\ G_{tp} > 0$
- $|\nu_p| < 1$
- $|\nu_{pt}| < (E_p/E_t)^{0.5}$
- $|\nu_{tp}| < (E_t/E_p)^{0.5}$
- $1 - \nu_p{}^2 - 2\nu_{tp}\,\nu_{pt} - 2\nu_p\,\nu_{tP}\,\nu_{PT} > 0$

Some materials do not present any symmetry at all. They are then referred to as anisotropic materials. The representation of their linear elastic behavior requires the full stiffness (compliance) matrix to be defined, i.e., twenty-one independent parameters are needed to populate the stiffness (compliance) matrix.

In this thesis it's important also to model the material in the plastic part. Fig. 2.8 shows an idealized stress-strain response of a polymer under uniaxial tension in the x-direction. It can be seen that this material exhibits nonlinear behavior as soon as the stress exceeds a threshold

value called yield stress σ_Y. If the specimen is unloaded at any point along A-B, a permanent deformation ε^P, or plastic deformation, is observed. If the stress/strain response is independent of the strain rate, then this material can be modeled using elasto-plasticity theory.
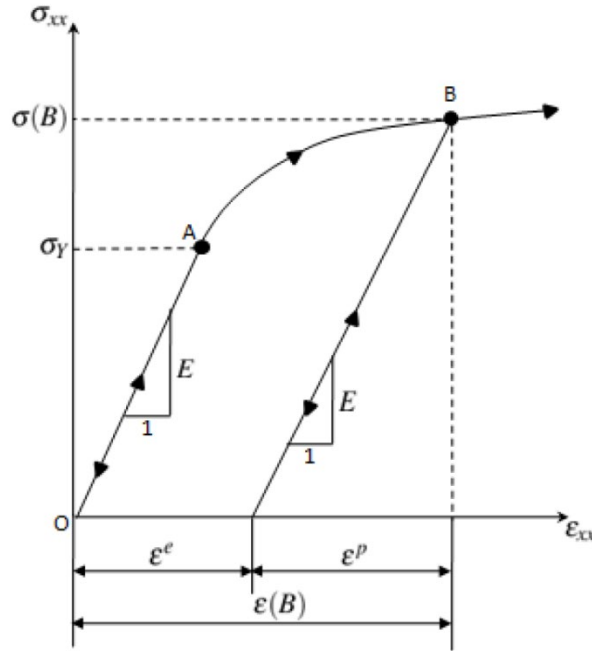

Fig. 2.8 Idealized stress/strain response of a polymer under uniaxial tension in the x–direction.

The elasto-plastic (EP) constitutive model available in Digimat is the J2-plasticity model. This model is based on the von Mises equivalent stress σ_{eq} , defined as:

$$\sigma_{eq} = \sqrt{J_2(\sigma)} = \left(\frac{3}{2}s : s\right)^{\frac{1}{2}} \tag{2.23}$$

where $J_2(\sigma)$ is the second invariant of the deviatoric stress tensor s, and is expressed as:

$$J_2(\sigma) = \left(\frac{3}{2}s : s\right) = \tag{2.24}$$

$$= \frac{3}{2}\left[\sigma - \frac{1}{3}Tr(\sigma)I\right] : \left[\sigma - \frac{1}{3}Tr(\sigma)I\right]$$

$$= \frac{1}{2}[(\sigma_{11} - \sigma_{22})^2 + (\sigma_{22} - \sigma_{33})^2 + (\sigma_{33} - \sigma_{11})^2] + 3[\sigma_{12}{}^2 + \sigma_{23}{}^2 + \sigma_{31}{}^2]$$

Remark: For uniaxial loadings, the von Mises equivalent stress is equal to the axial stress. In this constitutive model, the response is assumed to be linear elastic as long as the following condition is satisfied: $\sigma_{eq} < \sigma_Y$. Where σ_Y is a material parameter known as the initial yield stress. The total strain observed by the material is assumed to be the sum of the plastic strain and elastic strain

$$\varepsilon = \varepsilon^e + \varepsilon^p \tag{2.25}$$

The Cauchy stress and the elastic strain are then related by

$$\sigma = C : \varepsilon^e \tag{2.26}$$

where C is Hooke's operator. When σ_{eq} exceeds the initial yield stress, the response becomes nonlinear and plastic deformation appears. In this case, the Cauchy stress is given by

$$\sigma_{eq} = \sigma_Y + R(p) \tag{2.27}$$

Where $R(p)$ is the hardening stress and p the accumulated plastic strain, expressed as

$$p(t) = \int_0^t \dot{p}\,(\tau)d\tau \tag{2.28}$$

With

$$\dot{p} = \frac{2}{3}\sqrt{J_2(\dot{\varepsilon}^p)} = \sqrt{\frac{2}{3}\dot{\varepsilon}^p : \dot{\varepsilon}^p} \tag{2.29}$$

Remark: For uniaxial loadings, the accumulated plastic strain is equal to the axial plastic strain. The 2/3 factor enables to account for the transversal shrinkage due to the incompressibility of plastic strains. A yield function $f(\sigma, R)$ can be defined,

$$f(\sigma, R) = \sigma_{eq} - \sigma_Y - R(p) \leq 0 \qquad (2.30)$$

If $f(\sigma, R)$ is lower than zero, the material evolves in the elastic domain. Otherwise it is in the plastic region. The evolution of the plastic strain tensor ε^p is given by the normality rule

$$\dot{\varepsilon}^p = \dot{p} \frac{\partial f}{\partial \sigma} \qquad (2.31)$$

Three laws are available to model the isotropic hardening stress:

- Power law $\qquad\qquad\quad R(p) = kp^m$
- Exponential law $\qquad\quad R(p) = R_\infty \left[1 - \exp(-mp))\right]$
- Exponential and linear $\quad R(p) = kp + R_\infty \left[1 - \exp(-mp))\right]$

2.6 FAILURE

2.6.1 INTRODUCTION

To determine part failure some criteria named failure indicators are implemented in Digimat. Failure indicators are real valued functions comparing a given stress (strain) state combination to strengths (failure criteria) that must be assigned to a material analysis. They are written in a normalized dimensionless form in such a way that an indicator value smaller than 1 means a safe state, while failure is deemed to occur as soon as the chosen indicator reaches or exceeds 1. Failure indicators are used as a post-processing tool to identify critical or failing zones in a Digimat-CAE analysis or failure of material point in a Digimat-MF analysis.

The failure criteria presented are coming from laminated aerospace composites research in order to predict failure at the ply level, therefore, they have been historically used for composites such that as a thermoset polymer matrix (e.g., epoxy is reinforced with continuous and aligned stiff fibers, carbon fibers). Those indicators are used in a post-processing manner

at each ply level, in other words, the stress state in the ply is computed without any coupling with any damage mechanism within the ply. Those failure indicators are consequently valid when failure of the ply can be considered as being essentially of brittle nature, with negligible plastic deformation at the ply level. In Digimat, failure indicators are available for general composite systems, including ones with significant ductile matrix behavior (e.g., thermoplastic polymer matrix). The indicators can be generalized in Digimat to composite which are not laminates (no plies) and which are reinforced with misaligned short fibers thanks to the First Pseudo-Grain Failure (FPGF) method which will be treated afterwards.

Examples of available failure indicators are:

- Maximum component (stress-based or strain-based)
- Tsai-Hill 2D (stress-based or strain-based)
- Tsai-Hill 3D transversely isotropic (stress-based or strain-based)
- Tsai-Hill 3D (stress-based or strain-based)
- Azzi-Tsai-Hill 2D
- Tsai-Wu 2D (stress-based or strain-based)
- Tsai-Wu 3D transversely isotropic (stress-based or strain-based)
- Tsai-Wu 3D
- Multi-components 2D
- Hashin-Rotem 2D
- Hashin 2D
- Hashin 3D
- SIFT
- Christensen
- accumulated plastic strain
- User-defined

Unless notified otherwise, criteria are only stress based. Each of this model requires its own set of strength parameters to be defined (even though some of them are common to several models). Note also that all failure indicators can be applied at the pseudo-grain level, using

the FPGF scheme, in any axis system. In the following and unless otherwise indicated though, the strain and stress components as well as the strength parameters are defined in a local axis system such that direction 1 corresponds to the fibers axis, direction 2 is perpendicular to the fibers axis and is in the "ply plane", and direction 3 is orthogonal to that plane as in Fig. 2.9
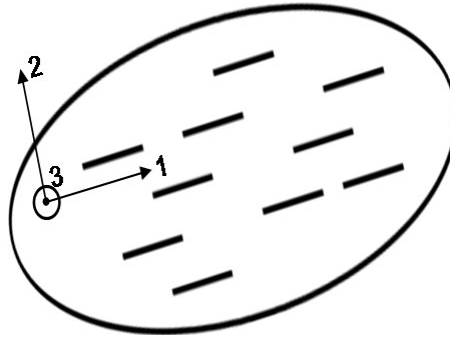
Fig. 2.9 Local axis system definition generally used when working with the FPGF scheme

Most of the failure criteria defined in Digimat are based on stress tensors, which provides an intuitive interpretation of their strength parameters from experimental stress-strain curves in typical directions. Some of these criteria were also given strain-based counterparts having a similar expression but using the strain components instead of the stress components.

In Digimat, the failure surface is described mathematically by a function defined in the stress-strain space. More precisely, failure is deemed to occur when the so-called failure function reaches 1, id est $F(\sigma, \varepsilon) \geq 1$. At each time step, Digimat outputs the value of a failure indicator f whose value is defined implicitly as the positive solution of the (non)linear equation.

$$F\left(\frac{\sigma}{f}, \frac{\varepsilon}{f}\right) = 1 \tag{2.31}$$

Hence, the failure indicator f can be interpreted as the inverse of a security factor; its definition implies that f = 1 when the current mechanical state is on the failure surface, i.e., $F(\sigma, \varepsilon) = 1$.

In the following particular examples, the failure indicator f can be computed explicitly:

- $f = F(\sigma)$ for stress or strain-component failure indicators, e.g., $F(\sigma) = max\left\{\frac{\sigma_{11}}{X_t}, 0\right\}$

- $f = \sqrt{F(\sigma)}$ Tsai-Hill failure indicators that can be written as $F(\sigma) = \sigma : \mathrm{F} : \sigma$

- f is the positive root of the second-order equation $\frac{\sigma : \mathrm{F} : \sigma}{f^2} + \frac{c : \sigma}{f^2} = 1$ for Tsai-Wu failure indicators written as $F(\sigma) = \sigma : \mathrm{F} : \sigma + c : \sigma$

Among the criterions previously mentioned we concentrate on the Tsai-Hill one which is widely used for anisotropic composite materials which have different strengths in tension and compression.

2.6.2 TSAI-HILL 3D TRANSVERSELY ISOTROPIC

This criterion assumes a material isotropy in the plane normal to axis 1 (default), 2 or 3. It has three input arguments (as it assumes identical strengths in tension and compression) and outputs one indicator. Inputs:

- Axial tensile strength, X > 0.
- In-plane tensile strength, Y > 0.
- Transverse shear strength, S > 0.

The output (failure indicator) is:

$f_A = \sqrt{\mathcal{F}_A(\boldsymbol{\sigma})}$ with

$\mathcal{F}_A(\boldsymbol{\sigma}) = \frac{\sigma_{11}^2}{X^2} - \frac{\sigma_{11}(\sigma_{22}+\sigma_{33})}{X^2} + \frac{\sigma_{22}^2+\sigma_{33}^2}{Y^2} + \left(\frac{1}{X^2} - \frac{2}{Y^2}\right)\sigma_{22}\sigma_{33} + \frac{\sigma_{12}^2+\sigma_{13}^2}{S^2} + \left(\frac{4}{Y^2} - \frac{1}{X^2}\right)\sigma_{23}^2$

when the normal to the plane of isotropy corresponds to axis 1,

$\mathcal{F}_A(\boldsymbol{\sigma}) = \frac{\sigma_{22}^2}{X^2} - \frac{\sigma_{22}(\sigma_{11}+\sigma_{33})}{X^2} + \frac{\sigma_{11}^2+\sigma_{33}^2}{Y^2} + \left(\frac{1}{X^2} - \frac{2}{Y^2}\right)\sigma_{11}\sigma_{33} + \frac{\sigma_{12}^2+\sigma_{23}^2}{S^2} + \left(\frac{4}{Y^2} - \frac{1}{X^2}\right)\sigma_{13}^2$

when the normal to the plane of isotropy corresponds to axis 2,

$\mathcal{F}_A(\boldsymbol{\sigma}) = \frac{\sigma_{33}^2}{X^2} - \frac{\sigma_{33}(\sigma_{11}+\sigma_{22})}{X^2} + \frac{\sigma_{11}^2+\sigma_{22}^2}{Y^2} + \left(\frac{1}{X^2} - \frac{2}{Y^2}\right)\sigma_{11}\sigma_{22} + \frac{\sigma_{13}^2+\sigma_{23}^2}{S^2} + \left(\frac{4}{Y^2} - \frac{1}{X^2}\right)\sigma_{12}^2$

when the normal to the plane of isotropy corresponds to axis 3

(2.32)

Failure is deemed to occur when the indicator reaches or exceeds the value of 1. The criteria is based on the components of the stress tensor, on the other hand, one can define a similar failure indicator based on the components of the strain tensor, which is also meaningful from a material point of view:

$$f_A = \sqrt{\mathcal{F}_A(\epsilon)} \text{ with}$$

$$\mathcal{F}_A(\epsilon) = \frac{\epsilon_{11}^2}{X^2} - \frac{\epsilon_{11}(\epsilon_{22}+\epsilon_{33})}{X^2} + \frac{\epsilon_{22}^2+\epsilon_{33}^2}{Y^2} + (\frac{1}{X^2} - \frac{2}{Y^2})\epsilon_{22}\epsilon_{33} + \frac{((2\epsilon_{12})^2+(2\epsilon_{13})^2)}{S^2} + (\frac{1}{Y^2} - \frac{1}{4X^2})(2\epsilon_{23})^2$$

when the normal to the plane of isotropy corresponds to axis 1,

$$\mathcal{F}_A(\epsilon) = \frac{\epsilon_{22}^2}{X^2} - \frac{\epsilon_{22}(\epsilon_{11}+\epsilon_{33})}{X^2} + \frac{\epsilon_{11}^2+\epsilon_{33}^2}{Y^2} + (\frac{1}{X^2} - \frac{2}{Y^2})\epsilon_{11}\epsilon_{33} + \frac{\epsilon_{12}^2+\epsilon_{23}^2}{S^2} + (\frac{4}{Y^2} - \frac{1}{X^2})\epsilon_{13}^2$$

when the normal to the plane of isotropy corresponds to axis 2,

$$\mathcal{F}_A(\epsilon) = \frac{\epsilon_{33}^2}{X^2} - \frac{\epsilon_{33}(\epsilon_{11}+\epsilon_{22})}{X^2} + \frac{\epsilon_{11}^2+\epsilon_{22}^2}{Y^2} + (\frac{1}{X^2} - \frac{2}{Y^2})\epsilon_{11}\epsilon_{22} + \frac{\epsilon_{13}^2+\epsilon_{23}^2}{S^2} + (\frac{4}{Y^2} - \frac{1}{X^2})\epsilon_{12}^2$$

when the normal to the plane of isotropy corresponds to axis 3

$$(2.33)$$

where X, Y and S are unitless maximum strains parameters (instead of strengths parameters).

2.6.3 FIRST PSEUDO-GRAIN FAILURE MODEL

In addition to the standard approach for which, by verifying whether the assigned failure criterion is reached, you control if the RVE breaks or not, since version 3.1, Digimat has introduced a new progressive failure mechanism that is called the First Pseudo-Grain Failure (FPGF) model. This approach is different because the stiffness of the RVE progressively decreases as when thinking to model damage. This model is developed specifically for short fibers reinforced polymer composites.

Fig. 2.10 introduces the concept of pseudo-grain for composites reinforced with short fibers inclusions in an RVE, which is the core of the FPGF model.

RVE : matrix
with fibers

homogenized RVE :
composite

decompose
fiber orientation
distribution
into
**unidirectional
pseudo grains**

RVE : ensemble
of unidirectional
pseudo grains
(up to 173)

• homogenize each
pseudo grain separately
(Mori-Tanaka)

• homogenize all
pseudo grains with each
other (Voigt)
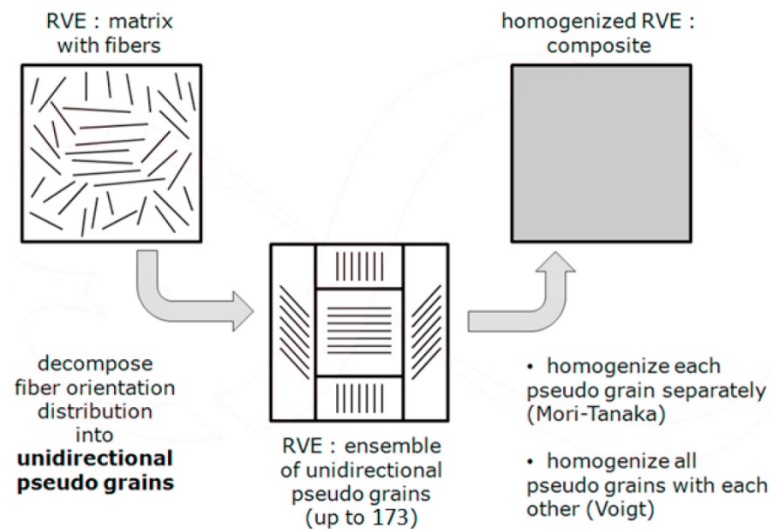
Fig. 2.10 Concept of pseudo-grain

In a real composite reinforced with fibers, the fibers are described by an orientation distribution (often represented by an orientation tensor). The basis of the FPGF model is to discretize the orientation distribution (Fig. 2.10, top left) into a limited number of perfectly aligned 'grains', called pseudo-grains (bottom of Fig 2.10). One single pseudo-grain can thus be considered as an internal, aligned composite, containing both the matrix phase and the fiber phase. Each pseudo-grain is a strictly 2-phases composite, a matrix combined with an inclusion phase. Note that pseudo-grains are a concept, a numerical artifact to perform mean-field homogenization on RVE presenting a non-fixed inclusion orientation. The pseudo-grains cannot be seen in the real composite.

As stated previously, the idea behind the FPGF model is to decompose the orientation distribution, expressed by a tensor, into a limited number of grains, each containing a perfectly aligned orientation of the inclusions.

Unless the inclusions are oriented in a random 3D state, in which case the importance of all pseudo-grains is the same, some orientation states are always more important than some others. To account for that, a weight is assigned to each pseudo-grain.

Then an external load applied to the RVE is redistributed over the pseudo-grains, so that each pseudo-grain is in a particular stress/strain state, that depends on its orientation with respect to the load. That means pseudo-grains (more or less) aligned with the direction of a strain load

get a high stress but a low strain in this direction, in comparison with pseudo-grains (more or less) transversely oriented with respect to the direction of a strain load, which then have a smaller stress in this direction but a larger strain. To compute the stress/strain state of one single pseudo-grain, a homogenization step of the matrix response with the inclusion response is first performed. Each pseudo-grain is homogenized separately using the Mori-Tanaka scheme (Level 1). Once this is done, the stress/strain state of the entire RVE (Level 2: macro composite) is computed by homogenizing the pseudo-grains with each other using an iso-strain Voigt scheme. The result is finally the stress/strain prediction of the macro composite, see Fig. 2.10, top right.

Regarding failure, the stress/strain state of each pseudo-grain is computed separately (Level 1); as a consequence, the FPGF scheme allows the user to apply any kind of failure indicator at the pseudo-grain level. Failure indicators can be applied to the phases that constitute the pseudo-grains, or simply to the composite a pseudo-grain represents, which is the way the FPGF model should generally be used. The application of failure indicators on pseudo-grains means that some pseudo-grains can fail without the necessity that the RVE totally fails. This differs significantly from the usual way of doing which consists of applying failure indicators either on the composite, or on the different phases of which it consists, for the overall RVE.

To resume the advantages of this method are:

- Increased resolution for failure detection
- Simple identification of failure criteria from experimental data:

Usually, experimental tensile tests on more or less unidirectional dumbbells are performed, which generates some strength thresholds. For most cases, the dumbbells are cut out of an injected plate either along the injection direction (for an aligned dumbbell), or transversely to the injection direction (for a transversely aligned dumbbell). The aligned dumbbell type provides composite tensile strength in the aligned direction xt1 (1 stands for aligned, see Fig. 2.11). The second type of dumbbell, in which fibers are transversely oriented with respect to the direction of the load applied, gives an estimate of the composite tensile strength in the transverse direction xt2 (2 stands for transversely aligned, see Fig. 2.11).
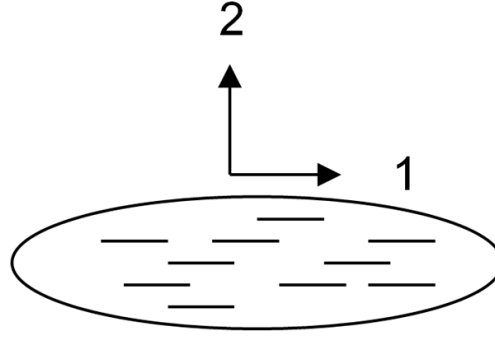
Fig. 2.11 Local axis definition in a pseudo-grain.

- An individual pseudo-grain is traduced as a unidirectional composite, which is close to the experimental set-ups which use more or less unidirectional dumbbells.

To conclude, no matter how many failure indicators are defined in the material law, there is always one FPGF output, called FPGF. That means if there are more than one failure indicator defined at the pseudo-grain level (FPGF), this output combines the global response of the RVE to all FPGF failure criteria. The output contains either the value of PGA and PGC that are used to define the failure of the RVE through the use of a critical value called:

- Critical fraction of failed pseudo-grains for PGA
- Critical mean value of failure criteria for PGC

The choice between PGA or PGC for the definition of the failure RVE is mutually exclusive. If you choose PGA (resp. PGC), the FPGF output contains the current value of PGA (resp. PGC). PGA is the weighted fraction of failed pseudo-grains, over the total weight of pseudo-grains, normalized by its critical value. The RVE is considered unsafe when the output value reaches 1. The output is therefore thresholded to 1.

$$PGA = \frac{\sum_{K=1}^{N} w_k F_k}{PGA_{critical}}$$

(2.34)

where: N is the total number of pseudo-grains, w_k is the individual pseudo-grain weight, which reflects its relative contribution to the fiber orientation distribution, F_k is a binary failure flag equal to 0 if the pseudo-grain is sane, and 1 if the pseudo-grain has failed. The total weight is set to 1.

PGC is a weighted average value of the failure criterion over the total weight of pseudo-grains (which is set to 1), normalized by its critical value. The main advantage of this output is its continuous evolution. This output has slightly different expressions following the "Threshold failure criterion output" option. If the option is deactivated (default), PGC is computed as:

$$PGC = \frac{\sum_{K=1}^{N} w_k f_k}{PGC_{critical}} \qquad (2.35)$$

where f_k is equal to the failure criterion computed for the pseudo-grain k. If the option is activated, PGC is computed as:

$$PGC = \frac{\sum_{K=1}^{N} w_k \max(f_k, 1)}{PGC_{critical}} \qquad (2.36)$$

which means that the failure criterion of a pseudo-grain is tresholded to 1.

2.7 MACROMECHANICS

Laminated fibrous composites are made by stacking of several laminae, as previously stated. In a laminated fibrous composite, the individual unidirectional laminae or plies are oriented in such a manner that the resulting structural component has the desired mechanical and/or physical characteristics in different directions. Thus, one exploits the inherent anisotropy of fibrous composites to design a composite material with appropriate properties. Once we have determined, analytically or otherwise, the characteristics of a fibrous lamina, we ignore its detailed microstructural nature and simply treat it as a homogeneous, orthotropic sheet, Fig 2.12. We then use the well-established theory of laminated plates or shells to analyze macro-mechanically such laminated composites.
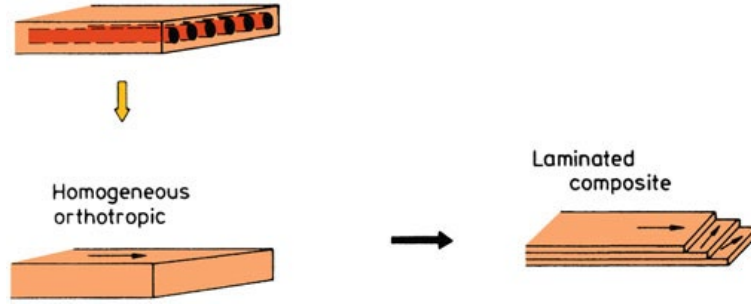
Fig. 2.12 Macro-mechanical analysis principle. A unidirectional ply is treated as a homogeneous, orthotropic material. Many such plies are stacked in an appropriate order (following laminated plate or shell theory) to make the composite.

To appreciate the significance of such a macro-mechanical analysis, we first review the basic ideas of the elastic constants of a bulk isotropic material and a lamina, a lamina as an orthotropic sheet, and finally the use of classical laminated plate theory to analyze macro-mechanically the laminated composites.

The relationship between stress and strain in linear elasticity is described by Hooke's law. Coming back to equation (2.16) it can be rewritten in indicial or tensorial notation like this:

$$\sigma_{ij} = C_{ijkl}\, \varepsilon_{kl} \qquad (2.37)$$

where C_{ijkl} are the elastic constants or stiffnesses. Equation (2.37), when written out in an expanded form, will have 81 elastic constants. It is a general practice to use a contracted matrix notation for writing stresses, strains, and elastic constants, following this scheme:

_ij_ or _kl_	11	22	33	23	31	12
_m_ or _n_	1	2	3	4	5	6

Then Eq. (2.37) can be rewritten as

$$\sigma_m = C_{mn}\, \varepsilon_n \qquad (2.38)$$

It can be shown from symmetry considerations that $C_{mn} = C_{nm}$. Conversely, we can write

$$\varepsilon_m = S_{mn}\sigma_{mn} \qquad (2.39)$$

where S_{mn}, the compliance matrix, is the inverse of the stiffness matrix C_{mn}. The expanded

matricial version of these equations are just the previously written Eq. (2.17) and (2.18)

We can make a laminated composite by stacking a sufficiently large number of thin laminae

in a specific order of fiber orientation, cured, and bonded. A lamina can be considered to be

in a state of generalized plane stress, a condition that force the through-thickness stress

components to zero (hence, the term plane stress), Thus $\sigma_3 = \sigma_4 = \sigma_5 = 0$ and Eqs. (2.17)

and (2.18) are reduced. In addition we can consider it as an orthotropic material; that is, it has

three mutually perpendicular axes of symmetry. Hooke's law for this kind of material was

reported in Eq (2.21). So finally we get to

$$
\begin{bmatrix} \varepsilon_1 \\ \varepsilon_2 \\ \varepsilon_6 \end{bmatrix} = \begin{bmatrix} S_{11} & S_{12} & 0 \\ S_{12} & S_{22} & 0 \\ 0 & 0 & S_{66} \end{bmatrix} \begin{bmatrix} \sigma_1 \\ \sigma_2 \\ \sigma_6 \end{bmatrix} \tag{2.40}
$$

And conversely,

$$
\begin{bmatrix} \sigma_1 \\ \sigma_2 \\ \sigma_6 \end{bmatrix} = \begin{bmatrix} Q_{11} & Q_{12} & 0 \\ Q_{12} & Q_{22} & 0 \\ 0 & 0 & Q_{66} \end{bmatrix} \begin{bmatrix} \varepsilon_1 \\ \varepsilon_2 \\ \varepsilon_6 \end{bmatrix} \tag{2.41}
$$

Where the notation Q_{ij} (reduced stifnesses) rather than C_{ij} is used for thin material. It is

worth emphasizing that Eqs. (2.40) and (2.41), showing terms with indices 16 and 26 to be

zero, represent a special case of orthotropy when the principal material axes of symmetry the

fiber direction and the direction transverse to it coincide with the geometric directions. If this

is not so, that is, if the material symmetry axes and the geometric axes do not coincide, then

we have the more general case of orthotropy:

$$
\begin{bmatrix} \sigma_x \\ \sigma_y \\ \sigma_s \end{bmatrix} = \begin{bmatrix} \bar{Q}_{11} & \bar{Q}_{12} & \bar{Q}_{16} \\ \bar{Q}_{12} & \bar{Q}_{22} & \bar{Q}_{26} \\ \bar{Q}_{16} & \bar{Q}_{26} & \bar{Q}_{66} \end{bmatrix} \begin{bmatrix} \varepsilon_x \\ \varepsilon_y \\ \varepsilon_s \end{bmatrix} \tag{2.42}
$$

where the $\bar{Q}_{ij}$ matrix is called the transformed reduced stiffness matrix because it is obtained by transformation from Q_{ij} (specially orthotropic) .The subscripts x and y represent the geometric axes x and y, and the subscript s refers to in plane shear components.

Fig 2.13 shows the situation for a unidirectional composite lamina where the two sets of axes do not coincide.
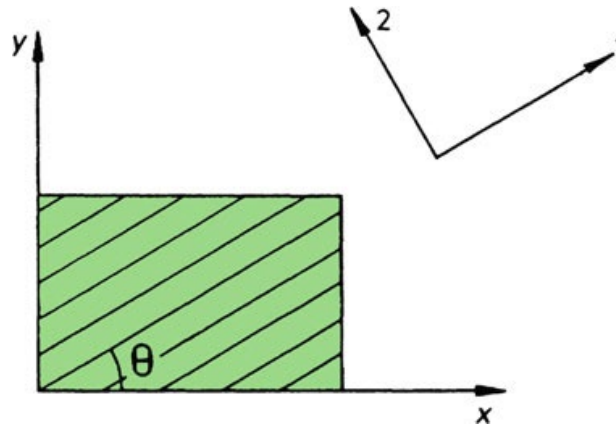
Fig. 2.13 An off axis unidirectional lamina

The properties in the 1–2 or material system of axes are known, and we wish to determine them in the x-y or geometric system or vice versa. In order to carry out the transformation of axes, we need to exploit the concept of direction cosines, a_{ij}. Table 2.14 gives the direction cosines for the transformation of axes shown in Fig. 2.13. Angle θ is positive when the x–y-axes are rotated counterclockwise with respect to the 1–2 axes. This transformation of axes is carried out easily in the matrix form.

Direction	x	y	
1	$a_{11} = m$	$a_{12} = n$	$m = \cos \theta$
2	$a_{21} = -n$	$a_{22} = m$	$m = \sin \theta$

Tab. 2.14 Direction cosines

For stresses, we can write

$$\begin{bmatrix} \sigma_1 \\ \sigma_2 \\ \sigma_6 \end{bmatrix} = [T]_\sigma \begin{bmatrix} \sigma_x \\ \sigma_y \\ \sigma_s \end{bmatrix} \qquad (2.43)$$

for strains

$$\begin{bmatrix} \varepsilon_1 \\ \varepsilon_2 \\ \varepsilon_6 \end{bmatrix} = [T]_\varepsilon \begin{bmatrix} \varepsilon_x \\ \varepsilon_y \\ \varepsilon_s \end{bmatrix} \qquad (2.44)$$

where $[T]_\sigma$ and $[T]_\varepsilon$ are the transformation matrices for stress and strain transformations, respectively, and are given by

$$[T]_\sigma = \begin{bmatrix} m^2 & n^2 & 2mn \\ n^2 & m^2 & -2mn \\ -mn & mn & m^2 - n^2 \end{bmatrix} \qquad (2.45)$$

$$[T]_\varepsilon = \begin{bmatrix} m^2 & n^2 & mn \\ n^2 & m^2 & -mn \\ -2mn & 2mn & m^2 - n^2 \end{bmatrix} \qquad (2.46)$$

where $m = cos\theta$ and $n = sin\theta$ .This method of using different transformation matrices for stress and stain transformations avoids the need of putting the factor 12 before the engineering shear strains to convert them to tensorial strain components suitable for transformation. Multiplying both sides of Eq. (2.43) by $[T]_\sigma^{-1}$ and remembering that $[T]_\sigma[T]_\sigma^{-1} = [I]$, we get

$$\begin{bmatrix} \sigma_x \\ \sigma_y \\ \sigma_s \end{bmatrix} = [T]_\sigma^{-1} \begin{bmatrix} \sigma_1 \\ \sigma_2 \\ \sigma_6 \end{bmatrix} \qquad (2.47)$$

From $[T]_\sigma$ you can get $[T]_\sigma^{-1}$ by simply substituting -θ for θ:

$$[T]^{-1}_{\sigma} = \begin{bmatrix} m^2 & n^2 & -2mn \\ n^2 & m^2 & 2mn \\ mn & -mn & m^2 - n^2 \end{bmatrix}$$

(2.48)

Substituting Eq. (2.41) in Eq. (2.47), we obtain

$$\begin{bmatrix} \sigma_x \\ \sigma_y \\ \sigma_s \end{bmatrix} = [T]_{\sigma}^{-1}[Q] \begin{bmatrix} \varepsilon_1 \\ \varepsilon_2 \\ \varepsilon_6 \end{bmatrix}$$

(2.49)

If we now substitute Eq. (2.44) in Eq. (2.49), we arrive at

$$\begin{bmatrix} \sigma_x \\ \sigma_y \\ \sigma_s \end{bmatrix} = [T]_{\sigma}^{-1}[Q][T]_{\varepsilon} \begin{bmatrix} \varepsilon_x \\ \varepsilon_y \\ \varepsilon_s \end{bmatrix} = [\bar{Q}] \begin{bmatrix} \varepsilon_x \\ \varepsilon_y \\ \varepsilon_s \end{bmatrix}$$

(2.50)

Where $[\bar{Q}]$ is the stiffness matrix for a generally orthotropic lamina as it was shown in Eq. (2.42). A corresponding stress–strain relationship in terms of compliances of a generally orthotropic lamina can be obtained.

Now that we have discussed the analysis of an individual lamina, we proceed to discuss the macroscopic analysis of laminated composites. Each ply is treated as a homogeneous, orthotropic sheet, and the laminated composite is analyzed using the classical theory of laminated plates. A hypothetical stacking sequence could be generated like in Fig. 2.15
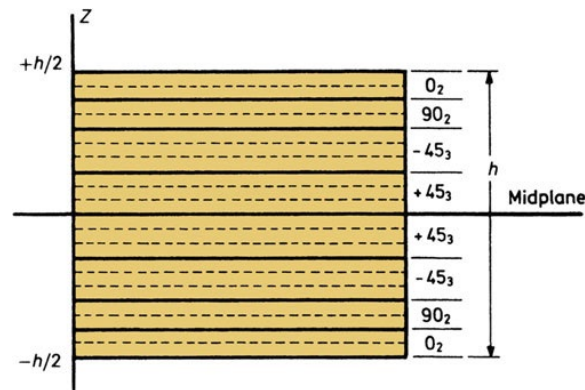
Fig. 2.15 A laminate composite with predefined stacking sequence

starting from the bottom of the laminate, that is, at z = − h/2, we have two plies at 0° orientation; then two plies at 90° orientation; followed by a group of three plies at −45° orientation; and lastly, a group of three plies at +45° orientation. The laminate is symmetric with respect to the midplane (z = 0); that is, the top half of the laminate is a mirror image of the bottom half.

To study the macro-mechanical behavior, we need some basic assumptions:

- The laminate thickness is small compared to its lateral dimensions
- It exists a perfect bond between any two laminae, so they cannot slide on each other
- A line originally straight and perpendicular to the laminate midplane remains so after deformation
- The Kirchhoff assumption, which states that in plane displacements are linear functions of the thickness, and therefore the interlaminar shear strains ε_{xz} and ε_{yz}, are negligible.

With these assumptions, we can reduce the laminate behavior to a two-dimensional analysis of the laminate midplane. We have the following strain–displacement relationships:

$$\varepsilon_x = \frac{\partial u}{\partial x} \qquad \varepsilon_{xy} = \frac{\partial u}{\partial y} + \frac{\partial v}{\partial x}$$

$$\varepsilon_y = \frac{\partial v}{\partial y} \qquad \varepsilon_{xz} = \frac{\partial u}{\partial z} + \frac{\partial w}{\partial x}$$

$$\varepsilon_x = \frac{\partial w}{\partial z} \qquad \varepsilon_{yz} = \frac{\partial v}{\partial z} + \frac{\partial w}{\partial y} \qquad (2.51)$$

Here, u, v, w are the displacements in the x-, y-, and z-directions, respectively. For i ≠ j, the ε_{ij} represent engineering shear strain components equal to twice the tensorial shear components. As per Kirchhoff's assumption, the in-plane displacements are linear functions of the thickness coordinate, z. Then

$$u = u_0(x, y) + zF_1(x, y) \qquad v = v_0(x, y) + zF_2(x, y) \qquad (2.52)$$

Where u_0 and v_0 are displacements of the midplane and F_1 and F_2 are functions to be determined, see below. It also follows from Kirchhoff's assumptions that interlaminar shear strains ε_{xz} and ε_{yz} are zero. Therefore, from Eqs. (2.51) and (2.52) we obtain

$$\varepsilon_{xz} = F_1(x,y) + \frac{\partial w}{\partial x} = 0$$

$$\varepsilon_{yz} = F_2(x,y) + \frac{\partial w}{\partial y} = 0 \tag{2.53}$$

It therefore follows that

$$F_1(x,y) = -\frac{\partial w}{\partial x} \quad and \quad F_2(x,y) = -\frac{\partial w}{\partial y} \tag{2.54}$$

The normal strain in the thickness direction ε_z is negligible so $w = w(x,y)$. That is, the vertical displacement of any point does not change in the thickness direction.

Substituting Eq. (2.54) into Eq. (2.52), we obtain

$$\varepsilon_x = \frac{\partial u}{\partial x} = \frac{\partial u_0}{\partial x} - z\frac{\partial^2 w}{\partial x^2} = \varepsilon_x{}^0 + zK_x \tag{2.55}$$

$$\varepsilon_y = \frac{\partial v}{\partial y} = \frac{\partial v_0}{\partial y} - z\frac{\partial^2 w}{\partial y^2} = \varepsilon_y{}^0 + zK_y \tag{2.56}$$

$$\varepsilon_{xy} = \frac{\partial u}{\partial y} + \frac{\partial v}{\partial x} = \frac{\partial u_0}{\partial y} + \frac{\partial v_0}{\partial x} - 2z\frac{\partial^2 w}{\partial x \partial y} = \varepsilon_{xy}{}^0 + zK_{xy} \tag{2.57}$$

Renaming ε_{xy} by ε_s and K_{xy} by K_s , we can rewrite the expression for ε_{xy} as

$$\varepsilon_s = \varepsilon_s{}^0 + zK_s \tag{2.58}$$

75

Here $\varepsilon_x{}^0$, $\varepsilon_y{}^0$ and $\varepsilon_s{}^0$ are the midplane strains, while K_x K_y and K_s are the plate curvatures. We can represent these quantities in a compact form as follows:

$$\begin{bmatrix} \varepsilon_x{}^0 \\ \varepsilon_y{}^0 \\ \varepsilon_s{}^0 \end{bmatrix} = \begin{bmatrix} \dfrac{\partial u_0}{\partial x} \\ \dfrac{\partial v_0}{\partial y} \\ \dfrac{\partial u_0}{\partial y} + \dfrac{\partial v_0}{\partial x} \end{bmatrix} \tag{2.59}$$

and

$$\begin{bmatrix} K_x \\ K_y \\ K_s \end{bmatrix} = - \begin{bmatrix} \dfrac{\partial^2 w}{\partial x^2} \\ \dfrac{\partial^2 w}{\partial y^2} \\ \dfrac{2\partial^2 w}{\partial x \partial y} \end{bmatrix} \tag{2.60}$$

Equations (2.55,2.56,2.57,2.58) can be put into the following form:

$$\begin{bmatrix} \varepsilon_x \\ \varepsilon_y \\ \varepsilon_s \end{bmatrix} = \begin{bmatrix} \varepsilon_x{}^0 \\ \varepsilon_y{}^0 \\ \varepsilon_s{}^0 \end{bmatrix} + z \begin{bmatrix} K_x \\ K_y \\ K_s \end{bmatrix} \tag{2.61}$$

With these bases, let's consider a composite made of n stacked layers or plies; see Fig. 2.16a. Let h be the thickness of the laminated composite. Then we can write, for the kth layer, the following constitutive relationship:

$$[\sigma_k] = [\bar{Q}]_k\, [\varepsilon_k] \tag{2.62}$$
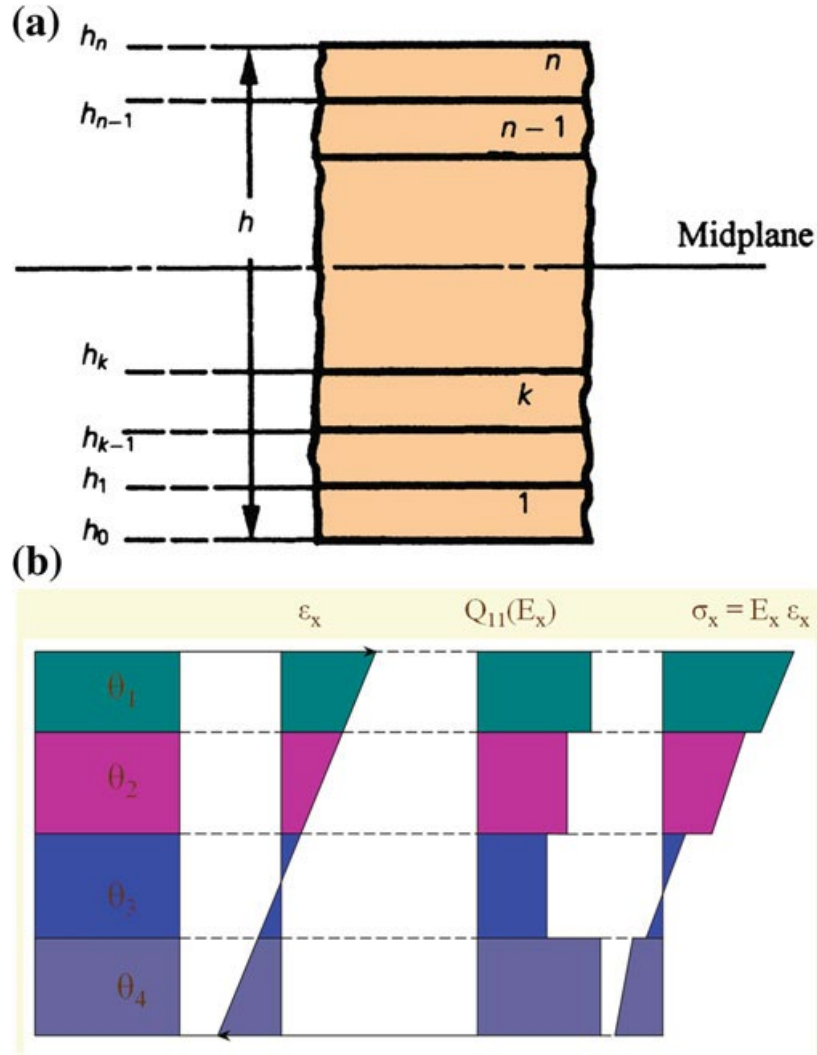
Fig. 2.16 a) laminated composite made up of n stacked plies. b) Variation of strain and stress through the thickness in a 4-ply laminated composite

From the theory of laminated plates, we have strain–displacement relationships given by Eq. (2.61). Substituting these relationships in Eq. (2.62), for the kth ply we get

$$[\sigma_k] = [\bar{Q}]_k \, [\varepsilon^0] + z[\bar{Q}]_k \, [K] \tag{2.63}$$

It is worth emphasizing that strains are continuous through the thickness while the stresses are not. This is in line with previous discussion including that stiffness of each ply is different being a function of the fiber orientation. This is shown schematically in a four-ply laminated

composite in Fig. 2.16b. Because the stresses in a laminated composite vary from ply to ply, it is convenient to define laminate force and moment resultants as shown in Fig. 2.17. These resultants of stresses and moments acting on a laminate cross section, defined as follows, provide us with a statically equivalent system of forces and moments acting at the midplane of the laminated composite.
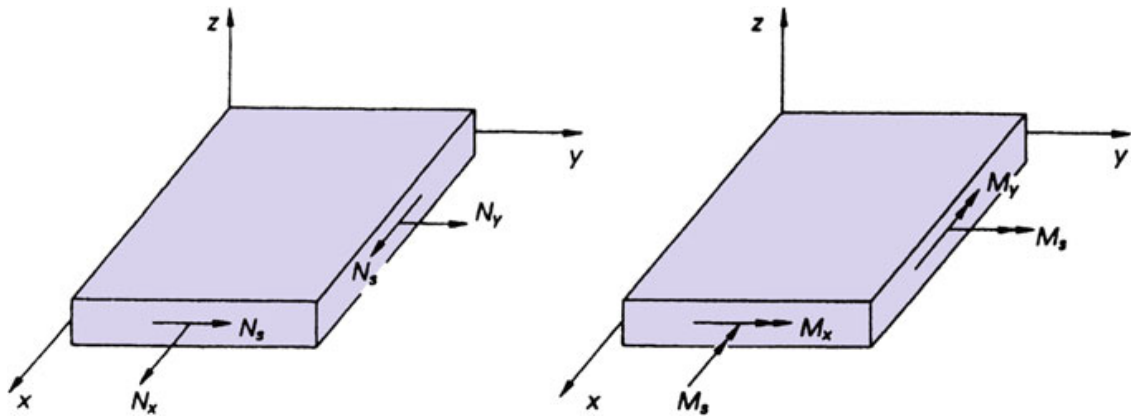
Fig. 2.17 Force (N) and moment (M) resultants in a laminated composite

In the most general case, such a composite will have $\sigma_x, \sigma_y, \sigma_z, \sigma_{xy}, \sigma_{yz}$ and σ_{zx} as the six stress components. Our laminated composite, however, is in a state of plane stress. Thus, we shall have only three stress components: σ_x, σ_y, and σ_{xy} (= σ_s). Accordingly, we define the three corresponding stress resultants as

$$N_x = \int_{-h/2}^{h/2} \sigma_x dz$$

$$N_y = \int_{-h/2}^{h/2} \sigma_y dz$$

$$N_s = \int_{-h/2}^{h/2} \sigma_x dz$$

<div align="right">(2.64)</div>

These stress resultants have the dimensions of force per unit length acting at the midplane and are positive in the same direction as the corresponding stress components. Additionally, moments are applied at the midplane, which are equivalent to the moments produced by the stresses with respect to the midplane. They are defined as:

$$M_x = \int_{-h/2}^{h/2} \sigma_x z dz$$

$$M_y = \int_{-h/2}^{h/2} \sigma_y z dz$$

$$M_{xy} = M_s = \int_{-h/2}^{h/2} \sigma_s z dz$$

<div align="right">(2.65)</div>

This system of three stress resultants (Eq. 2.64) and three moment resultants (Eq. 2.65) is statically equivalent to actual stress distribution through the thickness of the composite laminate. From Eqs. (2.62) and (2.53), we can write for the stress resultants a summation over the n plies:

$$
\begin{bmatrix} N_x \\ N_y \\ N_s \end{bmatrix} = \sum_{k=1}^{n} \int_{h_{k-1}}^{h_k} \begin{bmatrix} \sigma_x \\ \sigma_y \\ \sigma_s \end{bmatrix} dz
$$

$$
= \sum_{k=1}^{n} \left(\int_{h_{k-1}}^{h_k} \begin{bmatrix} \bar{Q}_{11} & \bar{Q}_{12} & \bar{Q}_{16} \\ \bar{Q}_{12} & \bar{Q}_{22} & \bar{Q}_{26} \\ \bar{Q}_{16} & \bar{Q}_{26} & \bar{Q}_{66} \end{bmatrix} \begin{bmatrix} {\varepsilon_x}^0 \\ {\varepsilon_y}^0 \\ {\varepsilon_s}^0 \end{bmatrix} dz \right.
$$

$$
\left. + \int_{h_{k-1}}^{h_k} \begin{bmatrix} \bar{Q}_{11} & \bar{Q}_{12} & \bar{Q}_{16} \\ \bar{Q}_{12} & \bar{Q}_{22} & \bar{Q}_{26} \\ \bar{Q}_{16} & \bar{Q}_{26} & \bar{Q}_{66} \end{bmatrix} \begin{bmatrix} K_x \\ K_y \\ K_s \end{bmatrix} z dz \right)
$$

(2.66)

Note that $[\varepsilon^0]$ and $[K]$ are not functions of z and in a given ply $[\bar{Q}]$ is not a function of z. Thus, we can simplify the preceding expression to

$$
\begin{bmatrix} N_x \\ N_y \\ N_s \end{bmatrix} = \sum_{k=1}^{n} \left(\begin{bmatrix} \bar{Q}_{11} & \bar{Q}_{12} & \bar{Q}_{16} \\ \bar{Q}_{12} & \bar{Q}_{22} & \bar{Q}_{26} \\ \bar{Q}_{16} & \bar{Q}_{26} & \bar{Q}_{66} \end{bmatrix} \begin{bmatrix} {\varepsilon_x}^0 \\ {\varepsilon_y}^0 \\ {\varepsilon_s}^0 \end{bmatrix} \int_{h_{k-1}}^{h_k} dz + \right.
$$

$$
\left. \begin{bmatrix} \bar{Q}_{11} & \bar{Q}_{12} & \bar{Q}_{16} \\ \bar{Q}_{12} & \bar{Q}_{22} & \bar{Q}_{26} \\ \bar{Q}_{16} & \bar{Q}_{26} & \bar{Q}_{66} \end{bmatrix} \begin{bmatrix} K_x \\ K_y \\ K_s \end{bmatrix} \int_{h_{k-1}}^{h_k} z \, dz \right)
$$

(2.67)

We can rewrite it as

$$
\begin{bmatrix} N_x \\ N_y \\ N_s \end{bmatrix} = \begin{bmatrix} A_{11} & A_{12} & A_{16} \\ A_{12} & A_{22} & A_{26} \\ A_{16} & A_{26} & A_{66} \end{bmatrix} \begin{bmatrix} {\varepsilon_x}^0 \\ {\varepsilon_y}^0 \\ {\varepsilon_s}^0 \end{bmatrix} + \begin{bmatrix} B_{11} & B_{12} & B_{16} \\ B_{12} & B_{22} & B_{26} \\ B_{16} & B_{26} & B_{66} \end{bmatrix} \begin{bmatrix} K_x \\ K_y \\ K_s \end{bmatrix}
$$

(2.68)

or

$$[N] = [A]\,[\varepsilon^0] + [B]\,[K] \qquad\qquad (2.69)$$

where

$$A_{ij} = \sum_{k=1}^{n} (\bar{Q}_{ij})_k\,(h_k - h_{k-1})$$

$$(2.70)$$

and

$$B_{ij} = \frac{1}{2} \sum_{k=1}^{n} (\bar{Q}_{ij})_k\,(h_k{}^2 - h_{k-1}{}^2)$$

$$(2.71)$$

Similarly, we can write for the moment resultants

$$\begin{bmatrix} M_x \\ M_y \\ M_s \end{bmatrix} = \begin{bmatrix} B_{11} & B_{12} & B_{16} \\ B_{12} & B_{22} & B_{26} \\ B_{16} & B_{26} & B_{66} \end{bmatrix} \begin{bmatrix} \varepsilon_x{}^0 \\ \varepsilon_y{}^0 \\ \varepsilon_s{}^0 \end{bmatrix} + \begin{bmatrix} D_{11} & D_{12} & D_{16} \\ D_{12} & D_{22} & D_{26} \\ D_{16} & D_{26} & D_{66} \end{bmatrix} \begin{bmatrix} K_x \\ K_y \\ K_s \end{bmatrix}$$

$$(2.72)$$

or in shorter form:

$$[M] = [B]\,[\varepsilon^0] + [D]\,[K] \qquad\qquad (2.73)$$

where

$$D_{ij} = \frac{1}{3} \sum_{k=1}^{n} (\bar{Q}_{ij})_k\,(h_k{}^3 - h_{k-1}{}^3)$$

$$(2.74)$$

and the B_{ij} are given by Eq. (2.71). We may combine Eqs. (2.69) and (2.73) and write the constitutive equations for the laminate composite in a more compact form. Thus,

$$\begin{bmatrix} N \\ \overline{M} \end{bmatrix} = \begin{bmatrix} A & B \\ B & D \end{bmatrix} \begin{bmatrix} \varepsilon^0 \\ \overline{K} \end{bmatrix}$$

(2.75)

Note that the stress resultant is a function of the midplane tensile strains ($\varepsilon_x{}^0$ and $\varepsilon_y{}^0$), the midplane shear strain $\varepsilon_s{}^0$, the bending curvatures (K_x and K_y), and the twisting (K_s). This is a much more complex situation than that observed in a homogeneous plate where tensile loads result in only tensile strains. In a laminated plate, we have coupling between tensile and shear, tensile and bending, and tensile and twisting effects. Specifically, the terms A_{16} and A_{26} bring in the tension–shear coupling, while the terms B_{16} and B_{26} represent the tension–twisting coupling. The D_{16} and D_{26} terms in a similar expression for M_x represent flexure–twisting coupling.

Chapter 3

FINITE ELEMENT METHOD

3.1 BASICS

The finite element method (FEM) is a discretization procedure that using mathematical models and techniques of numerical calculus makes possible the solution of engineering and physical problems that would be problematic to solve analytically.

To solve this type of problems, generally, (partial) differential equations have to be solved resulting in a system of algebraic equations. With FEM formulation the problem is subdivided into smaller sub-structures called "finite elements". The finite element can be modelled with simple equations assembled into a larger system that models the entire problem. The solution that can be obtained, even if it is not completely exact, can give useful indications for the analysis of problems whose analytical solution would be not always possible or very expensive.

The FEM is used to study a wide class of problems ranging from structural analysis, fluid dynamics, heat flow to electromagnetism.

Concerning the mechanics of the structure, the possibilities of FEM extends to non-linear, plasticity, visco-plasticity, static and dynamic impact problem.

In presenting the basics of the method the focus is on the elastic linear static problems, which are addressed with the goal of writing the stiffness relation (eq 3.1) for the basic elements.

$$\{F\} = [K]\{f\} \tag{3.1}$$

From this relation the target is to write the relations to describe the displacements field and then the stress and strain field for all the elements, starting from the nodal displacements. To get these results a procedure based on 7 steps is used for all the types of elements used in the finite element analysis. The 7 steps are:

1. Element identification and description.
2. Choice of a proper approximation function to describe approximately the displacements field of each point of the element.
3. Relate displacements field with nodal displacements of it through the so called "shape functions".
4. Write relations between displacements and strains fields for each element point.
5. Determine stresses field as a function of the strain one computed before.
6. To get the relation between the nodal loads and the displacements field: formulation of the stiffness matrix of the element.
7. Relate element stresses field with nodal displacements.

STEP 1

Firstly, characteristic points of the element, called nodes, are chosen and numbered. For each of them, displacements affected by the problem are identified (displacements field). To describe nodal forces and displacements, a local element reference frame to simplify the computations will be necessary.

Each element point displacements will be described through the vector $\{\delta\}$ and, in particular, for each node, a displacement vector $\{f_i\}$ and a force vector $\{F_i\}$ will be defined. Therefore, for n-nodes element, following relations will be obtained:

$$\{f\} = \{\{f_1\}, \{f_2\}, \{f_3\}, \ldots \ldots \{f_n\}\}^T \tag{3.2}$$

$$\{F\} = \{\{F_1\}, \{F_2\}, \{F_3\}, \ldots \ldots \{F_n\}\}^T \tag{3.3}$$

STEP 2

A polynomial function, that can univocally describe displacements field for each point of the

element is chosen. This function does not reflect precisely the problem, it's an approximation that must give interesting engineering results.

The function must fulfill four requirements, to have a monotonic convergence of the solution to the exact results:

1. Describe all the rigid motions of the element without the rise of any stress state on the element.

2. Describe all the constant strain states on the element (the continuity of the strain field is not required).

3. Ensure the continuity of the displacements field between contiguous elements on the structure. In some cases, partial exception to this requirement can be accepted. This requirement has to be strictly verified if different types of elements are connected together.

4. Be free of singularity points: the continuity of the displacements field inside the elements has to be ensured.

Defining as δ_i the i-th displacement, for each element point:

$$\delta_1(x_k) = \alpha_1 \Phi_{11}(x_k) + \alpha_2 \Phi_{12}(x_k) + \cdots + \alpha_n \Phi_{1n}(x_k)$$
$$\delta_2(x_k) = \alpha_1 \Phi_{21}(x_k) + \alpha_1 \Phi_{22}(x_k) + \cdots + \alpha_n \Phi_{2n}(x_k)$$
$$\ldots\ldots\ldots\ldots$$
$$\delta_i(x_k) = \alpha_1 \Phi_{i1}(x_k) + \alpha_1 \Phi_{i2}(x_k) + \cdots + \alpha_n \Phi_{in}(x_k)$$

$$(3.4)$$

where x_k are local reference frame coordinates of the considered point, Φ_{ij} are the chosen polynomial functions computed in that point and α_j are the coefficients of the linear combination of the function. The number of α_j has to be at least equal to the number of degrees of freedom of the element. Using the matrix form:

$$\{\delta(x_k)\} = [\phi(x_k)] \cdot \{\alpha\} \qquad (3.5)$$

Where $[\phi(x_k)]$ is the matrix with all the functions Φ_{ij} and $\{\alpha\}$ is the vector with all the α_j coefficients.

STEP 3

The chosen $\{(xk)\}$ should be such that it corresponds to nodal displacements, $\{f\}$, if it is calculated in the nodes' coordinates. This condition lets also to compute α_j terms. Therefore:

$$\{f\} = [\phi(x_k)] \cdot \{\alpha\} = [A] \cdot \{\alpha\} \tag{3.6}$$

where [A] is the matrix of Φ_{ij} functions computed at elements nodes; it is a square matrix because the number of α_j coefficients are equal to the components of vector $\{f\}$. The matrix $[A]$ can be inverted:

$$\{\alpha\} = [A]^{-1}\{f\} \tag{3.7}$$

consequently, all the values of $\{\alpha_j\}$ can be known and therefore, the displacements field is defined. The displacement fields can be written as a function of the nodal displacements

$$\{\delta(x_k)\} = [\phi(x_k)] \cdot [A]^{-1}\{f\} = [N(x_k)] \cdot \{f\} \tag{3.8}$$

where

$$[N(x_k)] = [\phi(x_k)] \cdot [A]^{-1} \tag{3.9}$$

is defined as the matrix of the shape functions, e.g. those functions that, multiplied by nodal displacements, describe the displacement field.

If $\phi(x_k) = N(x_k)$, that is the shape functions are used for the $\phi(x_k)$ functions the values of the α_j coefficients are equal to the nodal displacements. Usually, the polynomials used for the interpolating functions of the nodal displacements are called of the Lagrangian type. Polynomials of Hermitian type are used for beam and the shell elements.

STEP 4

In each point of the element the material is subjected to strain due to the applied

displacements field. The strain field is defined with the vector $\{\varepsilon(x)\}$. The components of this vector are joined to the displacements field (vector $\{(xk)\}$) using differential operations.

In rods, plane elements, solid elements, the normal strain $\{\varepsilon\}$ and the shear strain $\{\gamma\}$ are used to describe the strain of the material:

$$\{\varepsilon(x_k)\} = \frac{d\{\delta(x_k)\}}{d(x_k)} \tag{3.10}$$

In beams and shells (elements with strain outside the plane), the curvature is the best choice to model the strain of the material. The curvature is the second-degree differential operation of the function that describes the displacements field (deflection):

$$\{\varepsilon(x_k)\} = \frac{d^2\{\delta(x_k)\}}{d(x_k)^2} \tag{3.11}$$

The relation between the strain and the displacement is therefore a differential equation. In equation (3.9) some factors are constant, so it can be rewritten as

$$\{\varepsilon(x_k)\} = [diff\ \phi(x_k)]\cdot[A]^{-1}\cdot\{f\} = [C][A]^{-1}\cdot\{f\} = [B]\cdot\{f\} \tag{3.12}$$

where clearly the collection of terms was made like this : $[diff\phi(x_k)][A]^{-1} = [C(x_k)]$ and $[C][A]^{-1} = [B]$. In the matrix $[C(x_k)]$ there are the resulting functions of the differential operations on the approximating functions of the displacements field.

Moreover, recalling that the displacements field can be also described using the shape functions $[N(x_k)]$, the matrix $[B]$ can also be expressed as:

$$\{\varepsilon(x_k)\} = [diff\ N(x_k)]\cdot\{f\} = [B(x_k)]\cdot\{f\} \tag{3.13}$$

In the matrix $[B]$ there are the results of the differential operations on the shape functions $[N]$. The $[B]$ shows the dependency of the strain field to the nodal displacements.

STEP 5

Point by point, as consequence of strain field presence, material is subjected to a stress state $\{\sigma(x_k)\}$, that can be predicted by elasticity rules. The components of this vector are linked to the components of the vector $\{\varepsilon(x_k)\}$ through a matrix that includes the elastic properties of the material. In some cases, in the matrix there are also the geometric properties of the cross-section of the element.

$$\{\sigma(x_k)\} = [D] \cdot \{\varepsilon(x_k)\} \qquad (3.14)$$

Square matrix $[D]$ is the stiffness matrix. The stresses entities must be congruent with their parent strains. For example, in plane elastic problems (rods, plane elements) and with solid elements, the stress state is described with the normal stresses σ and the shear stresses τ as defined by the elasticity theory. When there is curvature with bending out of the plane (beams or shells) the bending moments are used.

After operations of mechanical machining or welding processes it is best to include residual stresses (stress field $\{\sigma_0\}$) that can be already present on the structure before the application of the loads. To manage also a pre-existent strain field like a thermal expansion, a more refined formulation can be written:

$$\{\sigma(x_k)\} = [D] \cdot \{\varepsilon(x_k) - \{\varepsilon_0\}\} + \{\sigma_0\} \qquad (3.15)$$

STEP 6

At this point, nodal forces can be determined, they are the consequence of the element stress field which depends on displacements field (nodal displacements in particular).

Stresses at elements interfaces are not balanced because the strain field continuity is not guaranteed by the approximate description of the displacement field. Interface stresses unbalance extent will be an important parameter in the evaluation of the quality of finite elements analysis results. The equivalent nodal loads cannot be evaluated computing the resultant of the stresses applied along the border of the element.

Forces are exchanged between two elements only through their common nodes, as

consequence, nodal forces should be computed in another way, in particular three main alternatives are usually adopted: by applying Virtual Works Principle, by differentiating potential energy or with Rayleigh-Ritz Method. In the following lines, Virtual Works Principle will be employed.

For the PVW, if a structure (the discretized one in our case), in equilibrium condition, is subjected to a virtual displacements field (coherent with the constraints of the structure), the virtual work done by the external forces applied to the structure (due to the displacement of the point of the application of the force) is equal to the virtual total work made by the internal stresses of the structure (due to the virtual strain field):

$$W_{ext} = W_{int} \tag{3.16}$$

The vector of the virtual nodal displacements is defined as $\{f^*\}$. The work made by the external forces is defined as the product between the force and the virtual nodal displacements:

$$W_{ext} = \{f^*\}^T \cdot [F] \tag{3.17}$$

Inside the element a virtual strain field is created due to the virtual nodal displacement applied to the structure. Reminding eq. (3.12):

$$\{\varepsilon^*\} = [B] \cdot \{f^*\} \tag{3.18}$$

Considering an infinitesimal part of the total volume of the element, with infinitesimal volume $dVol$, the virtual work made by the internal stresses is

$$dW_{int} = \{\varepsilon^*\}^T \cdot \{\sigma\} \cdot dVol \tag{3.19}$$

The total internal virtual work is obtained integrating this last result on the entire volume of the element:

$$W_{int} = \oint \{\varepsilon^*\}^T \cdot \{\sigma\} \cdot dVol$$

<div align="right">(3.20)</div>

The stress field can be calculated as:

$$\{\sigma\} = [D] \cdot [B] \cdot \{f\} \qquad \text{(3.21)}$$

The total virtual work of the internal stresses is therefore:

$$W_{int} = \oint \{f^*\}^T \cdot \{B\}^T \cdot [D] \cdot [B] \cdot \{f\} \cdot dVol$$

<div align="right">(3.22)</div>

Since both the virtual and real displacement vectors are constant with respect to the integral variable you can write:

$$W_{int} = \{f^*\}^T \oint \cdot (\{B\}^T \cdot [D] \cdot [B] \cdot dVol) \cdot \{f\}$$

<div align="right">(3.23)</div>

Applying the PVW eq (3.16-3.17):

$$\{F\} = \oint \cdot (\{B\}^T \cdot [D] \cdot [B] \cdot dVol) \cdot \{f\}$$

<div align="right">(3.24)</div>

Recalling the stiffness equation (3.1), the stiffness matrix of the element can be defined as

$$[K] = \oint \{B\}^T [D] \cdot [B] \cdot dVol$$

The stiffness parameters depend from the choices made at the beginning for the description of the displacements field. The previous integral can be solved in an analytical way only in few cases. More often it is convenient to solve it using numerical algorithms for integration. If external forces on the surface $\{p\}$ or external forces in the volume $\{v\}$ (i.e. due to centrifugal forces) are present the expression of the virtual work as to be modified:

$$W_{ext} = \{f^*\}^T \cdot [F] + \oint \{f^*\}^T \cdot [N]^T \{p\} \cdot dS + \oint \{f^*\}^T \cdot [N]^T \cdot \{v\} \cdot dVol$$

The previous equation, written with respect to the shape functions, can be reshaped as:

$$W_{ext} = \{f^*\}^T \cdot \left\{ \{F\} + \{F_p\} + \{F_v\} \right\}$$

Where $\{F_p\}$ is the vector of the nodal loads equivalent to the external forces on the volume:

$$\{F_p\} = \oint [N]^T \cdot \{p\} \cdot dS$$

And the vector $\{F_v\}$ is the vector of the nodal loads equivalent to the external forces on the volume:

$$\{F_V\} = \oint [N]^T \cdot \{v\} \cdot dVol$$

Moreover, a field of residual stress $\{\sigma_0\}$ or a field of independent strain $\{\varepsilon_0\}$ can be considered. In these cases, the internal virtual work is defined as:

$$W_{int} = \{f^*\}^T \left\{ \oint [B]^T \cdot [D] \cdot [B] \cdot \{f\} \cdot dVol \right.$$
$$\left. - \oint ([B]^T \cdot [D] \cdot \{\varepsilon_0\}) \cdot dVol + \oint ([B]^T \cdot \{\sigma_0\}) \cdot dVol \right\}$$

(3.30)

This expression can be rewritten as:

$$W_{int} = \{f^*\}^T \cdot \left\{ [K] \cdot \{f\} - \{F_\varepsilon\} - \{F_\sigma\} \right\}$$

(3.31)

Where $\{F_\varepsilon\}$ is the vector of the nodal loads equivalent to the strain field $\{\varepsilon_0\}$:

$$\{F_\varepsilon\} = \oint [B]^T \cdot [D] \cdot \{\varepsilon_0\} \cdot dVol$$

(3.32)

and $\{F_\sigma\}$ is the vector of the nodal loads equivalent to the stress field $\{\sigma_0\}$:

$$\{F_\sigma\} = - \oint [B]^T \cdot \{\sigma_0\} \cdot dVol$$

(3.33)

As a result, the general stiffness relation is:

$$\left\{ \{F\} + \{F_p\} + \{F_v\} + \{F_\sigma\} + \{F_\varepsilon\} \right\} = [K] \cdot \{f\}$$

(3.34)

STEP 7

Last step provides an equation which lets to compute directly stresses (especially in certain significant points of the element) starting from the knowledge of nodal displacements; this equation is used at the end of the analysis, once all nodal displacements have been computed, hen each element is re-examined in order to compute stresses present on it. Stress field equation, obtained in previous steps, is the starting point:

$$\{\sigma(x_k)\} = [D] \cdot [B] \cdot \{f\} = [H]\{f\}$$
(3.35)

The terms of the matrix $[B]$ are functions of the coordinates x_k , therefore the terms of the matrix $[H]$ are functions of the coordinates x_k.

For numerical calculation, significant element points at which stresses will be evaluated, must be chosen by the code or by the user.

Often, the nodes are used for this calculus, however it is not sure that they are the most significant solution for the evaluation of the stress state. A better choice is constituted by the points used by the Gauss's algorithm for the numerical integration of the terms of the stiffness matrix.

3.2 ABAQUS

3.2.1 ABAQUS BASICS

To deal with FEM simulations the software adopted in this thesis is Abaqus CAE from Dassault Systemès-Simulia. In the automotive industry Abaqus has a large penetration due to its capability to accurately model complex material behavior and to capture the important physical response of automotive components and systems in these applications, combined with the robustness of the software.

Abaqus consists of three main analysis products: Abaqus/Standard, Abaqus/Explicit, and Abaqus/Cfd plus other add-on analysis options available to further extend the possibilities.

Abaqus/standard is a general-purpose analysis product that can solve a wide range of linear and nonlinear problems involving the static, dynamic, thermal, electrical, and electromagnetic response of components. It solves a system of equations implicitly at each solution "increment."

In contrast, Abaqus/Explicit marches a solution forward through time in small time increments without solving a coupled system of equations at each increment (or even forming a global stiffness matrix); in fact Abaqus/Explicit is a special-purpose analysis product that uses an explicit dynamic finite element formulation, suitable for modeling brief, transient dynamic events, such as impact and blast problems, and efficient for highly nonlinear problems involving changing contact conditions.

Abaqus/Cfd is a computational fluid dynamics analysis product. It can solve a broad class of incompressible flow problems including laminar and turbulent flow, thermal convective flow, and deforming mesh problems.

A complete Abaqus analysis usually consists of three distinct stages: preprocessing, simulation, and post processing. These three stages are linked together by files as shown below in Fig. 3.1:
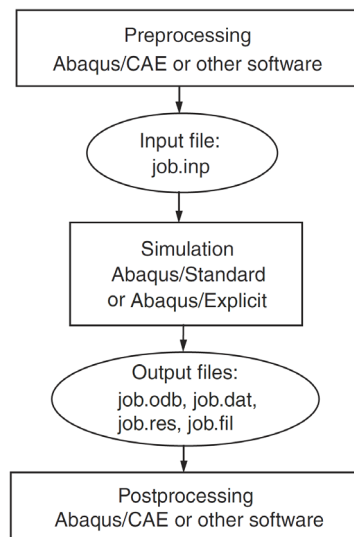
Fig. 3.1 Abaqus flow chart

In the preprocessing you must define the model of the physical problem and create an Abaqus input file using Abaqus/CAE or another preprocessor such as hypermesh, although the Abaqus input file for a simple analysis can be created and modified directly using a text editor.

The simulation, which normally is run as a background process, is the stage in which Abaqus/Standard or Abaqus/Explicit solves the numerical problem defined in the input file. Examples of output from a stress analysis include displacements and stresses that are stored in binary files ready for post processing. The complexity of the problem and the available computing power determine the time required to complete a run. At the end the post processing phase is the stage where outputs and results are evaluated in an interactive way using the visualization module of Abaqus/CAE or another postprocessor such as Hyperview. The visualization module, which reads the neutral binary output database file, has a variety of options for displaying the results, including color contour plots, animations, deformed shape plots and X–Y plots.

An Abaqus model is composed of several different components that together describe the physical problem to be analyzed and the results to be obtained: discretized geometry, element section properties, material data, loads and boundary conditions, analysis type, and output requests. The discretized geometry is composed by finite elements and nodes that define the basic geometrical and physical structure of the model under investigation. Elements are connected to one another by shared nodes. The coordinates of the nodes and the connectivity

of the elements (which nodes belong to which elements) are the backbone of the discretized geometry. The collection of all the elements and nodes in a model is called the mesh. Generally, the mesh will be only an approximation of the actual geometry of the structure. The element type, shape, and location, as well as the overall number of elements used in the mesh, affect the results obtained from a simulation. The greater the mesh density (i.e., the greater the number of elements in the mesh), the more accurate the results. As the mesh density increases, the analysis results converge to a unique solution, and the computer time required for the analysis increases. The solution obtained from the numerical model is generally an approximation to the solution of the physical problem being simulated. The extent of the approximations made in the model's geometry, material behavior, boundary conditions, and loading determines how well the numerical simulation matches the physical problem. Element section properties refers to the fact that Abaqus has a wide range of elements, many of which have geometry not defined completely by the coordinates of their nodes. Such additional geometric data are defined as physical properties of the element and are necessary to define the model geometry completely.

Loads distort the physical structure and, thus, create stress in it. The most common forms of loading include:

- point loads
- pressure loads on surfaces
- distributed tractions on surfaces
- distributed edge loads and moments on shell edges
- body forces, such as the force of gravity
- thermal loads

Boundary conditions are used to constrain portions of the model to remain fixed (zero displacements) or to move by a prescribed amount (nonzero displacements). In a static analysis enough boundary conditions must be used to prevent the model from moving as a rigid body in any direction; otherwise, unrestrained rigid body motion causes the stiffness matrix to be singular. A solver problem will occur during the solution stage and may cause the

simulation to stop prematurely popping a warning message. Rigid body motions can consist of both translations and rotations of the components. The potential rigid body motions depend on the dimensionality of the model. In a dynamic analysis inertia forces prevent the model from undergoing infinite motion instantaneously as long as all separate parts in the model have some mass; therefore, solver problem warnings in a dynamic analysis usually indicate some other modeling problem, such as excessive plasticity.

Abaqus can carry out many different types of simulations, among those, static and dynamic stress analyses are the most common. In a static analysis the long-term response of the structure to the applied loads is obtained. In other cases the dynamic response of a structure to the loads may be of interest: for example, the effect of a sudden load on a component, such as occurs during an impact.

3.2.2 ABAQUS STANDARD – ABAQUS EXPLICIT

Abaqus/Standard and Abaqus/Explicit are powerful tool suited to accomplish different tasks, according to the nature of the problem. For those problems that can be solved with either method, the efficiency with which the problem can be solved can determine which product to use. The key differences between the analysis products, are reported in table 3.2

Quantity	Abaqus/Standard	Abaqus/Explicit
Element library	Offers an extensive element library.	Offers an extensive library of elements well suited for explicit analyses. The elements available are a subset of those available in Abaqus/Standard.
Analysis procedures	General and linear perturbation procedures are available.	General procedures are available.
Material models	Offers a wide range of material models.	Similar to those available in Abaqus/Standard; a notable difference is that failure material models are allowed.
Contact formulation	Has a robust capability for solving contact problems.	Has a robust contact functionality that readily solves even the most complex contact simulations.
Solution technique	Uses a stiffness-based solution technique that is unconditionally stable.	Uses an explicit integration solution technique that is conditionally stable.
Disk space and memory	Due to the large numbers of iterations possible in an increment, disk space and memory usage can be large.	Disk space and memory usage is typically much smaller than that for Abaqus/Standard.

Tab. 3.2 Key differences between Abaqus/Standard and Abaqus/Explicit

For many analyses it is clear whether Abaqus/Standard or Abaqus/Explicit should be used. for example, in case of non "nonlinearity," Abaqus/Standard is more efficient for solving smooth nonlinear problems; on the other hand, Abaqus/Explicit is the clear choice for a wave propagation analysis. There are, however, certain static or quasi-static problems that can be simulated well with either program. Typically, these are problems that usually would be solved with Abaqus/Standard but may have difficulty converging because of contact or material complexities, resulting in a large number of iterations, cost and time since in Abaqus/Standard each iteration requires a large set of linear equations to be solved.

Whereas Abaqus/Standard must iterate to determine the solution to a nonlinear problem, Abaqus/Explicit determines the solution without iterating by explicitly advancing the kinematic state from the end of the previous increment, potentially being more efficient than Abaqus/Standard if the same analysis requires many iterations.

Another advantage of Abaqus/Explicit is that it requires much less disk space and memory. Using the explicit method, the computational cost is proportional to the number of elements and inversely proportional to the size reduction in element dimension.

Predicting implicit analysis computational cost is more difficult. This difficulty arises from the problem-dependent relationship between element connectivity and solution cost, a relationship that does not exist in the explicit method. As a general rule it may assumed that the computational cost is roughly proportional to the square of the number of degrees of freedom. The explicit method shows great cost savings against the implicit method as the model size increases, provided that the mesh is relatively uniform.
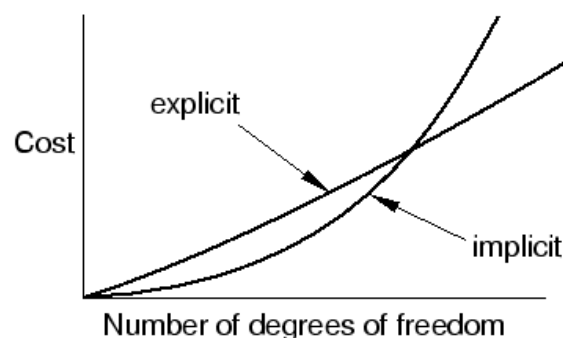
Fig. 3.3 Method cost choice based on number of dof

3.2.3 FINITE ELEMENTS AND RIGID BODIES

Finite elements and rigid bodies are the fundamental components of an Abaqus model. Finite elements are deformable, whereas rigid bodies move through space without changing shape. Any part of a body can be defined as a rigid one; most element types can be used in a rigid body definition with the advantage that the motion of a rigid body is described completely by no more than six degrees of freedom at a reference node. In contrast, deformable elements have many degrees of freedom and require expensive element calculations to determine the deformations. When such deformations are negligible or not of interest, modeling a component as a rigid body produces significant computational savings without affecting the overall results.

A wide range of elements is available in Abaqus. The elements available in Abaqus/Explicit are (with a few exceptions) a subset of those available in Abaqus/Standard. To help distinguish between them you can focus on five aspects:

- Family
- Degrees of freedom
- Number of nodes
- Formulation
- Integration

Each element in Abaqus has a unique name, such as S4R, or C3D10 that bring itself information on the five aspects. The naming convention in fact is this:

FAMILY

Fig. 3.4 shows the element families most used in a stress analysis. One of the major distinctions between different element families is the geometry type that each family assumes.
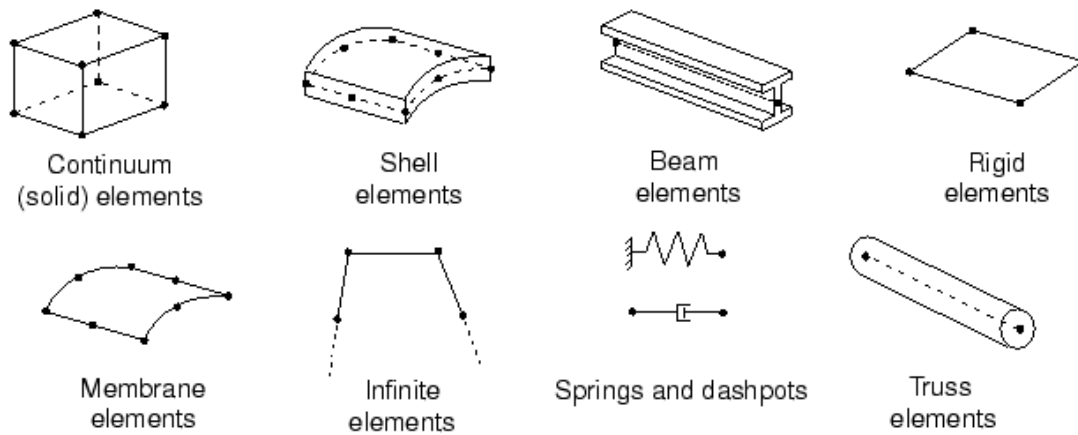
Fig. 3.4 Abaqus element types

The first letter or letters of an element's name indicate to which family the element belongs (i.e. "S" for shell elements, "C" for continuum ones...). For example, the S in S4R indicates this is a shell element, while the C in C3D8I indicates this is a continuum element.

DEGREES OF FREEDOM

The degrees of freedom (dof) are the fundamental variables calculated during the analysis. For a stress/displacement simulation the degrees of freedom are the translations at each node. Some element families, such as the beam and shell families, have rotational degrees of freedom as well. The following numbering convention is used for the degrees of freedom in Abaqus:

- 1 Translation in direction 1
- 2 Translation in direction 2
- 3 Translation in direction 3
- 4 Rotation about the 1-axis
- 5 Rotation about the 2-axis
- 6 Rotation about the 3-axis
- 7 Warping in open-section beam elements
- 8 Acoustic pressure, pore pressure, or hydrostatic fluid pressure
- 9 Electric potential

- 10 Connector material flow (units of length)
- 11 Temperature (or normalized concentration in mass diffusion analysis) for continuum elements or temperature at the first point through the thickness of beams and shells
- 12 Temperature at other points through the thickness of beams and shells

Directions 1, 2, and 3 correspond to the global 1-, 2-, and 3-directions, respectively, unless a local coordinate system has been defined at the nodes.

NUMBER OF NODES—ORDER OF INTERPOLATION

Displacements, rotations, temperatures, and the other degrees of freedom mentioned in the previous section are calculated only at the nodes of the element. At any other point in the element, the displacements are obtained by interpolating from the nodal displacements. Usually the interpolation order is determined by the number of nodes used in the element, as illustrated in Fig 3.5.

(a) Linear element
(8-node brick, C3D8)

(b) Quadratic element
(20-node brick, C3D20)

(c) Modified second-order element
(10-node tetrahedron, C3D10M)
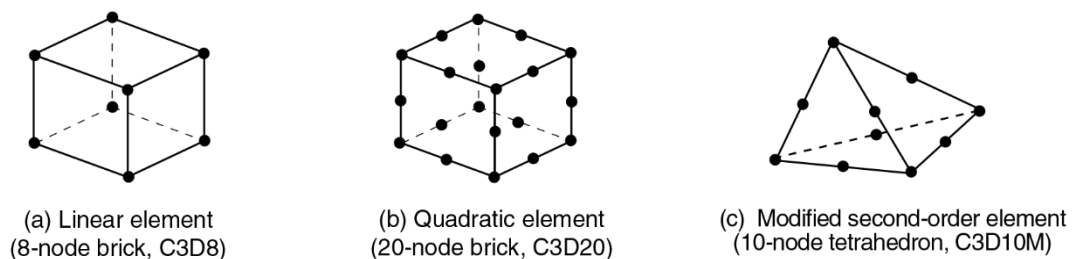
Fig. 3.5 Abaqus element interpolation examples

Elements that have nodes only at their corners (Fig 3.5a) use linear interpolation in each direction and are often called linear elements or first-order elements. Elements with mid-side nodes (Fig 3.5b) use quadratic interpolation and are often called quadratic elements or second-order elements.

Modified triangular or tetrahedral elements with mid-side nodes (Fig 3.5c) use a modified second-order interpolation and are often called modified elements or modified second-order elements.

Abaqus/Standard offers a wide selection of both linear and quadratic elements. Abaqus/Explicit offers only linear elements, with the exception of the quadratic beam and modified tetrahedron and triangle elements. Typically, the number of nodes in an element is clearly identified in its name. The beam element family uses a slightly different convention: the order of interpolation is identified in the name. Thus, a first-order, three-dimensional beam element is called B31, whereas a second-order, three-dimensional beam element is called B32. A similar convention is used for axisymmetric shell and membrane elements.

FORMULATION

An element's formulation refers to the mathematical theory used to define the element's behavior. The stress/displacement elements in Abaqus are based on the Lagrangian behavior (or material description of the behavior): the material associated with an element remains associated with the element throughout the analysis and material cannot flow across element boundaries.

In the alternative Eulerian or spatial description, elements are fixed in space as the material flows through them. Eulerian methods are used commonly in fluid mechanics simulations. Adaptive meshing combines the features of pure Lagrangian and Eulerian analyses and allows the motion of the element to be independent of the material. To accommodate different types of behavior, some element families in Abaqus include elements with several different formulations, for example the shell element family has three classes: one suitable for general-purpose shell analysis, another for thin shells, and yet another for thick shells.

Elements with alternative formulations are identified by an additional character at the end of the element name. For example, the continuum, beam and truss element families include members with a hybrid formulation in which the pressure (continuum elements) or axial force (beam and truss elements) is treated as an additional unknown; these elements are identified by the letter "H" at the end of the name like C3D8H or B31H.

Some element formulations allow coupled field problems to be solved. For example, elements whose names begin with the letter C and end with the letter T (such as C3D8T) possess both mechanical and thermal degrees of freedom and are intended for coupled thermal-mechanical simulations.

INTEGRATION

Abaqus uses numerical techniques to integrate various quantities over the volume of each element. Using Gaussian quadrature for most elements, Abaqus evaluates the material response at each integration point in each element. Some elements in Abaqus can use full or reduced integration, a choice that can have a significant effect on the accuracy of the element for a given problem.

Abaqus uses the letter "R" at the end of the element name to distinguish reduced integration elements (unless they are also hybrid elements, in which case the element name ends with the letters "RH"). For example, CAX4 is the 4-node fully integrated linear axisymmetric solid element and CAX4R is the reduced-integration version of the same element.

Abaqus/Standard offers both full and reduced-integration elements; Abaqus/Explicit offers only reduced-integration elements with the exception of the modified tetrahedron and triangle elements and the fully integrated first-order shell, membrane, and brick elements.

3.2.4 CONTINUUM ELEMENTS

Continuum or solid elements can be used to model the widest variety of components. Conceptually, continuum elements simply model small blocks of material in a component and since they may be connected to other elements on any of their faces, they can be used to build models of nearly any shape, subjected to nearly any loading, like bricks in a building.

Continuum stress/displacement elements in Abaqus have names that begin with the letter "C"; the next two letters indicate the dimensionality and usually, but not always, the active degrees of freedom in the element. The name "3D" indicates a three-dimensional element; "AX" an axisymmetric element, "PE" a plane strain element and "PS" a plane stress element. Three-dimensional continuum elements can be hexahedra (bricks), wedges, or tetrahedra. Whenever possible, hexahedral elements or second-order tetrahedral elements should be used; first-order tetrahedra (C3D4) have a simple, constant-strain formulation, and very fine mesh are required for an accurate solution.

Abaqus also provides several classes of two-dimensional continuum elements that differ from each other in their out-of-plane behavior. Two-dimensional elements can be quadrilateral or

triangular. Fig 3.6 shows the three classes that are used commonly:
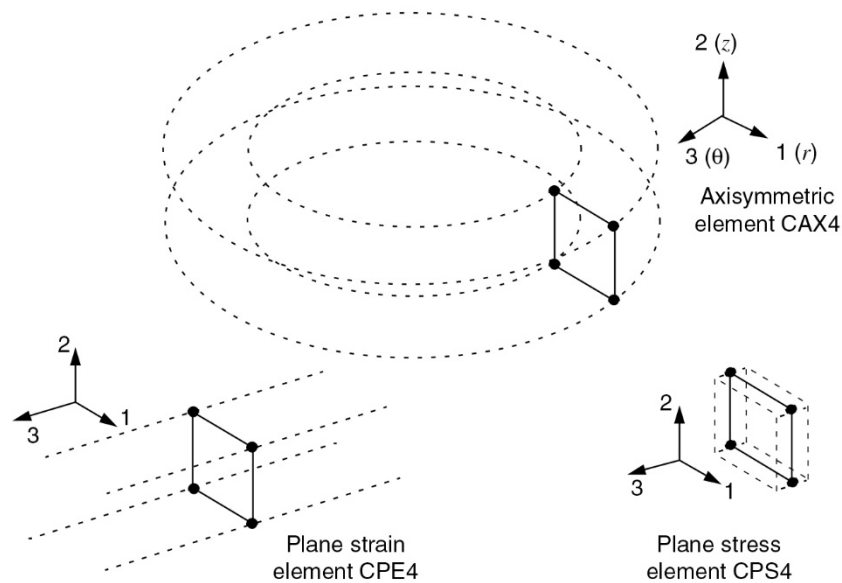
Fig. 3.6 Plane strain, plane stress, and axisymmetric elements without twist

Plane strain elements assume that the out-of-plane strain, ε_{33}, is zero; they can be used to model thick structures. Plane stress elements assume that the out-of-plane stress, σ_{33}, is zero; they are suitable for modeling thin structures.

Axisymmetric elements without twist, the "CAX" class of elements, model a 360° ring; they are suitable for analyzing structures with axisymmetric geometry subjected to axisymmetric loading.

Two-dimensional solid elements must be defined in the 1–2 plane so that the node order is counterclockwise around the element perimeter, as shown in Fig. 3.7
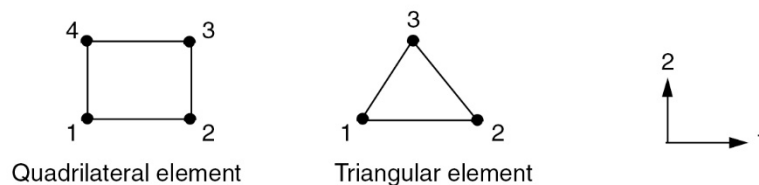
Fig. 3.7 Correct nodal connectivity for two-dimensional elements

DEGREES OF FREEDOM

All of the stress/displacement continuum elements have translational degrees of freedom at each node. Correspondingly, degrees of freedom 1, 2, and 3 are active in three-dimensional elements, while only degrees of freedom 1 and 2 are active in plane strain elements, plane stress elements and axisymmetric elements without twist.

ELEMENT PROPERTIES

All solid elements must refer to a solid section property that defines the material and any additional geometric data associated with the element. For three-dimensional and axisymmetric elements no additional geometric information is required: the nodal coordinates completely define the element geometry. For plane stress and plane strain elements the thickness of the elements may be specified or a default value of 1 will be used.

The property used will be "SOLID SECTION" that can be followed by the parameter "COMPOSITE" (only Abaqus/Standard analyses) if the solid is made up of several layers of material. This parameter can be used only with three-dimensional brick solid elements that have only displacement degrees of freedom.

The COMPOSITE and MATERIAL parameters are mutually exclusive.

FORMULATION AND INTEGRATION

Alternative formulations available for the continuum family of elements in Abaqus/Standard include an incompatible mode formulation (the last or second-to-last letter in the element name is I) and a hybrid element formulation (the last letter in the element name is H). In Abaqus/Standard you can choose between full and reduced integration for quadrilateral and hexahedral (brick) elements. In Abaqus/Explicit you can choose between full and reduced integration for hexahedral (brick) elements; however, only reduced integration is available for quadrilateral first-order elements. Both the formulation and type of integration can have a significant effect on the accuracy of solid elements.

ELEMENT OUTPUT VARIABLES

By default, element output variables such as stress and strain refer to the global Cartesian

coordinate system. Thus, the -component of stress at the integration point shown in Fig 3.8a acts in the global 1-direction. Even if the element rotates during a large-displacement simulation, as shown in Fig 3.8b, the default is still to use the global Cartesian system as the basis for defining the element variables
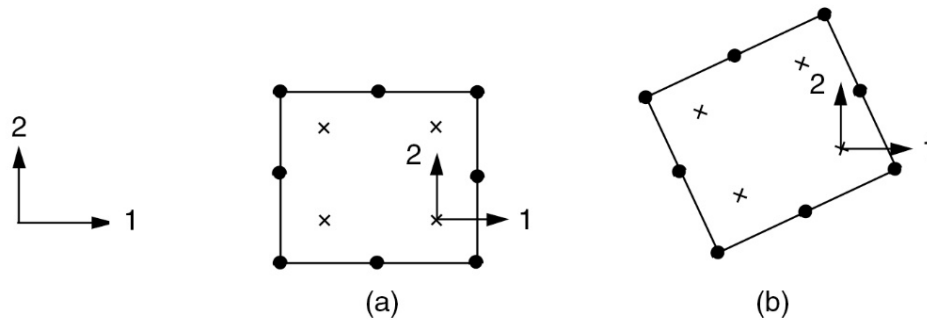
Fig. 3.8 Material direction for continuum elements

There is also the possibility to define a local coordinate system for element variables. This local coordinate system rotates with the motion of the element in large-displacement simulations. A local coordinate system can be very useful if the object being modeled has some natural material orientation, such as the fiber directions in a composite material.

3.2.5 SHELL ELEMENTS

Shell elements are used to model structures in which one dimension (the thickness) is significantly smaller than the other dimensions and the stresses in the thickness direction are negligible. Their diffusion in structural applications such as the automotive ones is vast; components with one negligible dimension (like metal and/or composite sheets) are very common. The advantage of using shell elements is that they allow to reduce a lot the simulation computational cost without decreasing too much the results accuracy.

Shell element names in Abaqus begin with the letter "S." Axisymmetric shells all begin with the letters "SAX". The first number in a shell element name indicates the number of nodes in the element.

Two types of shell elements are available in Abaqus: conventional shell elements and

continuum shell elements. Conventional shell elements discretize a reference surface by defining the element's planar dimensions, its surface normal, and its initial curvature. Continuum shell elements, on the other hand, resemble three-dimensional solid elements in that they discretize an entire three-dimensional body yet are formulated so that their kinematic and constitutive behavior is similar to conventional shell elements.

The most used shell type in strain-stress explicit analyses is the general-purpose one: they account for finite membrane strains and arbitrarily large rotations; hence from now on "shell elements" refers to this category.

In Abaqus/Standard general three-dimensional shell elements are available with three different formulations: general-purpose, thin-only, and thick-only. The general-purpose shells and the axisymmetric shells with asymmetric deformation account for finite membrane strains and arbitrarily large rotations. The three-dimensional "thick" and "thin" element types provide for arbitrarily large rotations but only small strains. The general-purpose shells allow the shell thickness to change with the element deformation. All of the other shell elements assume small strains and no change in shell thickness, even though the element's nodes may undergo finite rotations. Triangular and quadrilateral elements with linear and quadratic interpolation are available. Both linear and quadratic axisymmetric shell elements are available. All of the quadrilateral shell elements (except for S4) and the triangular shell element S3/S3R use reduced integration. The S4 element and the other triangular shell elements use full integration. Table 3.9a summarizes the shell elements available in Abaqus/Standard.

All the shell elements in Abaqus/Explicit are general-purpose. Finite membrane strain and small membrane strain formulations are available. Triangular and quadrilateral elements are available with linear interpolation. A linear axisymmetric shell element is also available. Table 3.9b summarizes the shell elements available in Abaqus/Explicit.

	General-Purpose Shells	Thin-Only Shells	Thick-Only Shells
a	S4, S4R, S3/S3R, SAX1, SAX2, SAX2T, SC6R, SC8R	STRI3, STRI65, S4R5, S8R5, S9R5, SAXA	S8R, S8RT

	Finite-Strain Shells	Small-Strain Shells
b	S4, S4R, S3/S3R, SAX1	S4RS, S4RSW, S3RS

Tab. 3.9 a) Three classes of shell elements in Abaqus/Standard **b)** Two classes of shell elements in Abaqus/Explicit

For most explicit analyses the large-strain shell elements are appropriate. If, however, the analysis involves small membrane strains and arbitrarily large rotations, the small-strain shell elements are more computationally efficient. The S4RS and S3RS elements do not consider warping, while the S4RSW element does.

DEGREES OF FREEDOM

The three-dimensional elements in Abaqus/Standard whose names end in the number "5" (e.g.S4R5, STRI65) have 5 degrees of freedom at each node: three translations and two in-plane rotations (i.e., no rotations about the shell normal). However, all six degrees of freedom are activated at a node if required; for example, if rotational boundary conditions are applied or if the node is on a fold line of the shell.

The remaining three-dimensional shell elements have six degrees of freedom at each node (three translations and three rotations). The axisymmetric shells have three degrees of freedom associated with each node:

- 1 Translation in the r-direction.
- 2 Translation in the z-direction.
- 6 Rotation in the r–z plane.

ELEMENT PROPERTIES

All shell elements must refer to a shell section property that defines the thickness and material

properties associated with the element. The "SHELL SECTION" property will be used after. The stiffness of the shell cross-section can be calculated either during the analysis or once at the beginning of the analysis. If you choose to have the stiffness calculated during the analysis, Abaqus uses numerical integration to calculate the behavior at selected points through the thickness of the shell. These points are called section points, as shown in Fig 3.10. The associated material property definition may be linear or nonlinear. You can specify any odd number of section points through the shell thickness.
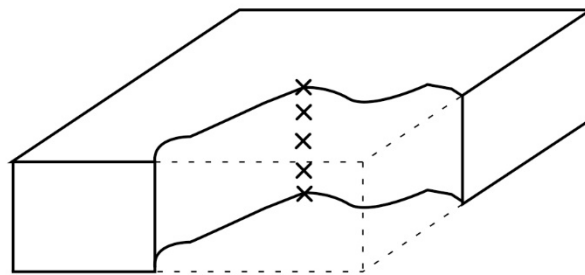
Fig. 3.10 Integration points

If you choose to have the stiffness calculated once at the beginning of the analysis, you can define the cross-section behavior to model linear or nonlinear behavior. In this case Abaqus models the shell's cross-section behavior directly in terms of section engineering quantities (area, moments of inertia, etc.), so there is no need for Abaqus to integrate any quantities over the element cross section, saving cost. This approach is recommended when the response of the shell is linear elastic.

ELEMENT OUTPUT VARIABLES

The element output variables for shells are defined in terms of local material directions that lie on the surface of each shell element. In all large-displacement simulations these axes rotate with the element's deformation. You can also define a local material coordinate system that rotates with the element's deformation in a large-displacement analysis.

3.3 MOLDFLOW

3.3.1 INTRODUCTION

Autodesk Moldflow® Insight simulation software provides a complete set of advanced plastics engineering simulation tools for use on digital prototypes. Providing in-depth analysis and optimization of plastic parts and their associated mold, Autodesk Moldflow® Insight software offers powerful functionality that can simulate the most advanced molding process in use today like injection molding, compression molding and others. This software is used vastly in the automotive business by OEM and their suppliers to reduce the need for physical prototypes and get innovative products to market faster.

Autodesk Moldflow® Insight allows you to simulate the filling and packing phase of the injection molding process to help predict the flow behavior of plastic melts and help achieve high quality manufacturing. Engineers can optimize gate locations, balance runner systems, evaluate processing conditions and predict and correct molded parts defects. Mold makers can analyze the effects of non-uniform mold temperatures, determine optimized valve-gate timing sequences and compare flow through hot versus cold runner systems. The optimization is done experimenting "what if" scenarios using different materials (from the vast library available), part geometries, mold designs and processing conditions before committing to a final design. Autodesk Moldflow® Insight helps manufacturers to "get it right the first time" so they can avoid cost and time delays due to non-optimized process.

In our thesis the analysis is dedicated only to the injection molding filling phase since the objective is to obtain information on the fiber orientation, not on the manufacturability of the part. A workflow of the analysis is reported in Fig. 3.11.

The preparation of the mesh will be treated after, the material is selected among more than 8000 grades of thermoplastic and thermosetting materials of the library or it can be imported manually. The single or multi-gate location is a critical factor in part quality since it vastly influences the flow paths: the gate must be placed to get a balanced and unidirectional filling,

in a thick area, preventing jetting and weld lines in weak regions. Air traps and overpacking must also be avoided.

Problem	Possible Solutions
Short Shot	1,2,3,4,5
Poor Filling Pattern	1,2,3,5
Poor Weld Lines	1,2,3,4,5
Air Traps	1,2,3,5
High Stress	1,2,3,4,5
High Pressure	1,2,3,4,5
High Clamp Force	1,2,3,4,5
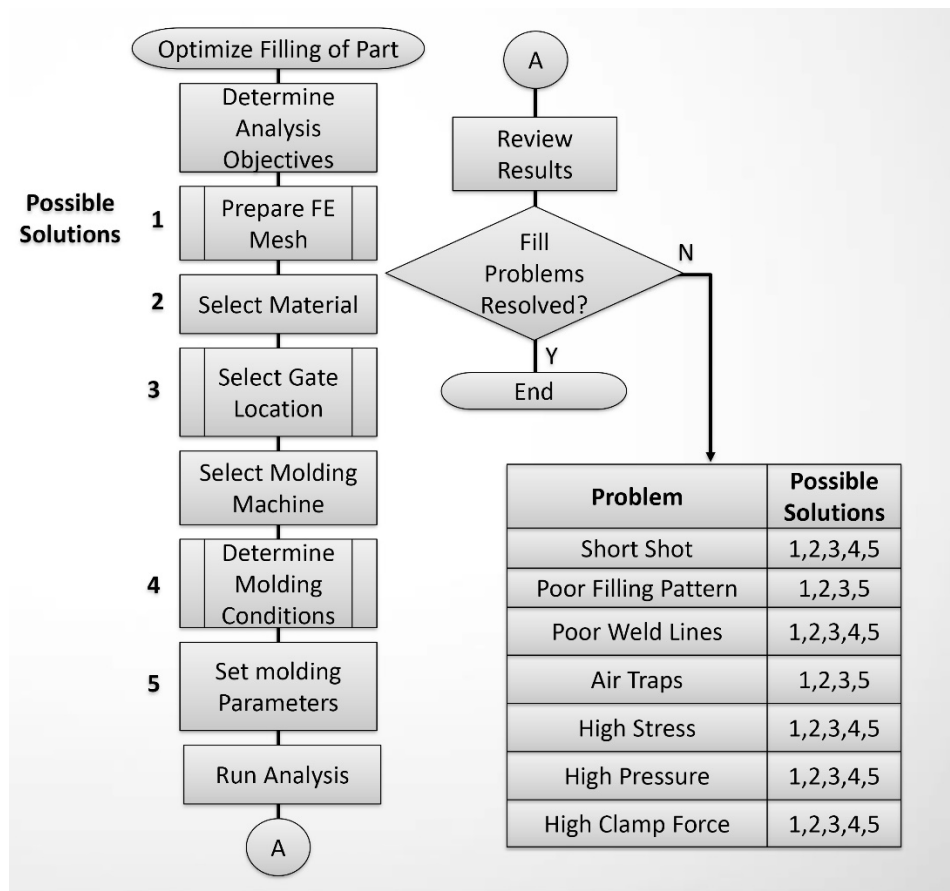
Fig. 3.11 analysis workflow

Determining the molding condition and the parameters is a tricky part of the simulation. In general the first parameters to set are the max pressure and clamp force (given by the machine type). Then you have to set mold surface temperature, melt temperature, filling control, velocity/pressure switch over and pack/holding control.

Mold temperature typically is the one already known from the present equipment or it can be changed if it is part of the optimization. Melt temperature, flow rate and injection time instead are often changed to have a good filling. Pressure drop is an important parameter to monitor during all the simulation.

The analysis can be run in local server on cloud, generating log files to see the progress. Each

type of problem detected can be addressed operating back on the design choices as shown in Fig 3.12.

At the end of the analysis you have over 30 possible results to review. Typical checked outcomes are the fill time graph, that shows if the filling was balanced without hesitation (Fig 3.12a), the Pressure at V/P switchover, the temperature at flow front, the frozen layer at filling end (Fig 3.12b), weld lines placement and angle (Fig 3.12c), volumetric shrinkage and pressure profile (Fig 3.12d).
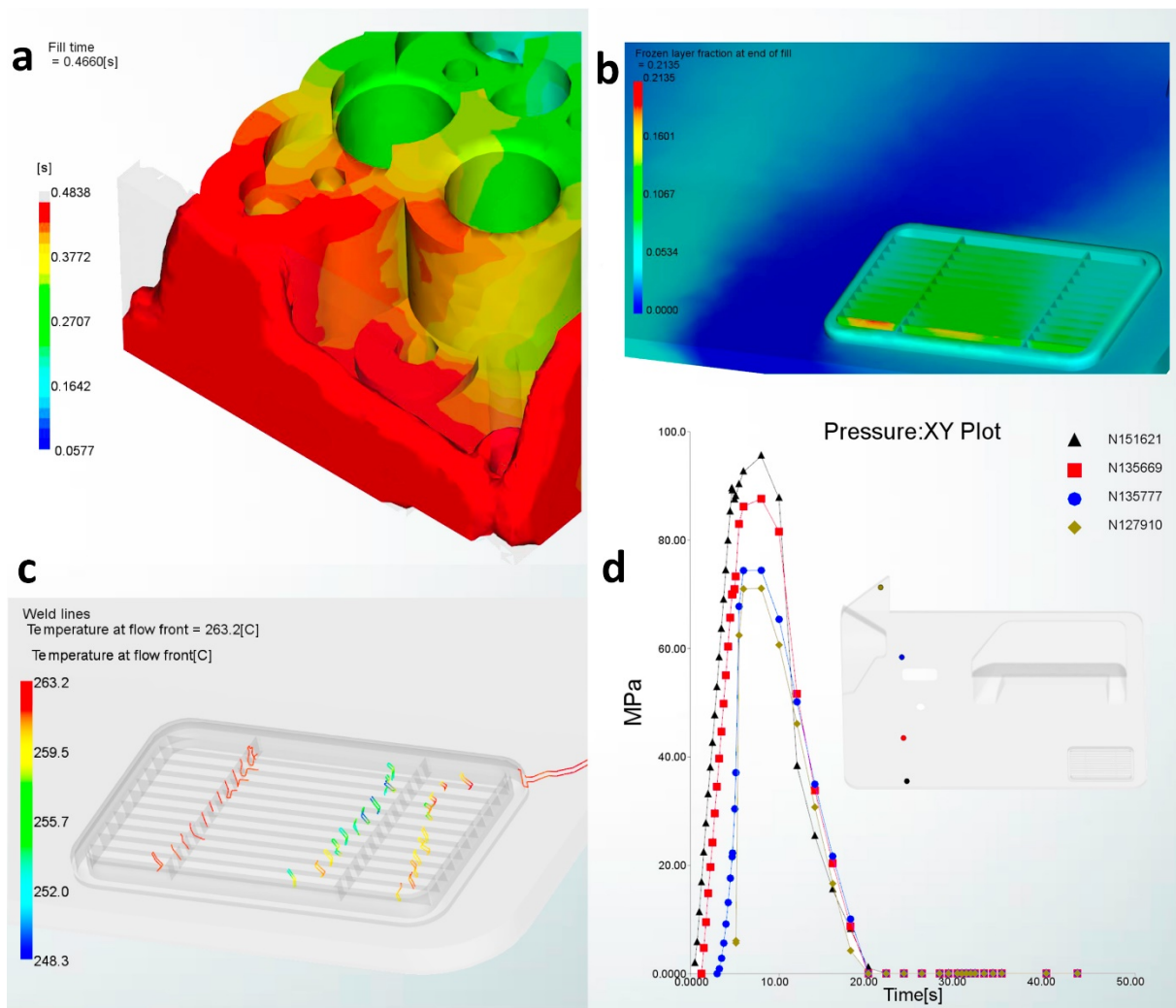
Fig. 3.12 general examples of results

the preparation of the model to launch the analysis is discussed in the next paragraph.

3.3.2 MESHING

In Autodesk Moldflow® Insight the model to be submitted for analysis must be discretized in finite element just as in Abaqus previously. Elements used are two-node linear elements (beams), three-node triangular elements (shell) and four-node tetrahedral elements (3D). The mesh type or analysis technology you select determines which molding processes and which analysis sequences are available for selection.

There are 4 types of mesh available:

- Midplane analysis technology
- Dual Domain analysis technology
- 3D analysis technology
- Beam elements

MIDPLANE MESH

A Midplane mesh consists of a web of 3-noded triangular elements and forms a 2D representation of a solid model. The local thickness of the part is added to each element to simulate the part volume. The aspect ratio of mesh elements can affect analysis performance. High aspect ratios can cause a slower analysis and affect the results. With the longest side in the direction of flow, the end node of high aspect ratio elements will add an excessive resistance factor to flow front calculations. Avoid very high aspect ratio triangles, which have their longest side in the direction of flow. If very high aspect ratios cannot be avoided, the longest side should, if possible, be at right angles to the flow direction.
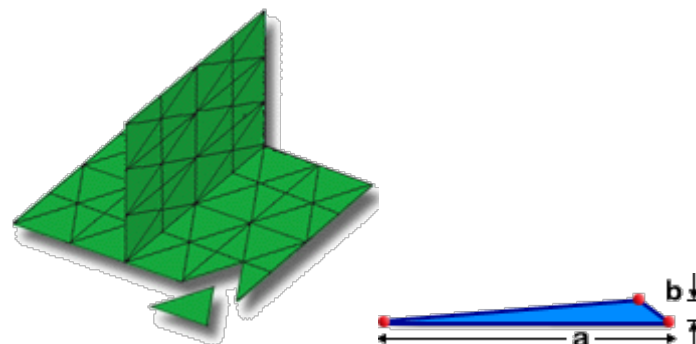
Fig. 3.13 midplane mesh and aspect ratio

The mesh density should be increased until there is no significant change in result detail. Mesh orientation is used to provide a consistent means of differentiating between the two sides of a two-dimensional, 3-noded element. The convention is to call one side of the element the top, and the other side the bottom.

DUAL DOMAIN MESH

Dual Domain analysis technology allows you to perform detailed analyses directly on thin-wall, surface meshed models (Flow width should be at least four times the thickness). The Dual Domain analysis works by simulating the flow of the melt on both the top and bottom parts of the mold cavity. Mesh orientation is used to provide a consistent means of differentiating between the two sides of a two-dimensional, 3-noded element. The simplest convention is to call one side of the element the top, and the other side the bottom. Attention must be payed to boundary edges that indicate holes or tears in the mesh and must be corrected either in the original CAD system used to create the model or using the mesh editing tools.
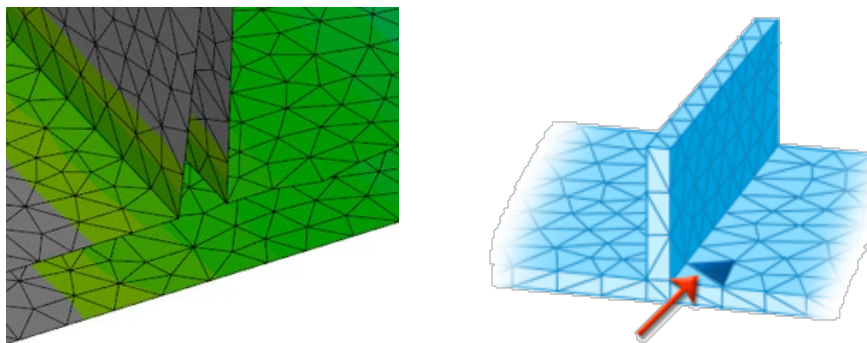
Fig. 3.14 dual domain mesh and boundary edges

3D MESH

A 3D mesh represents the CAD model by filling the volume of the model with four-node, tetrahedral elements (tetra). 3D meshes work well for parts that are thick or solid because tetra give a true 3D representation of the model. A 3D analysis does not make the assumptions that are made for Midplane or Dual Domain analyses. Therefore, 3D analyses often require

additional computational time to complete. This makes a 3D mesh more appropriate for thick models with complicated shapes, while Midplane and Dual Domain meshes are more applicable for thin-walled, shell-like parts.
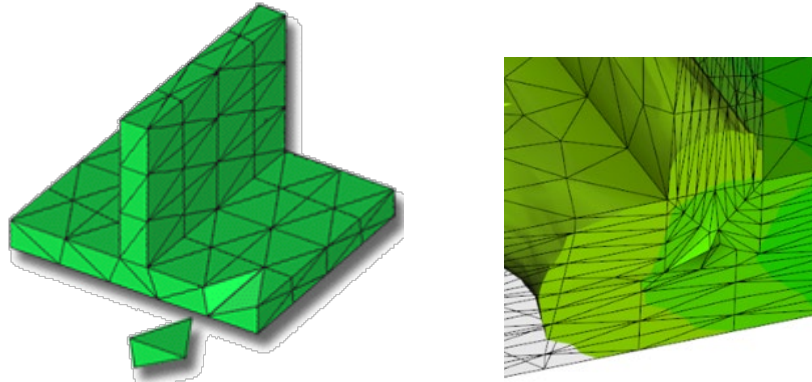
Fig. 3.15 3D mesh examples

BEAM ELEMENTS

Beam elements are two-node elements used to represent runner system components, cooling channels, gas channels, and tapered or non-tapered structural beams on the part. The nodes represent the centerline of the element and a radius defines the cross-sectional size.

In dual domain and midplane mesh the flow front grows from injection point to connected nodes; when a node fills other nodes are added, see Fig 3.16. Melt temperature is homogeneous entering the mold and polymer freezes as it hits the mold wall.
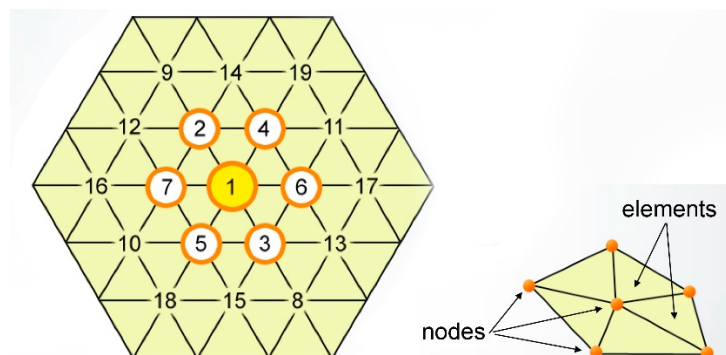
Fig. 3.16 flow propagation

The Tetrahedral Mesh instead is used for thick and "chunky" geometries, utilizing full 3D Navier-Stokes model and solving at each node for the variables pressure, velocity vector and temperature. It also considers heat conduction in all directions and optionally gravity and inertia.

3.4 DIGIMAT RP

3.4.1 INTRODUCTION

To conclude the chapter dedicated to the CAE tools, the implementation of Digimat-RP module is discussed to better understand its potentiality and application in the thesis. Digimat-RP is a powerful software which enables to bridge the gap between processing simulation (injection molding) and predictions carried out on the structural side, e.g., implicit & explicit structural FEA. In short, Digimat-RP enables an integrative approach to multi-scale material and structure modeling by taking into account the process-induced material microstructure in the FEA of the final part structure.

In order to take full advantage of Digimat-RP, it is strongly recommended to ensure that the structural FEA model and the Digimat material satisfy the following prerequisites:

- The regions of the structural FEA model where a Digimat material is to be used should have a specific material assigned to them in the original structural FEA model. If several different Digimat materials are to be used, then each associated region should have its own unique material.

- If it is intended to perform the coupled simulation on the local machine, the targeted FEA code should be properly installed and configured in order to run coupled Digimat analyses.

- The structural FEA model must be complete and ready to run with the targeted FEA code before going to Digimat-RP.

Since the power of this software is to merge these pieces of information the workspace area is formed by four windows that, used in succession, define the workflow:

- Structural model window, where you import the structural model and select the

component to assign a Digimat material and its manufacturing data

- Digimat material window, where all the material parameters can be edited

- Manufacturing data window to insert data coming from manufacturing process

- Solution settings window

The Structural model window is the main window of the workspace, it contains a 3D visualization of the meshed model and the list of components available. A component in Digimat-RP is defined as a region of the FEA model which is assigned to a given material model. Supported manufacturing technologies include injection molding of short fiber (SFRP) and long fibers (LFRP) reinforced polymers, compression molding for SFRP and LFRP, fused filament fabrication, fused deposition modeling and selective laser sintering.

It can accept input files from different commercial software such as Nastran, Abaqus, Ls-Dyna and so on. Speaking about Abaqus solid and shell elements are supported including:

- Tetra 4 *C3D4* elements

- Tetra 10 *C3D10* elements

- Wedge 6 *C3D6* elements

- Wedge 15 *C3D15* elements

- Hexa 8 *C3D8* elements

- Hexa 20 *C3D20* elements

- Tri 3 *S3* and *STRI3* elements

- Tri 6 *STRI6* elements

- Quad 4 *S4* elements

- Quad 8 *S8* elements

It is possible to load CAE input file containing unsupported elements. In that case, all supported elements will be loaded and displayed with the possibility to assign a material and all unsupported element will be skipped. When generating the coupled analysis files at the end of the workflow, unsupported elements will be copied without modification.

The material window contains the required features to define the Digimat materials used in

the coupled analysis. It is divided into two tabs: the model tab which contains parameters related to the physical definition of the composite material and the solution tab which contains numerical parameters not directly related to the physical material.
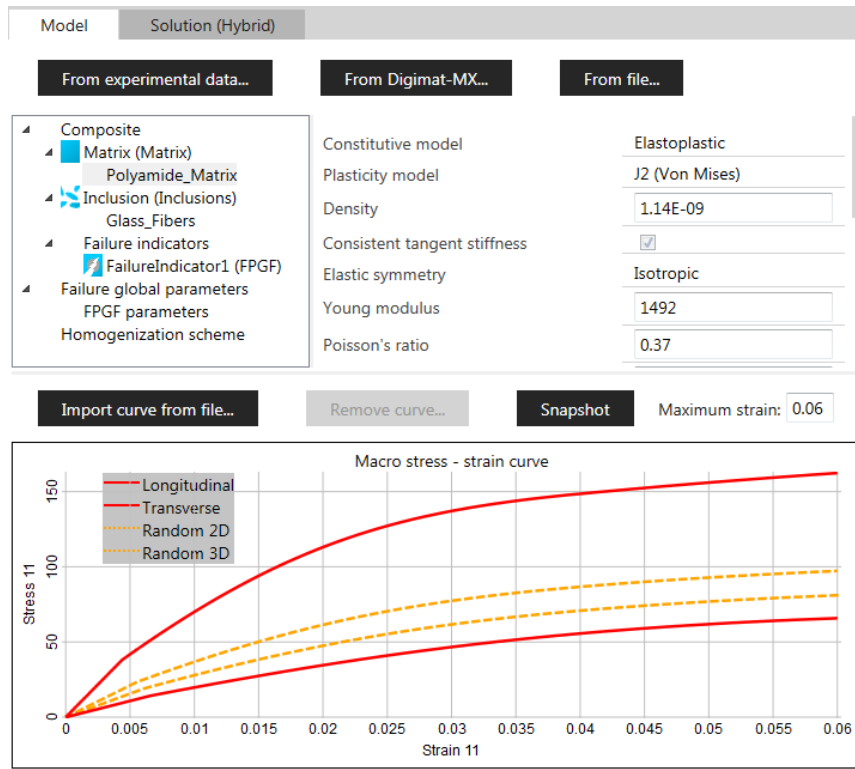
Fig. 3.17 the model tab, general example

The material model card can be obtained from the database (Digimat-MX), from a general file or by reverse engineering from experimental data.

The reverse engineering process involves some steps: first a description of the material grade (matrix material, fiber material and fiber amount), second a selection of required performance (linear stiffness, non-linear stiffness or non-linear stiffness combined with failure), third the input experimental data must be provided as stress-strain curves from at least two loading directions. Finally, a definition of the microstructure with fiber orientation tensors can be either identified automatically, or user-defined via the import of a .csv file following the CSV laminate file format.

Reverse engineering computation will then start based on the number of CPUs defined. After

completion of the reverse engineering, a new results tab becomes available which allows to review the obtained parameters as well as optimize them to obtain a better fit with a new computation.

Failure indicators are also specified in this phase.

The manufacturing data window is accessible as soon as a valid Digimat material is defined for a component. In particular in this thesis the information of fiber orientation is obtained coming from Moldflow 3d trough an intermediate step in Digimat-Map that will be discussed now before concluding with the solution setting.

3.4.2 DIGIMAT MAP

Digimat-MAP is a 3D mapping software included in the Digimat suite used to transfer fiber orientations, residual stresses, temperatures, weld lines, porosity or volume fractions between dissimilar injection molding and structural FEA meshes. It helps structural engineers to generate the optimal mesh refinement and make the appropriate element choice to capture changes in the composite material microstructure properties.
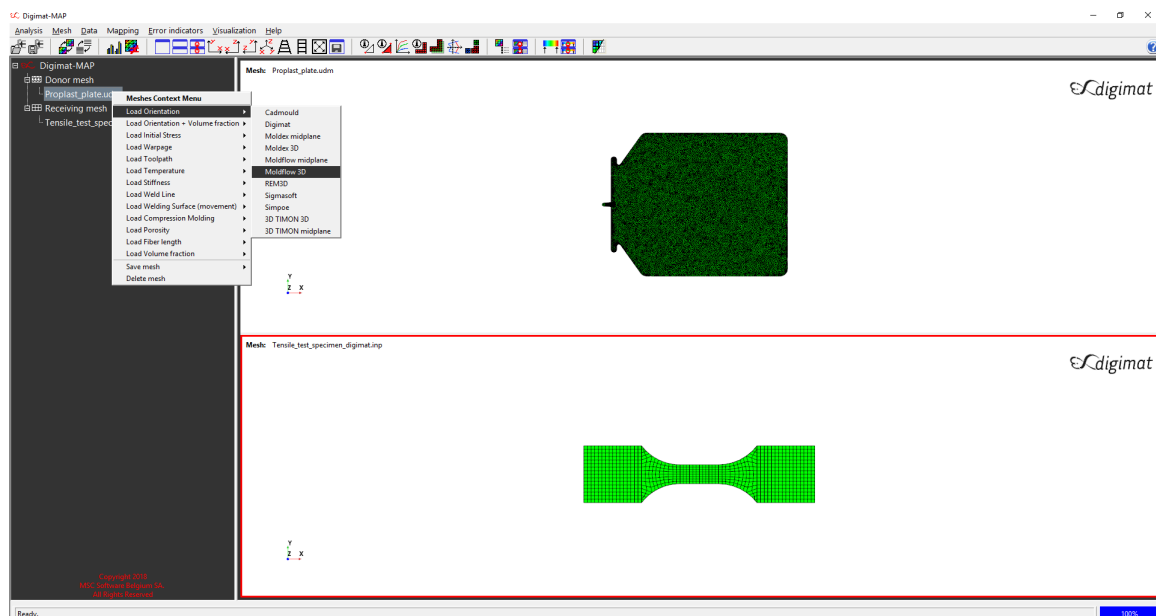
Fig. 3.18 Digimat Map graphical interface

The mapping process is done between a donor mesh on which the orientation tensor field, stress tensor field, temperature, weld lines field, fiber length and/or volume fraction field have been calculated and a receiving mesh, to which the donor information will be mapped. For both donor and receiving meshes, quadratic elements are supported in addition of linear elements; the input data is mapped on every integration point of the receiving mesh according to some algorithms:

- Node to node is available only for nodal data such as temperatures. This is the default algorithm for nodal data mapping. With this algorithm, the nodes of the receiving mesh are first localized in the donor mesh. Data is then mapped between the nodes.

- Integration point / node to integration point is the default algorithm for data at integration points (for example, stresses and orientations) and is the most recommended method for such type of data. First, the integration points of the receiving mesh are localized in the donor mesh and then data is mapped from the nodes of the donor mesh to the integration points of the receiving mesh. This means there is a sort of smoothing occurring in this method. Finally, in the receiving mesh, data is interpolated or extrapolated from the integration points to the nodes for visualization purposes only.

- Integration point / node to node / integration point is available for data at integration points. The difference with the default algorithm is that the mapping is done between the nodes of the donor and receiving meshes such that you actually have two smoothing steps instead of only one, given that an interpolation is required to transfer data from the nodes in the receiver mesh to the integration points. However, this method produces better visual results since the mapping step is done between nodes.

- Element to integration point is available for data at integration points. In this method, the integration points of the receiving mesh are localized in the donor mesh. The data value of the element in the donor mesh is then directly transferred to the integration point in the receiving mesh (there is no interpolation based on shape functions). This method is the 2nd most recommended after the Integration point /Node to Integration point method.

- Element to node / integration point is available for data at integration points. Each node of the receiving mesh is localized in the elements of the donor mesh and the data value of this element is transferred to the node of the receiving mesh. The value at the integration points in the receiving mesh are then interpolated from the value at the corresponding nodes.
- Other mapping methods are available for specific data types. For example, weld line data mapping uses a Point to Element method, and toolpath mapping also uses its own method. In these specific cases, the 5 previously mentioned methods are not applicable.

A tolerance parameter is used to check if the integration point/node is really external to an element (i.e., at a distance greater than the tolerance) or if it has to be considered for further mapping operations with that element. By default a tolerance is automatically computed based on the mean element size in the donor mesh.

The structural mesh of some analysis is usually different from the mesh used to simulate the injection process so geometric transformations can be operated to bring the meshes in the same space frame. The "superpose meshes" function scales (Fig. 3.19a), translates and rotates the donor mesh to get it exactly superposed to the receiving mesh; this is done by specifying three common points/nodes in the donor and the receiving meshes. Digimat-MAP then computes and applies the appropriate geometric transformations.

Focusing on fibers orientation most injection simulation software allows to predict the distribution of them in a part even through the thickness, which is critical to correctly account for anisotropic properties of composite. The orientation is expressed by a 3x3 symmetric tensor. The terms are denoted as a_{ij} and the information is stored at the integration points of the mesh (Fig 3.19b). Fiber orientation tensors can be imported for first order continuum and shell elements. The element's orientation is constant over it (or over its layer for shell elements) and is defined at its center.

After the mapping process a status box appears containing shortcuts to the typical actions that should be performed afterwards: error assessment or saving the mapped data. The global error indicator compares the relative number of elements with a given value (for stress

component s_{ij} or orientation tensor component a_{ij}) between the donor mesh and the receiving mesh. The local error indicator provides information on the mapping quality for each element of the donor mesh individually.
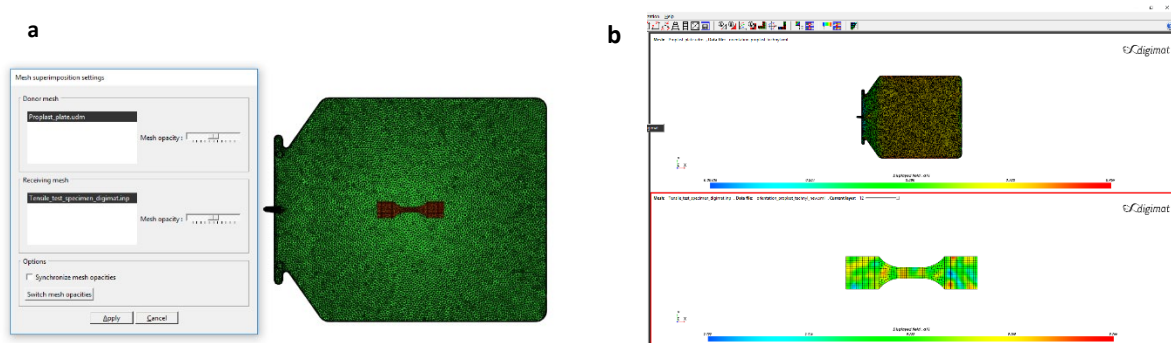
Fig. 3.19 a) Digimat map mesh superpose **b)** Mapped fiber orientation example result

3.4.3 DIGIMAT RP SOLUTION SETTINGS

The Solution settings window is available at the end of a component workflow. It enables to review the numerical settings for the analysis as well as to choose the coupling solution method to be used for the FEA run. Digimat is capable of performing three principle types of multi-scale solutions:

- o MICRO (full micro/macro multi-scale modeling)
  - Linear & nonlinear material properties
  - Micro & macro output
  - Failure & FPGF criteria at phase & composite level.
- o HYBRID (reduced micro/macro multi-scale coupling)
  - Linear & nonlinear material properties
  - Macro output
  - Failure & FPGF criteria at phase & composite level.

- o MACRO (reduced micro/macro multi-scale coupling)
    - Linear material properties
    - Macro output

MICRO SOLUTION

Choosing this method means using strong multi-scale coupling techniques. For micro solution, Digimat interactively computes material properties and communicates with the structural code at each iteration of the overall computation in order to compute the macroscopic stress response, using homogenization techniques and to update composite tangent stiffness. In no way the composite material properties are computed at the initiation of the analyses and then kept constant. The method can be applied to all different kind of anisotropic, nonlinear, strain-rate and/or temperature dependent material behavior with all failure indicators available.

HYBRID SOLUTION

Choosing the hybrid solution method means using weak multi-scale coupling techniques for linear and/or nonlinear material properties. For the hybrid solution, Digimat pre-computes macroscopic material properties which are then used in order to communicate with the structural code at each iteration of the overall computation. This method was introduced to save computation time and increase calculation robustness. It is limited to the following material behavior of two-phase composites (with or without clustering) and balanced or unbalanced woven composites with basic yarns:

- elastic,
- thermoelastic,
- viscoelastic,
- thermoviscoelastic
- elastoplastic (j2p and Drucker-Prager),
- thermoelastoplastic,
- elasto-viscoplastic,
- thermoelasto-viscoplastic,

- viscoelastic-viscoplastic

The hybrid solution method is based on the reduction of the material model to the computation of macroscopic material properties:
- (strain-rate dependent) (non)linear stress/strain curves
- (strain-rate dependent) failure indicators (stress and strain based)

In the case of material with thermal dependences, these macroscopic material properties are also temperature dependent.

The reduction technique involves a pre-processing step performed before the start of the analysis. It computes hybrid parameters that are stored at the end of the .mat file. The gain in CPU time results from solely taking into account the pre-computed macroscopic material properties during I/O operations with the FEA solver(s) in the user-defined subroutine(s).

Hybrid parameters are computed from a large number of Digimat-MF simulation on the material file chosen by the user. A given number of orientations and loadings are tested. The pre-processing step is therefore equivalent to launching a large campaign of experimental tests on various orientations and loadings. For each orientation, mesoscopic model is identified. The set of mesoscopic model defines our macroscopic model.

MACRO SOLUTION

Choosing the macro solution method means using weak multi-scale coupling techniques for linear material properties. For the macro solution, Digimat pre-computes macroscopic material properties which are then used by the structural code at each iteration of the overall computation. The method is limited to the following material behavior: elastic and thermo-elastic. Even though material properties are still communicated via the Digimat interface, there is no interactive computation of material properties during the run of the structural software. Therefore, no update of the material properties is performed between Digimat and the FE solver and only linear elastic materials can be used. Such computations are very limitative and far from being accurate for nonlinear materials which is why the usage is not very recommended.

LINEAR SOLUTION

On top of the three methods micro, hybrid and macro solutions which are available in Digimat RP to interface structural FEA software, there's a fourth method called the linear solution which makes it possible to couple Digimat with MSC Nastran, Optistruct, Permas and Abaqus without any preexisting integration of Digimat-CAE.

Digimat-RP works with these types of models just like with any other type of structural model. The main difference is that the LINEAR solution is the only coupling method available for Nastran SOL1XX, OptiStruct and PERMAS models.

Currently, the LINEAR solution only supports:

- Shell or solid elements
- Linear mechanical analyses (excluding thermal expansion phenomena) such as linear static, modal and frequency response analyses
- Linear thermo-mechanical analyses but excluding damping effects;
- Two-phase, elastic Digimat materials (OptiStruct, PERMAS and Abaqus models) or two-phase, elastic or viscoelastic Digimat materials (Nastran SOL1XX models).

The LINEAR solution only achieves a weak coupling between Digimat and the finite element model similarly to the macro solution. More particularly, the macroscopic linear properties of the Digimat materials are pre-computed prior to the finite element analysis which then runs without Digimat re-computing anything as the solution proceeds. To the contrary of the macro solution, the material properties are explicitly written to the input files of the coupled analysis instead of being communicated in real time by Digimat; the coupled model can run without Digimat, with a classical installation of the structural FEA software. The modifications Digimat-RP makes to the structural model only affect the material properties and the coordinate systems.

The other data in the structural model remain unchanged.

Chapter 4

TEST SPECIMEN

4.1 INTRODUCTION AND WORKFLOW

As we anticipated, there is a high interest in the automotive sector to use composite material made parts to ensure low weight, corrosion resistance, good energy and vibration absorption, complex shape molding. For this reason, it is investigated a method to improve the numerical simulation accuracy that could account for the composite material anisotropy and different mechanical behavior according to the fiber orientation in the thickness of the part.

The proposed method to be validated is shown in Fig 4.1. We start from a chosen material with known constitutive parameters and mechanical properties obtained by experimental testing and in parallel a virtual model is arranged. The virtual line proceeds by simulating the injection of a test plate of the desired material in Autodesk Moldflow Insight with the following extraction of the fiber orientation result that will be mapped in Digimat Map on a structural mesh. The structural mesh is the Abaqus model of a standardized test specimen subjected to traction. With all this "ingredients" the coupled analysis Digimat-Abaqus can be launched in the Digimat-RP module locally or on a server. The only missing input is the material "card" for the simulation. In general and future use the material card will be a validated asset available for the company, obtained from the experimenting department or requested to the material supplier; in this case of "study" the card is reverse engineered in Digimat-MX starting from tested specimens.
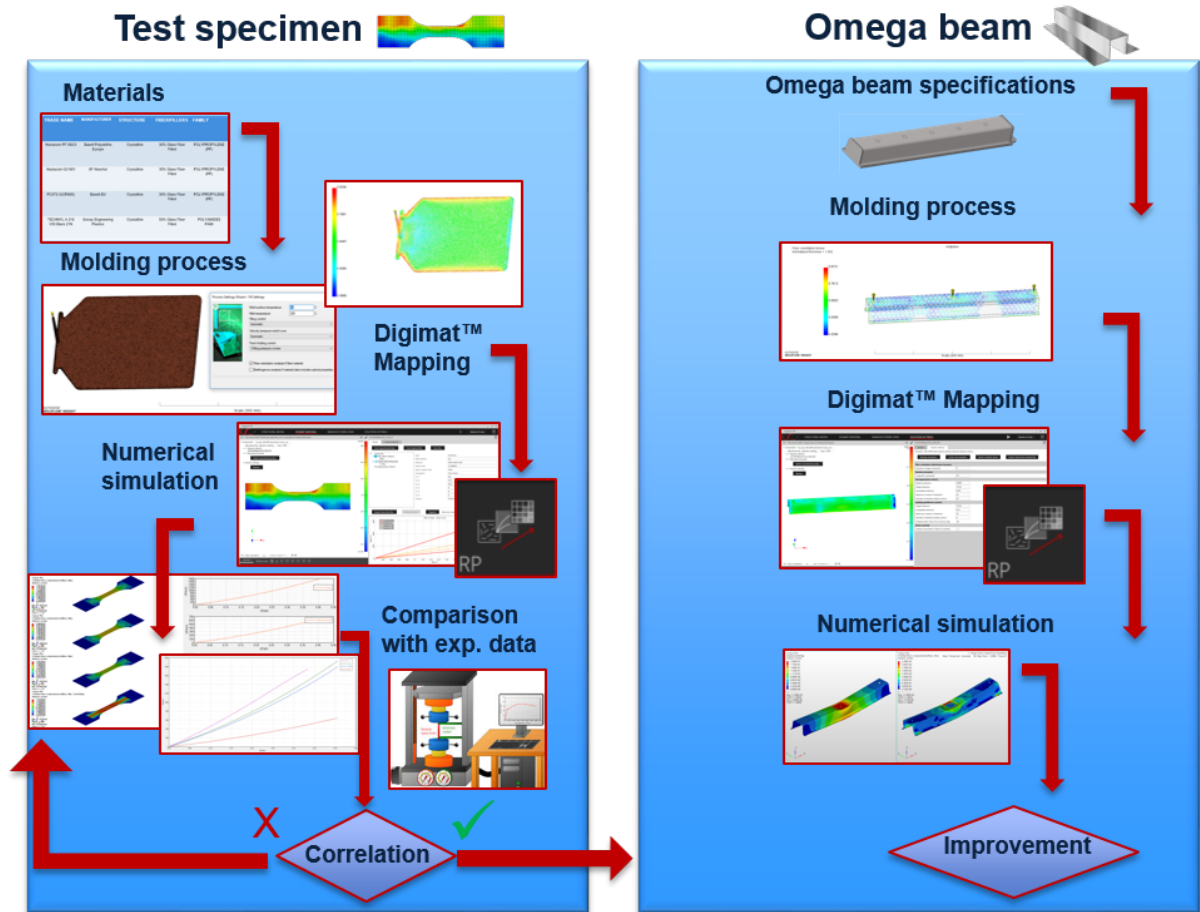
Fig. 4.1 methodology validation workflow

If the numerical coupled simulation gives results in line with the experimental ones the methodology can be further tested with a more complex component like an omega beam (chapter 5).

4.2 EXPERIMENTAL TESTS

The experimental tests were conducted on a 30% glass fiber reinforced Polypropylene homopolymer with low melt flow, high stiffness, low coefficient of linear thermal expansion and low creep under load at elevated temperature.

Typical Properties	Nominal Value	Units	Test Method
Physical			
Melt Flow Rate, (230 °C/5.0 kg)	5	g/10 min	ISO 1133-1
Melt Volume Flow Rate, (230 °C/5.0 kg)	5	cm³/10 min	ISO 1133-1
Density, (23 °C)	1.15	g/cm³	ISO 1183-1/A
Mechanical			
Tensile Modulus, (23 °C)	6500	MPa	ISO 527-1, -2
Tensile Stress at Break, (23 °C)	90	MPa	ISO 527-1, -2
Tensile Strain at Break, (23 °C)	3.5	%	ISO 527-1, -2
Impact			
Charpy Impact Strength - Notched, (23 °C)	11	kJ/m²	ISO 179-1/1eA
Charpy Impact Strength - Unnotched, (23 °C)	48	kJ/m²	ISO 179-1/1eU
Thermal			
Vicat Softening Temperature, (B50)	140	°C	ISO 306
Deflection Temperature Under Load			
(0.45 MPa, Unannealed)	155	°C	ISO 75B-1, -2
(1.80 MPa, Unannealed)	140	°C	ISO 75A-1, -2
Flammable			
Flame Rating - UL			
(1.5 mm)	HB		UL 94
(3.0 mm)	HB		UL 94

Tab. 4.2 PP GF30 datasheet

The test specimen was cut from a 3mm thick injected test plate (Fig. 4.3a) with standard quotes (Fig 4.3b) obeying the ASTM D1022 specifications for polymers tensile test.

a

b
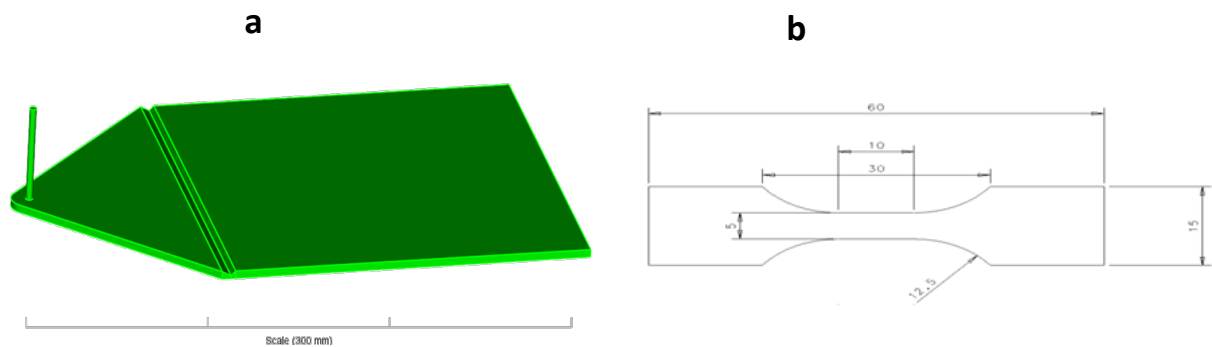
Fig 4.3 a) injected test plate **b)** ASTM D1022 specimen dimension

The specimen dimensions are also reported accurately in Tab. 4.4.

	Specimen type (dimension in mm)	
t_3	Overall lenght	60
t_1	Lenght of narrow parallel-sided portions	10
r	Radius	12.5
t_2	Distance between broad parallel-sided portions	30
b_2	Width at ends	15
b_1	Width at narrow portion	5
l_1	Preferred thickness	3

Tab. 4.4 ASTM D1022 specimen dimensions

The tensile test was led by GML, the company's material department, with a hydro pulse Schenck equipment and digital image correlation to measure the displacement. The digital image correlation apparatus is composed of a tensile test machine, a light source and a high-speed camera that can trace specific points on the specimen to give accurate results and true stress true strain curves.

The specimens are extracted in different conditions: two orientation angles 90° and 0° (see Fig 4.5a), different temperatures and strain rates. From previous know-how acquired with crystallographic inspection on similar specimens (Fig 4.5c), the three principal components of the orientation tensor a_{11}, a_{22} and a_{33} should have an evolution in thickness similar to Fig 4.5b: high orientation in the skin and sub-skin layers and a rotated orientation in the core. This is the reason why physically the stress-strain curves differ according to the specimen cutting orientation from the test plate.
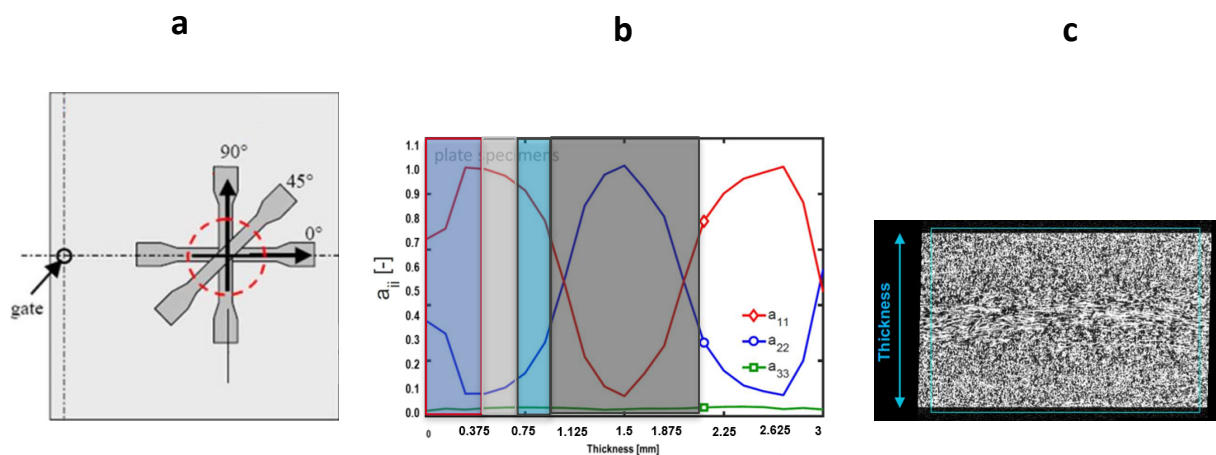
Fig 4.5 a) specimen orientation angle **b)** fiber orientation tensor in the thickness **c)** common microstructure

In this thesis data referring to 23° at quasi static strain rate will be used to correlate the coupled numerical simulation with the actual data, see Fig 4.6.

a
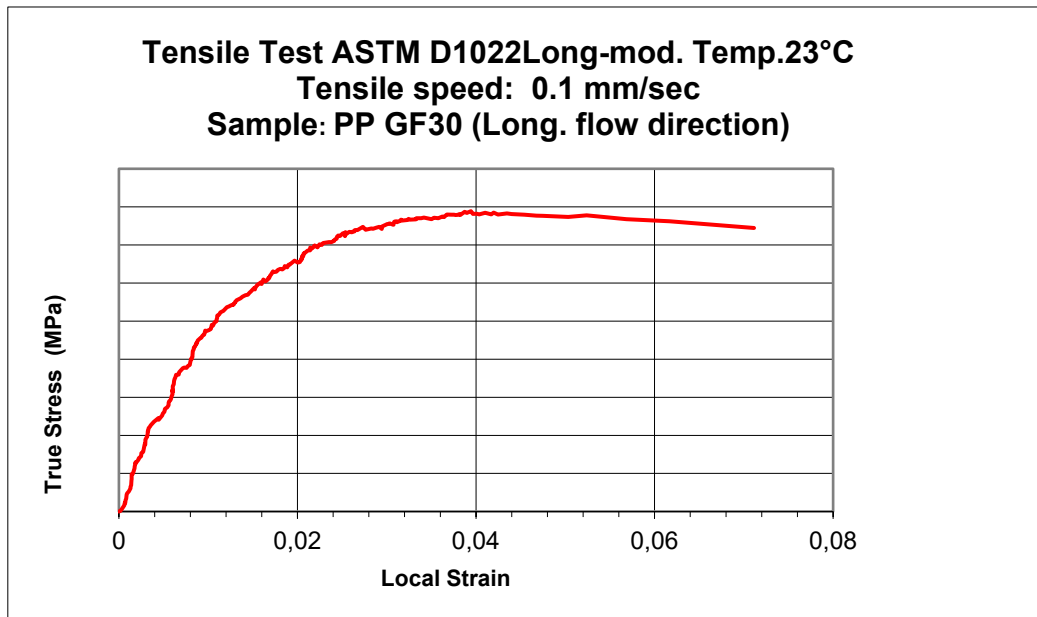
b
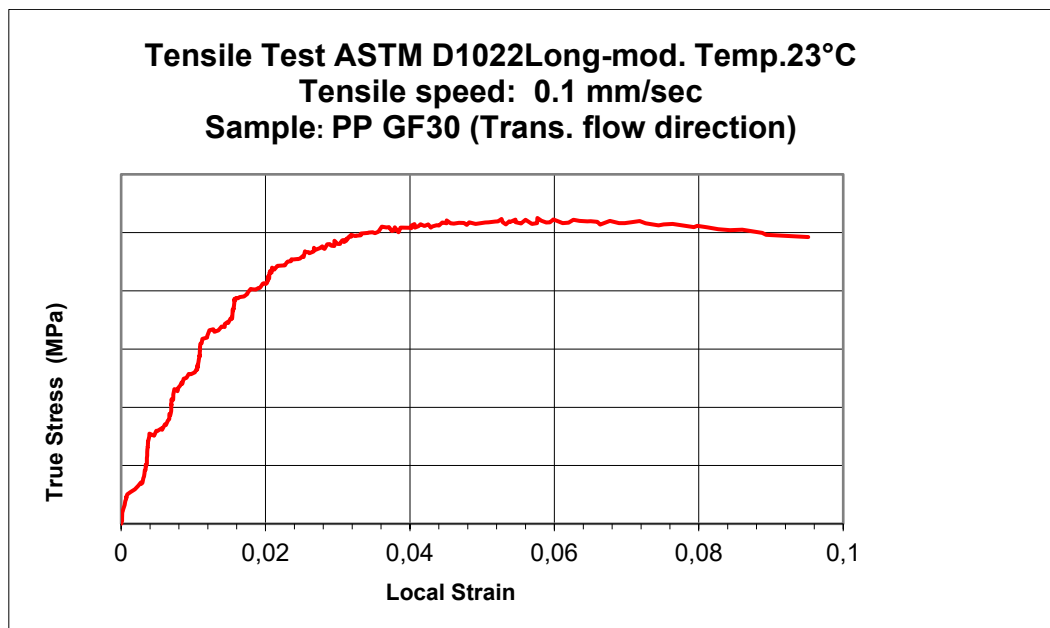
Fig 4.6 a) Longitudinal true stress-true strain curve **b)** transversal true stress-true strain curve

This ends the experimental side of the method. In parallel the virtual models that will bring us to the final coupled analysis are prepared starting from the injection molding simulation.

4.3 VIRTUAL MODEL

The virtual model in Autodesk Moldflow is composed of a 3d geometry of the test plate that will be 3d meshed trying to keep a consistent reference system orientation with the Abaqus model, which is another item necessary to the coupled analysis. Next material, gate location and process settings are chosen to guarantee a proper injection see Fig 4.7.

TRADE NAME	MOLD TEMP [C°]	MELT TEMP [C°]	FILLING CONTROL : FLOW RATE [cm^3/s]
PP GF30	35	230	80
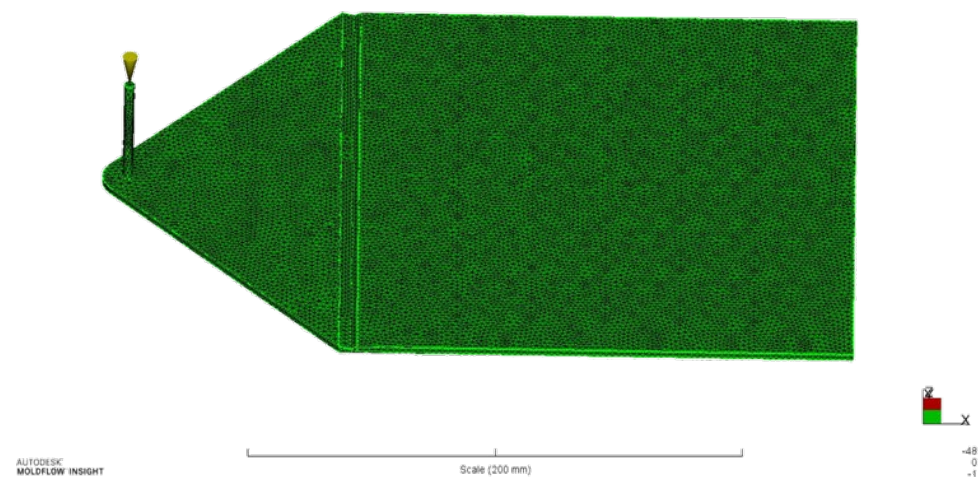
Fig 4.7 Moldflow model

Amongst the outputs of this simulation the average (over the thickness) fiber orientation expressed as a value between 0 and 1 of the first principal direction (flow main direction) is extrapolated as an .xml file and shown in the contour of Fig. 4.8. This information needs to be mapped on the structural mesh of an Abaqus model (Fig 4.10) and the proper module to do

the job is Digimat-MAP (Fig. 4.11). The orientation is mathematically a 3x3 symmetric tensor; the terms are denoted as a_{ij} and the information is stored at the integration points of the mesh. Fiber orientation tensors can be imported for first order continuum and shell elements. The element's orientation is constant over it (or over its layer for shell elements) and is defined at its center. So the central part of the test plate (Fig. 4.9), where a reasonably constant orientation is found, is chosen to be the donor in Digimat-MAP for some test specimens in transversal and longitudinal direction, utilizing the integration point / node to integration point algorithm described in Chapter 3.
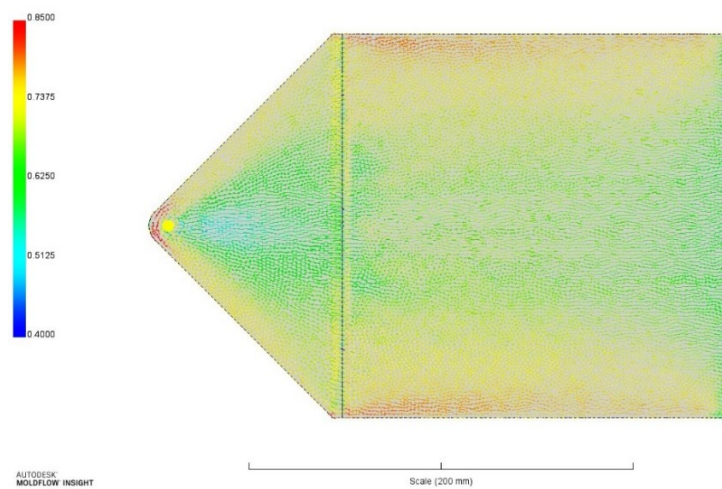
Fig 4.8 Average fiber orientation contour
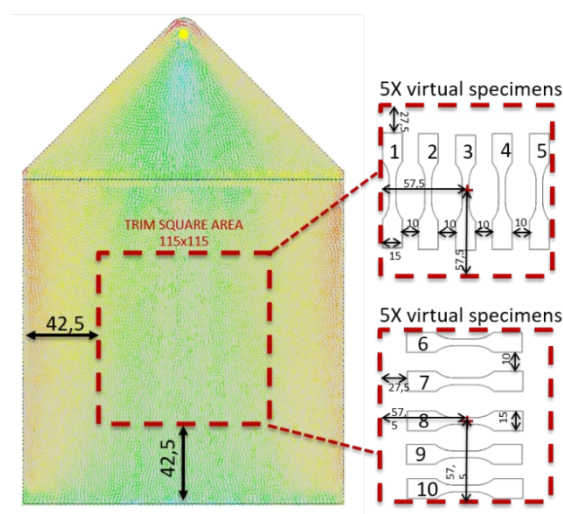
Fig 4.9 Mapping region
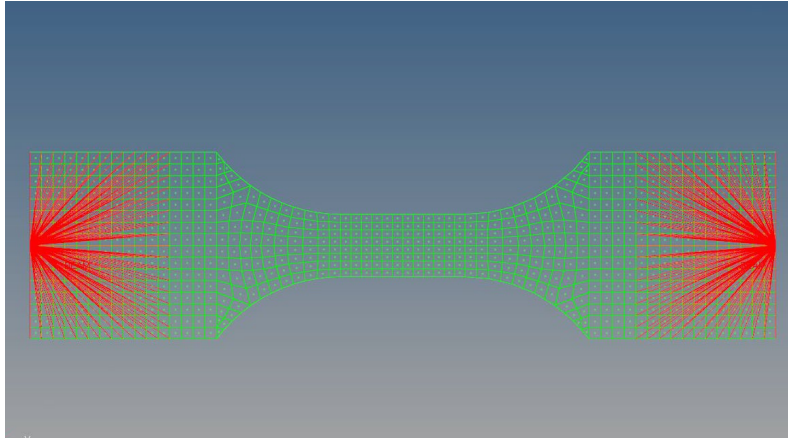
Fig 4.10 Abaqus specimen model
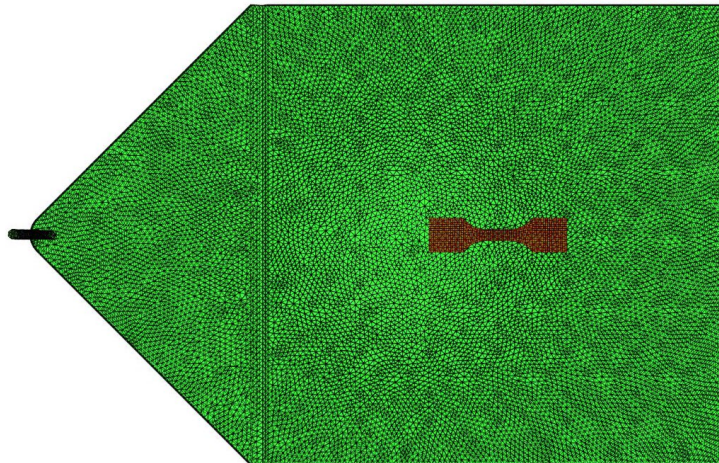
Fig 4.11 Digimat-MAP superpose mesh

The Abaqus model contains the shell mesh constrained at the extremities in all DOF except the ones free to replicate the tensile test at slow strain rate condition. At this point the only element missing to launch the coupled analysis is a material card for Digimat-RP.

4.4 COUPLED ANALYSIS

The material card will be reverse- engineered starting from experimental data in the dedicated module of Digimat-MX, the material database solution. In the importation the specimen must be specified according to the standard, creating a new preset if not already available (Fig 4.12). The strain rate chosen was the lower one since the modeling target is a static analysis.

Fig 4.12 Data import according to standards

For chopped fiber (short), experimental data must be loaded in the format of stress-strain curves. Selected stress-strain curves must correspond to a single grade, and to a single temperature as it is in our case with the 0° and 90° curves at 23°C.

The material model of choice will be the non-linear stiffness plus failure J2 plasticity model

combined with FPGF failure. This means that the material card creation process is an optimization algorithm that will target the experimental data operating on material parameters in two steps:

- Reverse engineering the constitutive law of the material in terms of Young's module, Poisson's ration, yield stress, hardening modulus and exponent, linear hardening modulus, plastic strain multiplier, aspect ratio.
- Reverse engineering of a failure indicator by means of the parameters axial tensile strength, in-plane tensile strength, transverse shear strength for Tsai-Hill 3D Transversely Isotropic strain-based failure criteria (chapter 2.6.2).

At this point the software algorithm can run the process to obtain the material card as a Digimat .daf analysis file. This process is not definitive, it requires various degrees of optimization acting on parameters and also on the optional microstructure tab to better approximate the experimental curves. The parameters are always varied keeping consistency with the physical specifications of the real material grade, utilizing the company know-how. In Fig 4.13 there's a picture of the process work in progress.
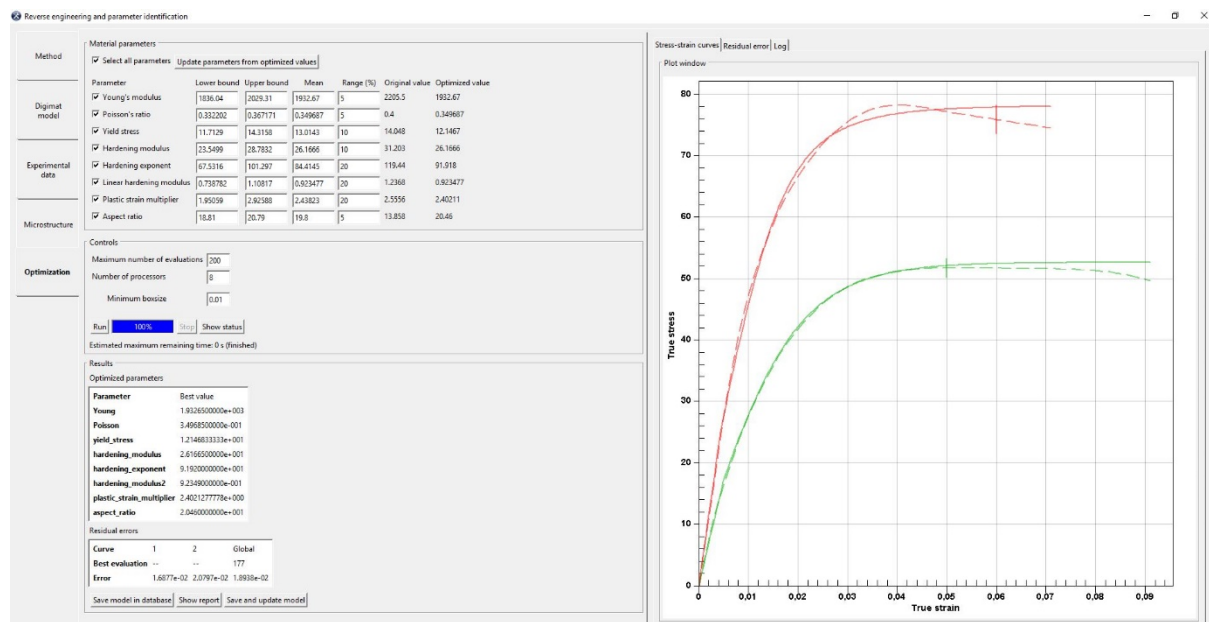
Fig 4.13 Material card optimization in progress

At the end of the process a material card revision one is obtained and ready to be used in the final coupled analysis in Digimat-RP where the Abaqus mesh marries the fiber orientation information coming from manufacturing process before being launched to virtually simulate a tensile test. This first card attempt is far from acceptable both in replicating the experimental stress and strains and failure onset. Fig 4.14 shows the Digimat-RP window and the final result with the coupled analysis performed on the various longitudinal and transversal specimens with a resulting bad correlation. The solution method for Digimat-RP is set on "hybrid solution" with First Pseudo-Grain Failure (FPGF) failure method as described in Chapters 3.4.3 and 2.6.3.
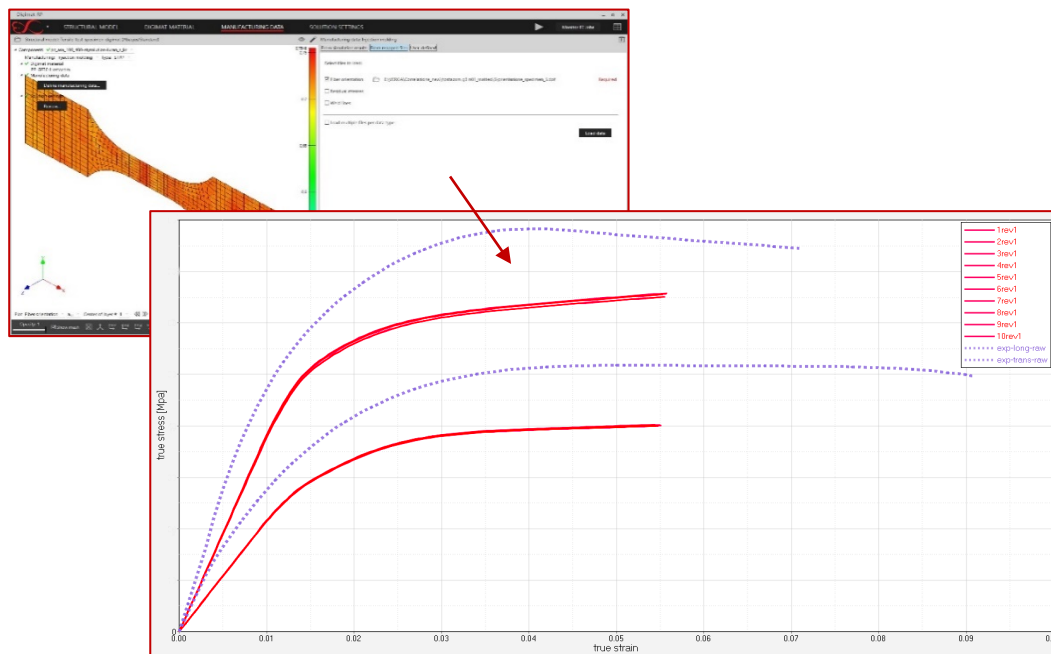
Fig 4.14 Revision one coupled analysis

The card optimization process is iterated trough new attempts (up to revision five) while investigating the issues relevant to guarantee a good final result. First methodology modification is concerning the initial stress-strain curves fed to Digimat-MX. To allow an efficient work of the optimization algorithm you need to clean the curves from the small metrology oscillations coming from experimental lab. For this reason, the elastic and plastic portion of the curves are mathematically fitted with a linear and a polynomial approximation (Fig 4.15 – 4.16).

Tensile Test ASTM D1022 Long-mod. Temp.23°C
Tensile speed: 0.1 mm/sec
Sample: PP GF30 (Long. flow direction)
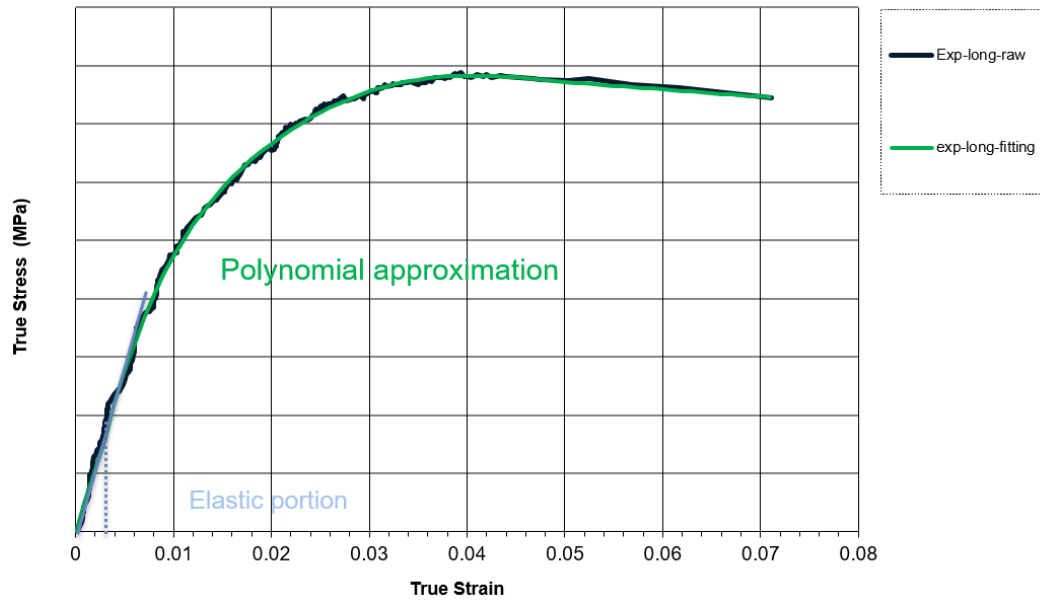
Fig 4.15 Longitudinal experimental specimen data fitting

Tensile Test ASTM D1022 Long-mod. Temp.23°C
Tensile speed: 0.1 mm/sec
Sample: PP GF30 (Transv. flow direction)
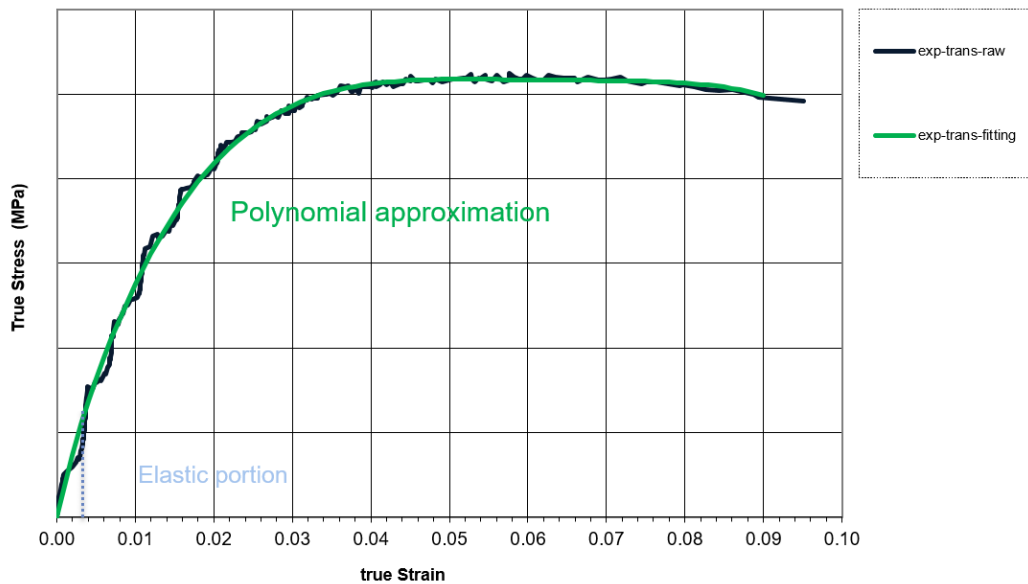
Fig 4.16 Transversal experimental specimen data fitting

137

In addition to this also the microstructure optional tab in the reverse engineering process is tweaked to better represent reality. In particular at material card revision four the microstructure that presents different fiber orientation is described by dividing the thickness of the specimen in only "skin", "intermediate" and "core" while in revision five the layers are multiplied up to eleven with orientation vector components taken directly from the injection molding simulation, since this information is available and easily accessible (Fig 4.17).
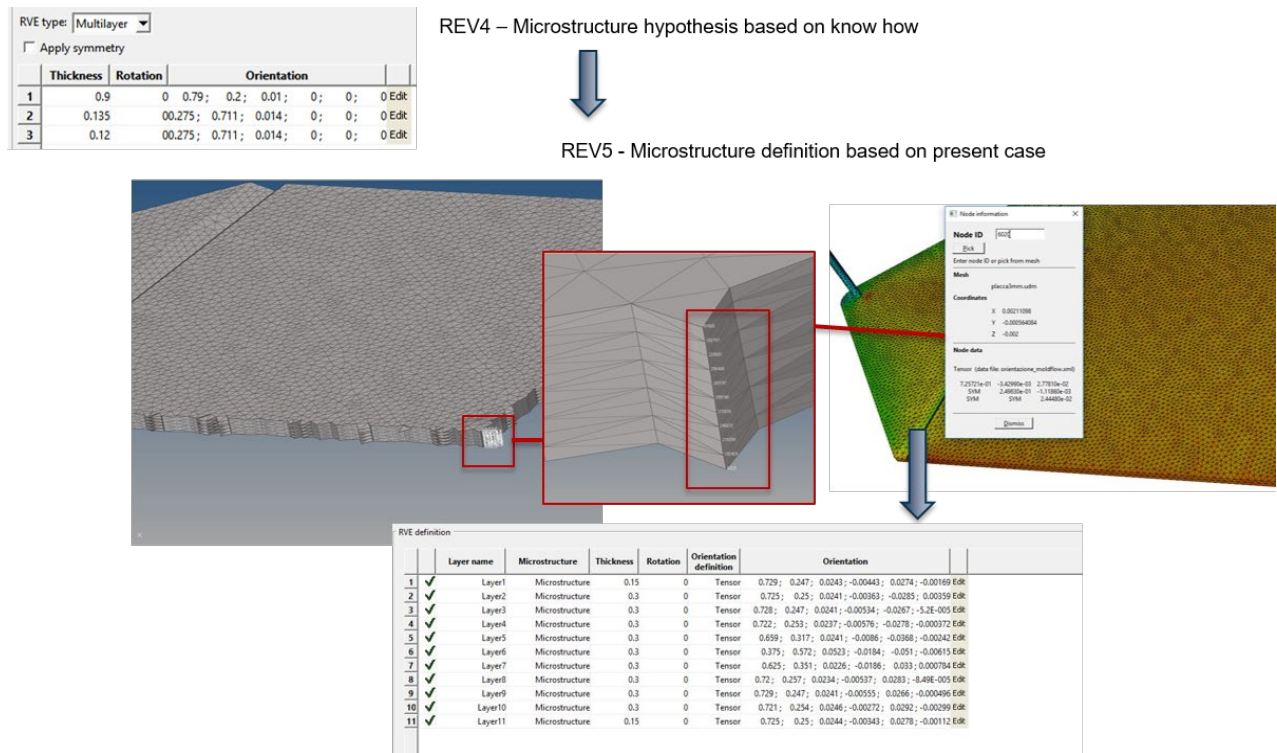
Fig 4.17 Microstructure improved description in reverse engineering

Lastly with these improvements and some manual calibration the final material card revision five is obtained with the expected performance of Fig 4.18, which is Digimat-MF internal tensile test simulation tool. In Fig 4.19 instead there's the result coming from the coupled analysis with Abaqus tensile test model and specimens' contour. You can see that both the longitudinal and transversal experimental curves are well approximated by the stress-strain curves measured on the virtual specimen. The failure index also reaches the unity in a point close to the original experimental failure strain. This means that at this level the methodology

can implement proficiently the fiber orientation actual arrangement and improve the numerical simulation guaranteeing the proper material response region by region.
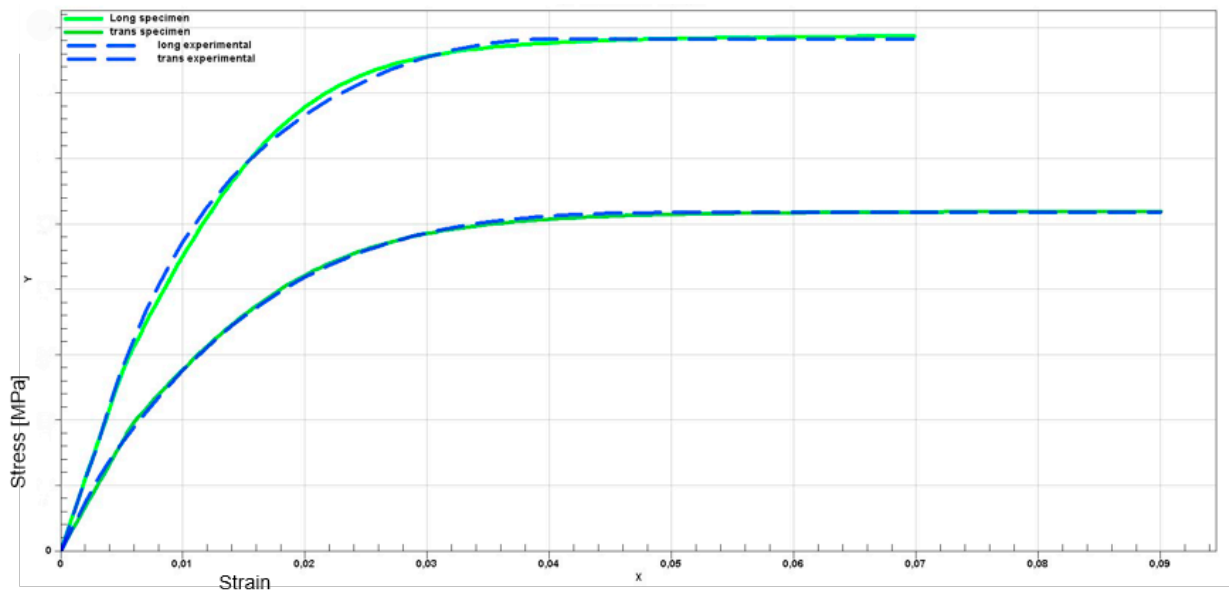
Fig 4.18 Final material card
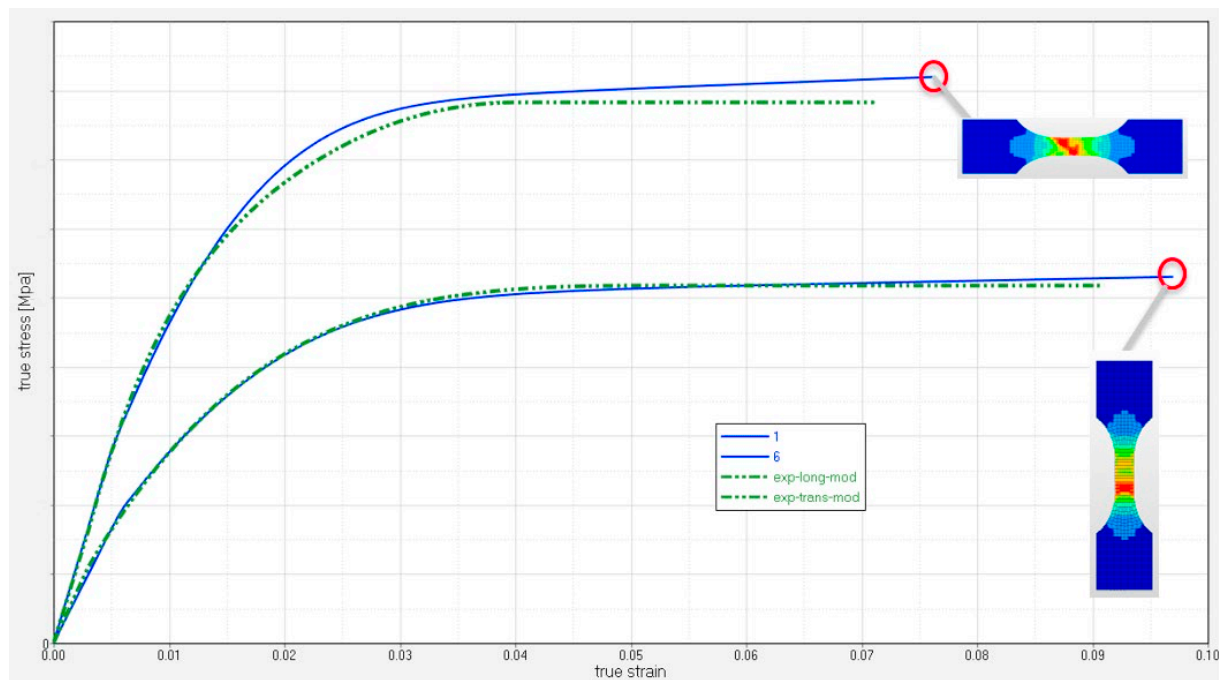
Fig 4.19 Final coupled analysis of the virtual tensile test

4.5 FINAL CONSIDERATIONS

Once the methodology is proven effective a new effort is made to extend the conclusion of the work: choosing from the vast database of Digimat-MX material analysis files, the virtual Abaqus-Digimat tensile test coupled analysis with information coming from Moldflow injection simulation is redone to evaluate the variability of behavior in the trim area of a test plate. The polymeric material of choice is in Tab 4.20

NAME	STRUCTURE	FIBER/FILLERS	FAMILY
PA6.6 GF50	Crystalline	50% Glass Fiber Filled	Polyamides

Tab 4.20 Pa6.6 GF50 specs

The methodology is the same applied before, with the mapping phase executed on 14 different specimen positions in the trim square area of 115mm of this new test plate utilized in the company. In addition to the longitudinal and transversal extraction direction, four specimens are rotated of 30° with respect to the first principal direction, see Fig 4.21. The contour area showing the average fiber orientation can be dividend in a red highly oriented zone due to injection molding border effect, a yellow area of transition and a large green area with moderately high orientation in flow direction. This latest area is large enough to guarantee the possibility to cut and extract a good number of specimens for experimental testing on an unknown material. The coupled analysis Abaqus-Digimat RP simulating the tensile test confirms that the variability in this area, where the injection molding predicts a homogenous fiber orientation, is indeed not affecting considerably the stress-strain behavior (Fig. 4.22).
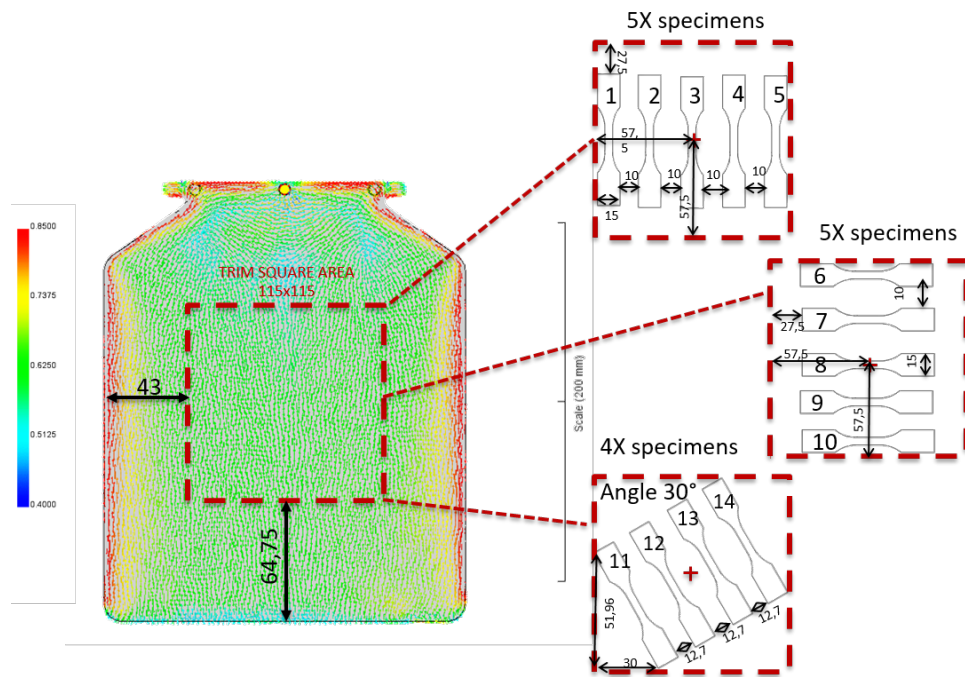
Fig 4.21 Fiber orientation and trim square area candidate
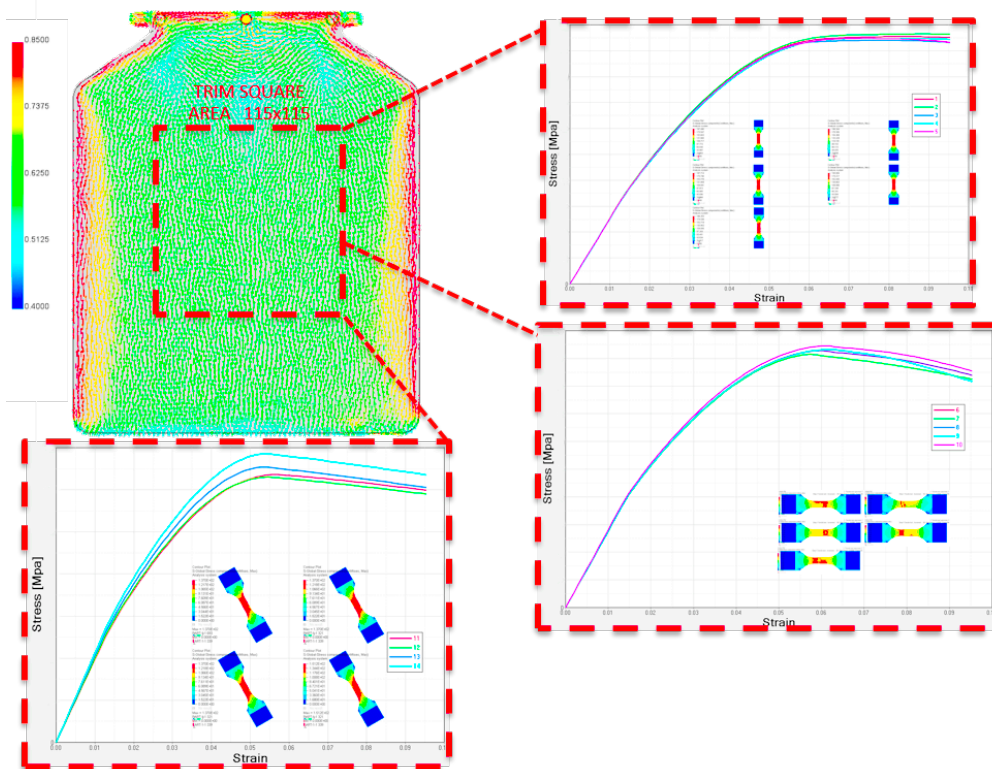
Fig 4.22 Low variability effect in the trim square area

To conclude the present chapter, the material card revision five developed for the PP GF30 is validated and used as input for the next chapter. To make the methodology efficient in case of a material not present in the database, it would be best if the material testing department could smooth and regularize the experimental true stress and strain curve; a square trim area is suggested for glass fiber reinforced composites similar to our test. In addition, it would be interesting to request from the material testing laboratory a third (or more) inclined experimental curve (for example at 30° or 60°) to feed as an input to Digimat-MX module in order to investigate the benefit on the robustness of the reverse engineering of the card and on the final correlation with a coupled analysis.

Chapter 5

OMEGA BEAM

5.1 INTRODUCTION

Starting from the validated card material of chapter 4 the methodology is extended to a more complex component: an injection molded omega beam made of the same polypropylene. The component is made in a single shot without fastenings even if it can be conceptually viewed as a ribbed internal part and an omega beam external cover (Fig 5.1).

Beam

+

Ribs

Single-shot molded component
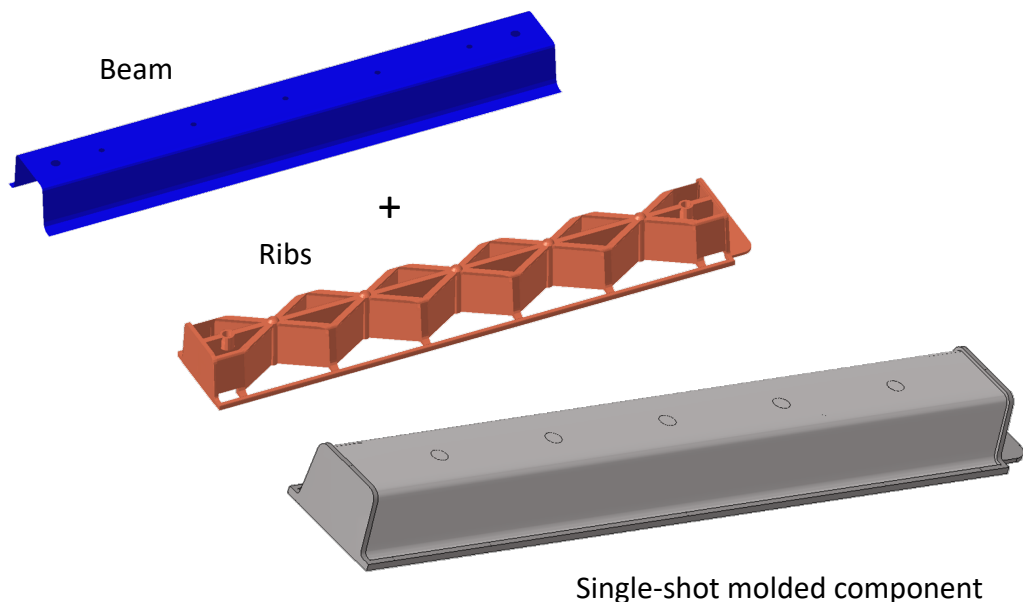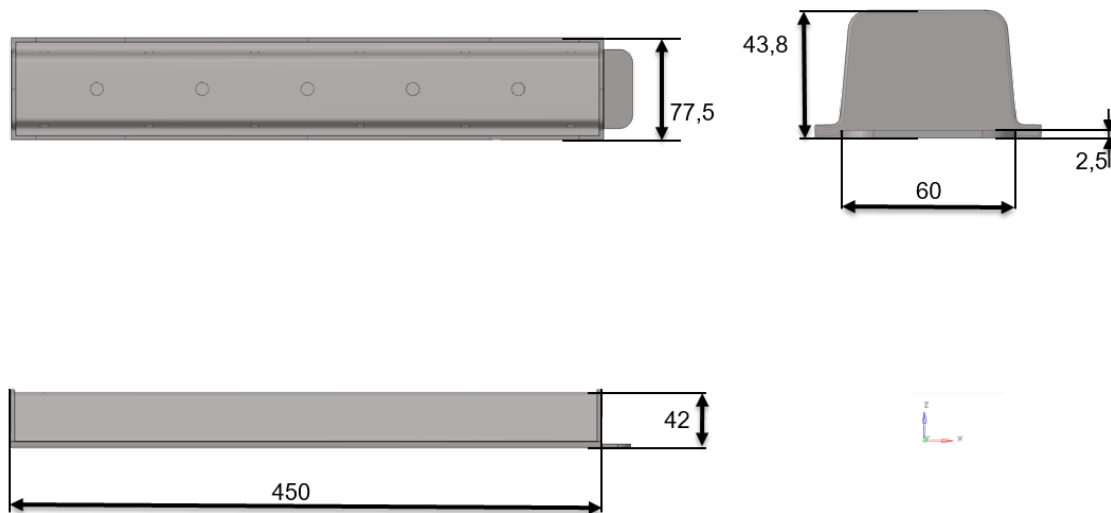
Fig 5.1 Omega beam

Fig 5.2 Omega beam dimensions

Fig 5.3 Omega beam finished part

In Fig 5.2 and Fig 5.3 there are dimensions and final realization of the part by the supplier. The holes on the side are due to manufacturing constraints; they will be reproduced also in the cad model. As before the methodology is to start from the simulation of the molding process to acquire the fiber orientation information; then it can be mapped on the structural mesh to virtually observe the refined accuracy of the result given by the more realistic modeling on a natural frequency extraction analysis and on a three point bending flexural test. The experimental correlation was not performed.

5.2 MOLDFLOW SIMULATION

The Moldflow simulation of the single gate injection molding filling phase was done with a 3d mesh and two possible parameters sets: one with supplier constraints (Fig 5.4) and one to guarantee complete filling (Fig 5.5). The final result on fiber orientation is not changing relevantly in both cases and is reported in Fig 5.6. The shape complexity determines a considerable variation in fiber orientation according to the examined region of the component. This can foresee a relevance in the application of the multi-scale approach to have a realistic response of the material.
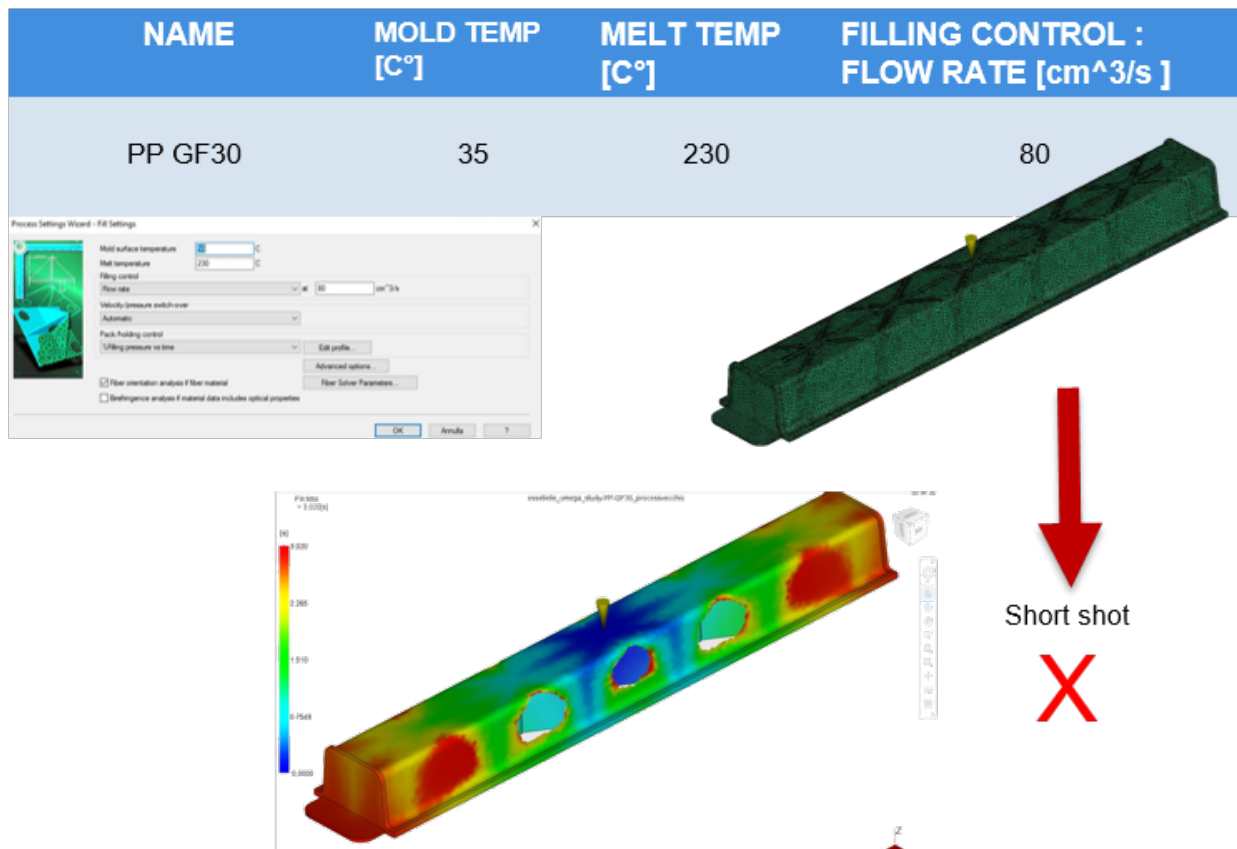
Fig 5.4 Filling simulation – short shot

NAME	MOLD TEMP [C°]	MELT TEMP [C°]	FILLING CONTROL : FLOW RATE [cm^3/s]
PP GF30	80	280	automatic
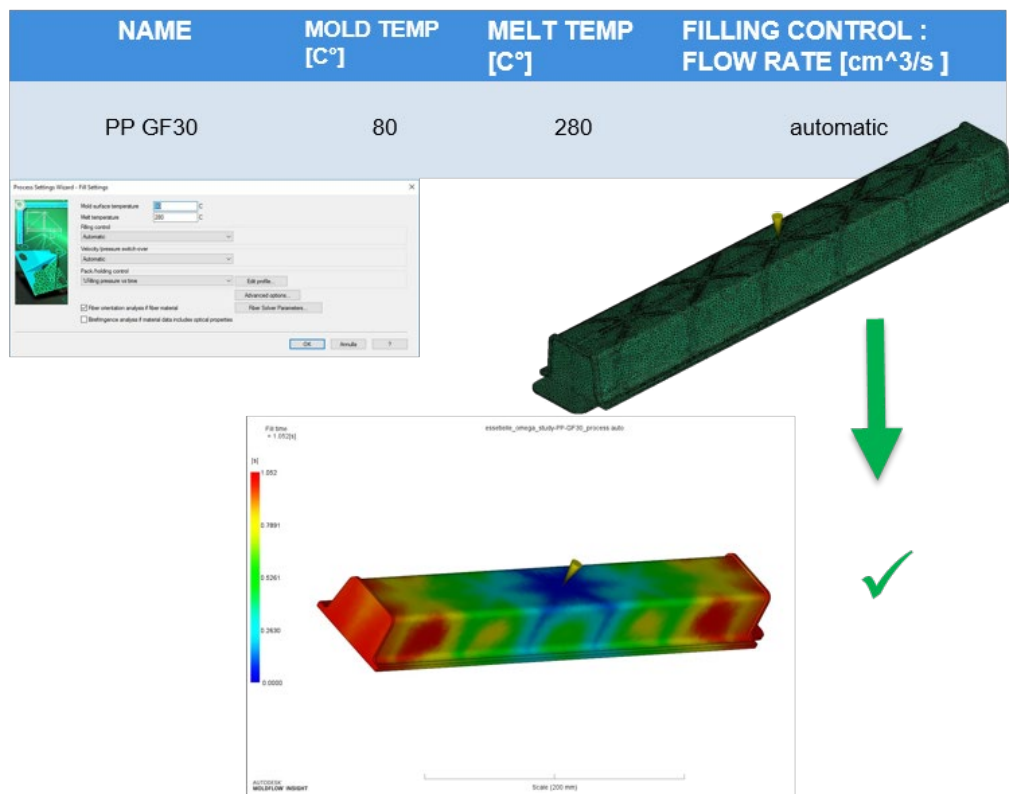
Fig 5.5 Filling simulation – feasible design
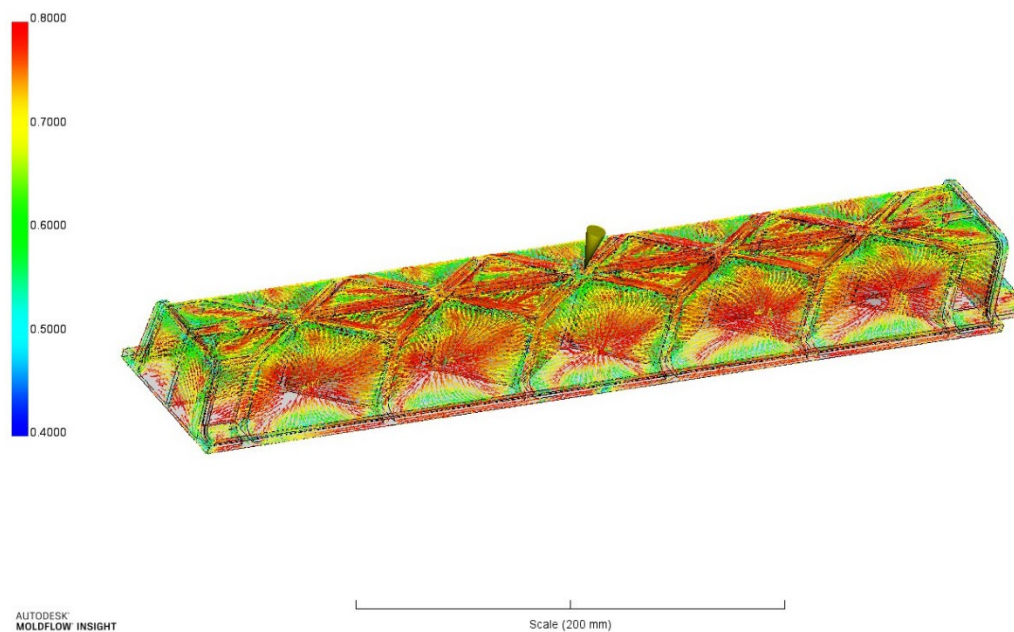
Fig. 5.6 Average fiber orientation result

5.3 MODAL ANALYSIS

An interesting type of analysis available that can be executed in coupling condition between Abaqus and Digimat is the frequency extraction procedure that in Abaqus is performed extracting the eigenvalues to calculate the natural frequencies and the corresponding mode shapes of a system.

The eigenvalue problem for the natural frequencies of an undamped finite element model is

$$(-\omega^2 M^{\mathrm{MN}} + K^{\mathrm{MN}})\phi^N = 0 \qquad (5.1)$$

Where M^{MN} is the mass matrix (which is symmetric and positive definite), K^{MN} is the stiffness matrix (which includes initial stiffness effects if the base state included the effects of nonlinear geometry, ϕ^N is a linear perturbation procedure and M an N are degrees of freedom.

When K^{MN} is positive definite, all eigenvalues are positive. Rigid body modes and instabilities cause K^{MN} to be indefinite. Rigid body modes produce zero eigenvalues. Instabilities produce negative eigenvalues and occur when you include initial stress effects. Abaqus/Standard solves the eigenfrequency problem only for symmetric matrices. The Abaqus/Standard default eigenvalue extraction method is the Lanczos one; for this you need to provide the maximum frequency of interest or the number of eigenvalues required.

The Abaqus mesh for the omega beam is done with C3D10M quadratic tetrahedral elements; they are 'modified' formulation elements using bilinear interpolation and hence, they are not a true second-order element. Basically, this means that C3D10M will be unable to capture curvature as smoothly as C3D10 elements but on the contrary a significant improvement in contact results when used with finite sliding, node to surface formulation and direct enforcement method is obtainable.

In Fig 5.7 there's the Abaqus 3D meshed component, in Fig 5.8 the beam is mapped with fiber orientations with the help of Digimat-MAP.

The test is conducted in this way: the first five natural frequencies of different assigned material models are compared with each other and in particular with the model that will benefit of the multi-scale approach with mapped fiber orientation.
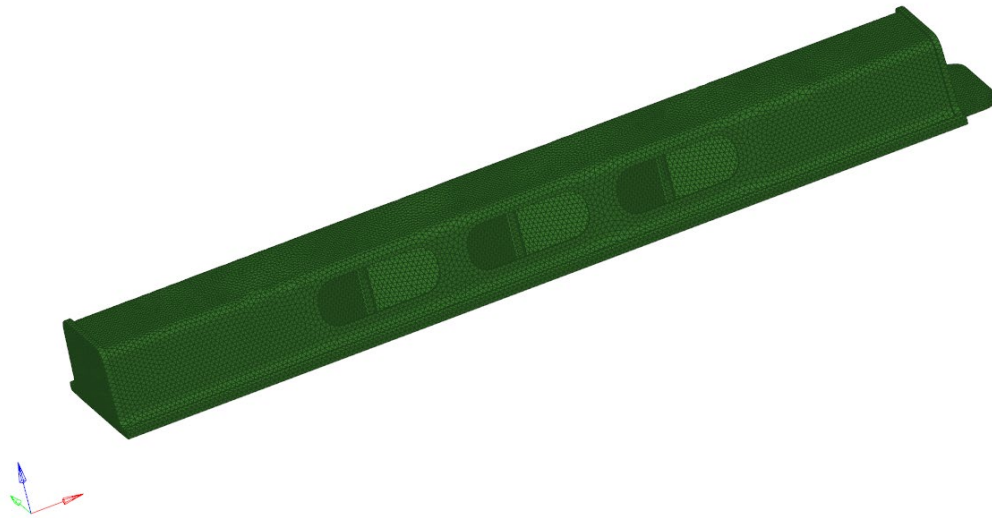
Fig. 5.7 Abaqus meshed omega beam
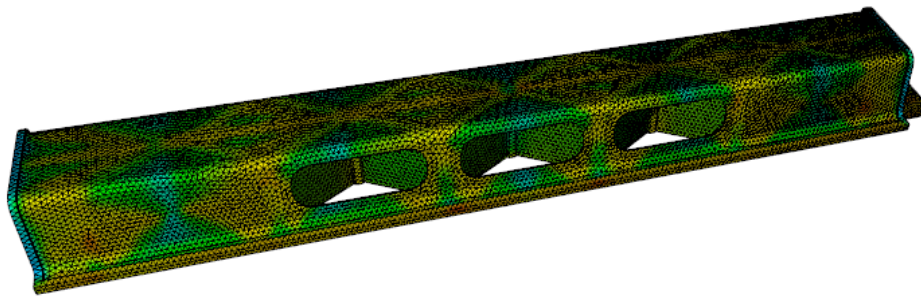
Fig. 5.8 Omega beam mapped in Digimat-MAP

The models simulated with "classical" approach have fixed assigned material with this scheme:

- Elastic isotropic material with Young's modulus E=3650 Mpa to represent a simulation with fibers with poor alignment with respect to principal flow during injection.
- Elastic isotropic material with Young's modulus E=4550 Mpa which corresponds to 0.7x the elastic modulus obtained in EN ISO 527-1 traction tests. This is an indicative

value used in "classical" design approach.

- Elastic isotropic material with Young's modulus E=5387 Mpa to represent a simulation with fibers with medium alignment with respect to principal flow during injection.

- Elastic isotropic material with Young's modulus E=6500 Mpa which corresponds to the elastic modulus obtained in EN ISO 527-1 traction tests. This is an indicative value used to impose a high fiber orientation and consequently mechanical properties in a "classical" approach

- Multi-scale approach with hybrid solution in Digimat-RP.

The calculations are done both for a complete filling beam (Fig 5.9) and for a short-shot one (Fig 5.10). It can be easily seen that with the multi-scale approach method the numerical simulation gives a realistic "midway" result (green arrows) on the natural frequencies, making clear the advantage of using this refined methodology.
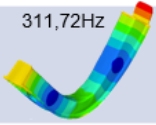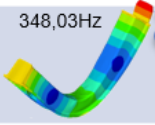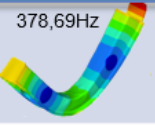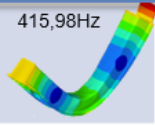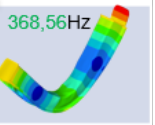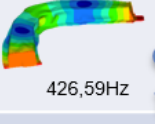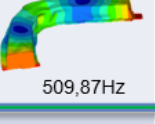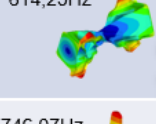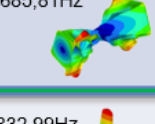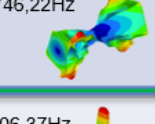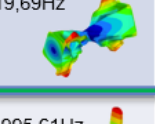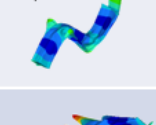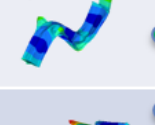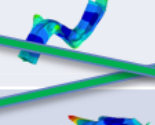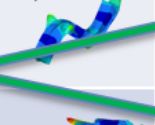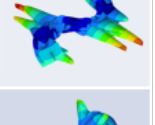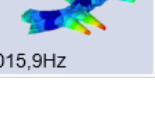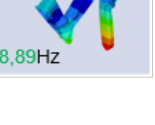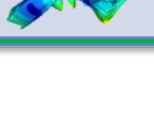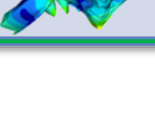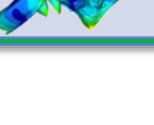
material hyp. / Vibration modes	Elastic isotropic Trans fiber E=3650Mpa	Elastic isotropic E=4550Mpa (0,7*iso 527-1)	Elastic isotropic Long fiber E=5387Mpa	Elastic isotropic E=6500Mpa (iso 527-1)	Digimat material card + moldflow orientation
1st nat freq	311,72Hz	348,03Hz	378,69Hz	415,98Hz	368,56Hz
2nd nat freq	382,08Hz	426,59Hz	464,17Hz	509,87Hz	435,49Hz
3rd nat freq	614,25Hz	685,81Hz	746,22Hz	819,69Hz	684,17Hz
4th nat freq	746,07Hz	832,99Hz	906,37Hz	995,61Hz	859,86Hz
5th nat freq	761,25Hz	849,93Hz	924,81Hz	1015,9Hz	878,89Hz

Fig. 5.9 Natural frequency extraction for complete filling beam
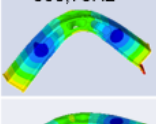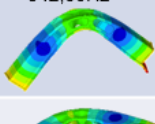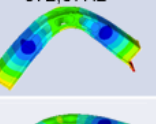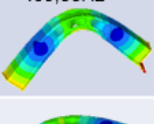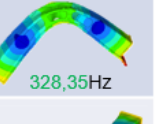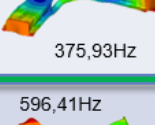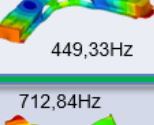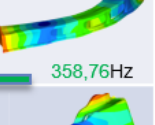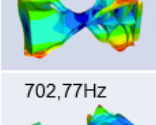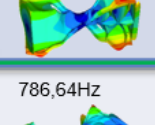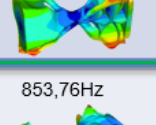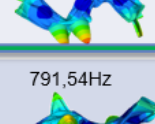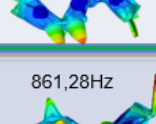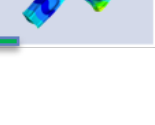
material hyp. / Vibration modes	Elastic isotropic Trans fiber E=3650Mpa	Elastic isotropic E=4550Mpa (0,7*iso 527-1)	Elastic isotropic Long fiber E=5387Mpa	Elastic isotropic E=6500Mpa (iso 527-1)	Digimat material card + moldflow orientation
1st nat freq	306,76Hz	342,50Hz	372,67Hz	409,36Hz	328,35Hz
2nd nat freq	336,71Hz	375,93Hz	409,05Hz	449,33Hz	358,76Hz
3rd nat freq	534,17Hz	596,41Hz	648,95Hz	712,84Hz	515,04Hz
4th nat freq	702,77Hz	786,64Hz	853,76Hz	937,82Hz	722,83Hz
5th nat freq	708,95Hz	791,54Hz	861,28Hz	946,07Hz	742,78Hz

Fig. 5.10 Natural frequency extraction for short shot beam

5.4 THREE-POINT BENDING FLEXURAL TEST

The second virtual experiment performed is a three-point bending flexural test which consists in bending the beam that is previously constrained symmetrically in two points at the extremities while loaded at the center by an impactor. The test is performed at 23° C with the impactor proceeding at 1 mm/s (quasi-static condition). A scheme is reported in Fig 5.11.
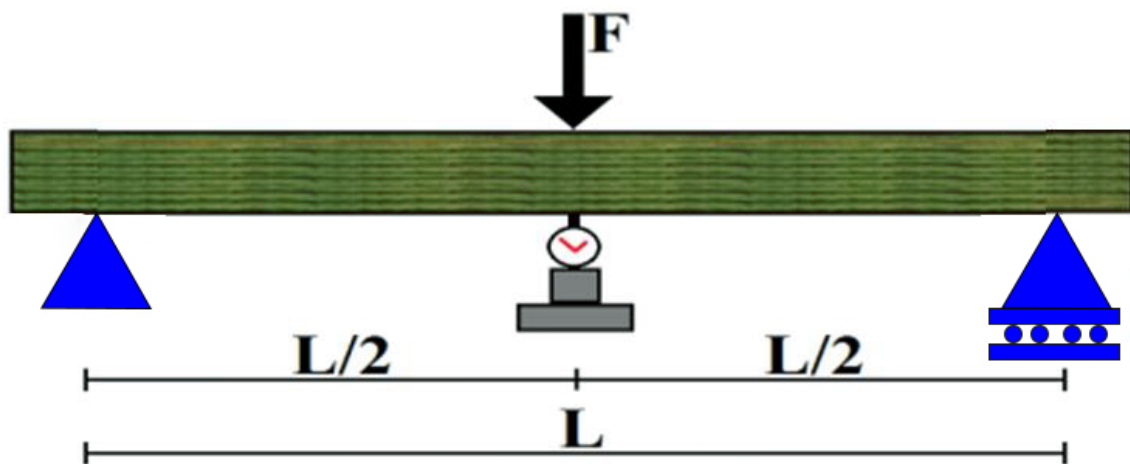
Fig. 5.11 Test scheme

The starting Abaqus file contains all the commands to simulate the virtual test as a dynamic stress/displacement analysis using explicit integration in Abaqus/Explicit plus the meshed geometry of the beam, the impactor and the supports (Fig 5.12). The beam is meshed as before with C3D10M elements; the supports and impactor are made in cast iron so they are much stiffer and stronger with respect to the beam material and, consequently, their deformation can be considered negligible. Therefore they are modeled as rigid bodies in order to reduce computational cost and time without losing accuracy. In addition, loads can be read directly by evaluating reaction forces on reference nodes that govern those rigid bodies motion. The impactor is moving downward on Z axis, the supports are constrained, the beam stands on them: we need to model contact.
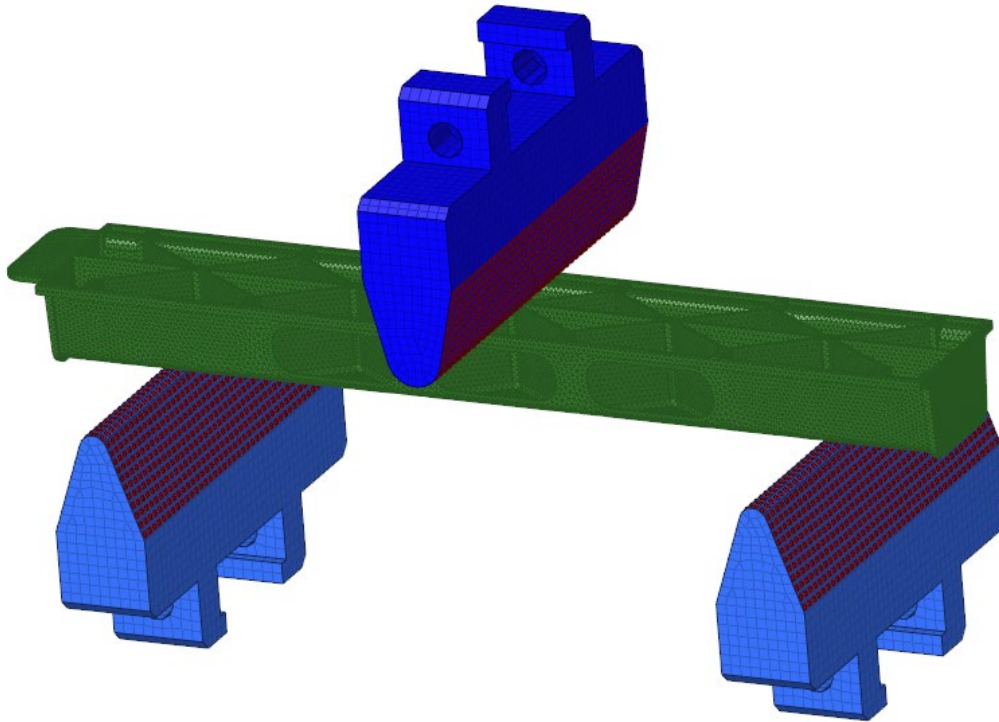
Fig. 5.12 Physical components of the test in Abaqus

Many engineering problems involve contact between two or more components. In these problems a force normal to the contacting surfaces acts on the two bodies when they touch each other. If there is friction between the surfaces, shear forces may be created that resist the tangential motion (sliding) of the bodies. The general aim of contact simulations is to identify the areas on the surfaces that are in contact and to calculate the contact pressures generated. In a finite element analysis contact conditions are a special class of discontinuous constraint, allowing forces to be transmitted from one part of the model to another. The constraint is discontinuous because it is applied only when the two surfaces are in contact. When the two surfaces separate, no constraint is applied. The analysis has to be able to detect when two surfaces are in contact and apply the contact constraints accordingly. Similarly, the analysis must be able to detect when two surfaces separate and remove the contact constraints.

Contact simulations in Abaqus/Standard can either be surface based or contact element based. Contact simulations in Abaqus/Explicit are surface based only.

Surface-based contact can utilize either the general ("automatic") contact algorithm or the contact pair algorithm. The general contact algorithm allows for a highly automated contact definition, where contact is based on an automatically generated all-inclusive surface definition. Both algorithms require specification of contact properties between surfaces (for example, friction).

Coulomb friction is a common friction model used to describe the interaction of contacting surfaces. The model characterizes the frictional behavior between the surfaces using a coefficient of friction μ.

The default friction coefficient is zero. The tangential motion is zero until the surface traction reaches a critical shear stress value, which depends on the normal contact pressure, according to the following equation:

$$\tau_{crit} = \mu p \qquad (5.2)$$

Where μ is the coefficient of friction and p is the contact pressure between the two surfaces. This equation gives the limiting frictional shear stress for the contacting surfaces. The contacting surfaces will not slip (slide relative to each other) until the shear stress across their interface equals the limiting frictional shear stress μp . For most surfaces μ is normally less than unity.

In Abaqus/Standard the discontinuity between the two states—sticking or slipping—can result in convergence problems during the simulation. In general, friction presents no additional computational difficulties for Abaqus/Explicit.

Surfaces are created with the *SURFACE option by identifying all of the element faces that form the surface. This is done in much the same way as defining distributed pressure loads. The definition of surfaces is optional for general contact because an all-inclusive element-based surface is automatically created when the *CONTACT option is used.

*SURFACE INTERACTION defines surface interaction properties. The surface interaction properties will govern any contact interactions that reference this command. *CONTACT

PROPERTY ASSIGNMENT assign contact properties for the general contact algorithm. This option is used to modify contact properties for specific contact interactions within the domain considered by general contact. It must be used in conjunction with the *CONTACT and *SURFACE INTERACTION options.

For example, if you want to apply a certain friction coefficient to all but a few surfaces in your model, you can assign a global friction coefficient and override this property for a given pair of user-defined surfaces using the *CONTACT PROPERTY ASSIGNMENT option.

In this actual three-point bending flexural virtual test the subsequent lines of command were used:

```
*SURFACE INTERACTION, NAME = Interaction
*FRICTION
 0.3,
*CONTACT
*CONTACT INCLUSIONS, ALL EXTERIOR
*CONTACT PROPERTY ASSIGNMENT
, , Interaction
```

The *CONTACT INCLUSIONS, ALL EXTERIOR is a line to specify self-contact for a default unnamed, all-inclusive surface that includes all element-based surface facets and, in Abaqus/Explicit only, all analytical rigid surfaces. This is the simplest way to define the contact domain. 0.3 is the friction coefficient described before.

The Abaqus file is joined in Digimat-RP with the material card of the PP GF30 coming from chapter 4 and with the mapped fiber orientation shown in Fig. 5.8 to finally launch a coupled analysis with multi-scale approach set on hybrid solution.

To have a visual comparison of the benefit of the application of the multi-scale approach with composite materials, the virtual test is done also with Abaqus-only analysis with simple material hypothesis: plastic with low orientation of the fiber (low Young's modulus) and plastic with higher fiber orientation (high Young's modulus). The reaction force on the impactor is plotted versus its displacement (Fig 5.13)
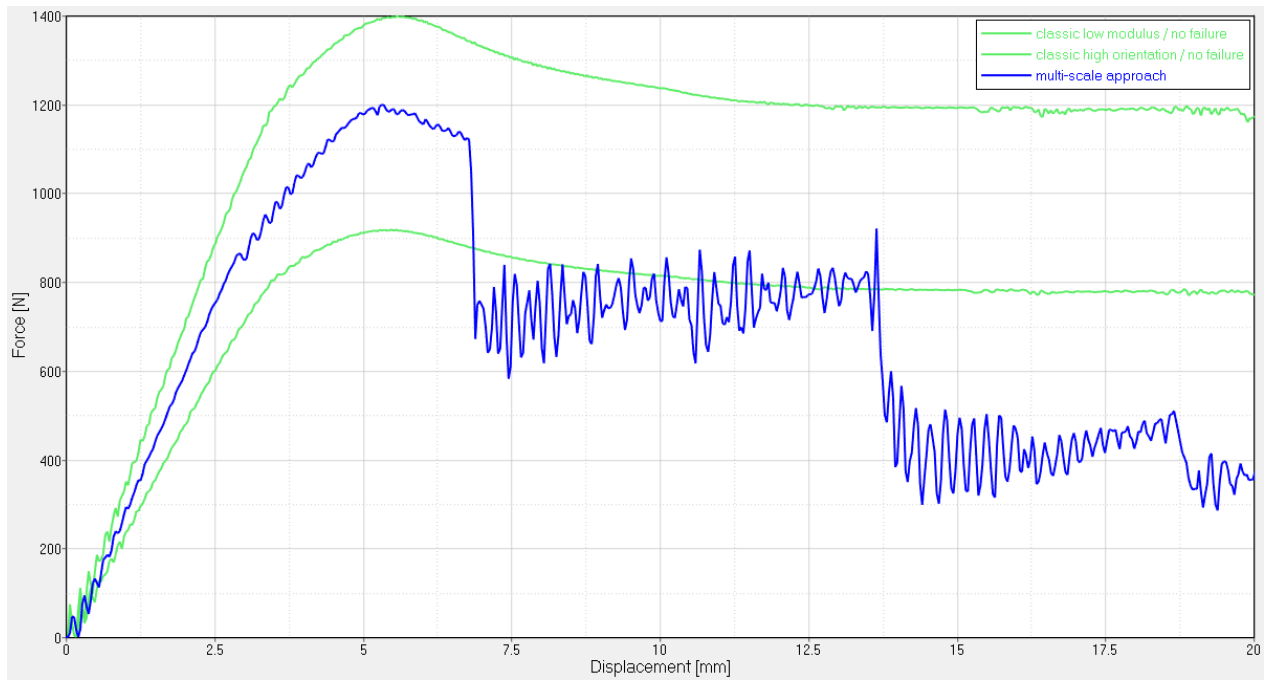
Fig. 5.13 Force-displacement plot

As expected the peak of the multi-scale approach curve at about 5 mm is midway between the two other reference cases to demonstrate the ability of the method to represent a complex real scenario component. Mind that the "classical" curves are not modeled as a composite material but as simple elasto-plastic one, only to provide a reference for the elastic and peak region, while the multi-scale approach curve is a full composite modeled material, with j2 plasticity material model and element deletion in case of failed element whit FPGF criteria. This is what causes the sudden decrease from the peak when a considerable number of elements start to fail.

Speaking of failure in the next figures there is the visual dynamics of the test (multi-scale approach) with the impactor bending the beam and the elements failing. The colored elements in each picture are the ones approaching single failure. In Fig 5.14 the test is at the beginning, in Fig 5.15 the central contact point is already reached failure stress, the central rib surface is twisting and the sides are starting to bend. This is linked to the first drop in force in Fig 5.13. In Fig 5.16 the situation is exasperated and the sides are buckling; we have the second big force drop. Lastly in Fig 5.17 the sides and the central ribs are completely cracked.
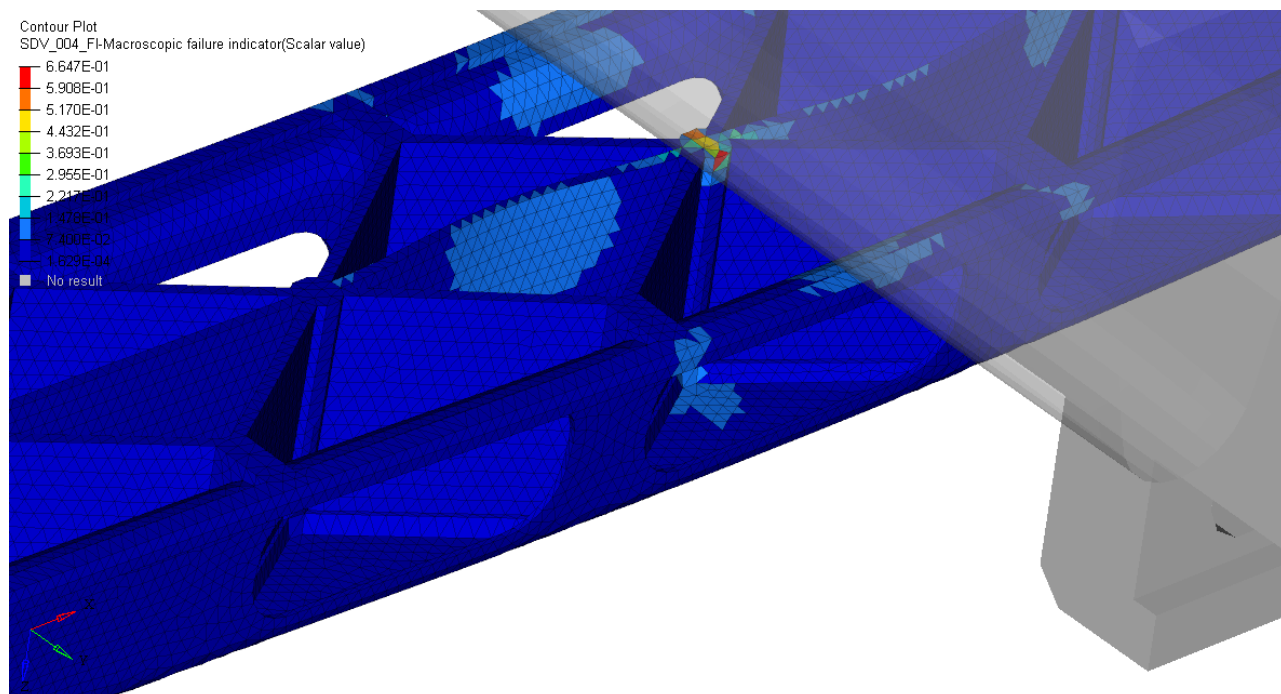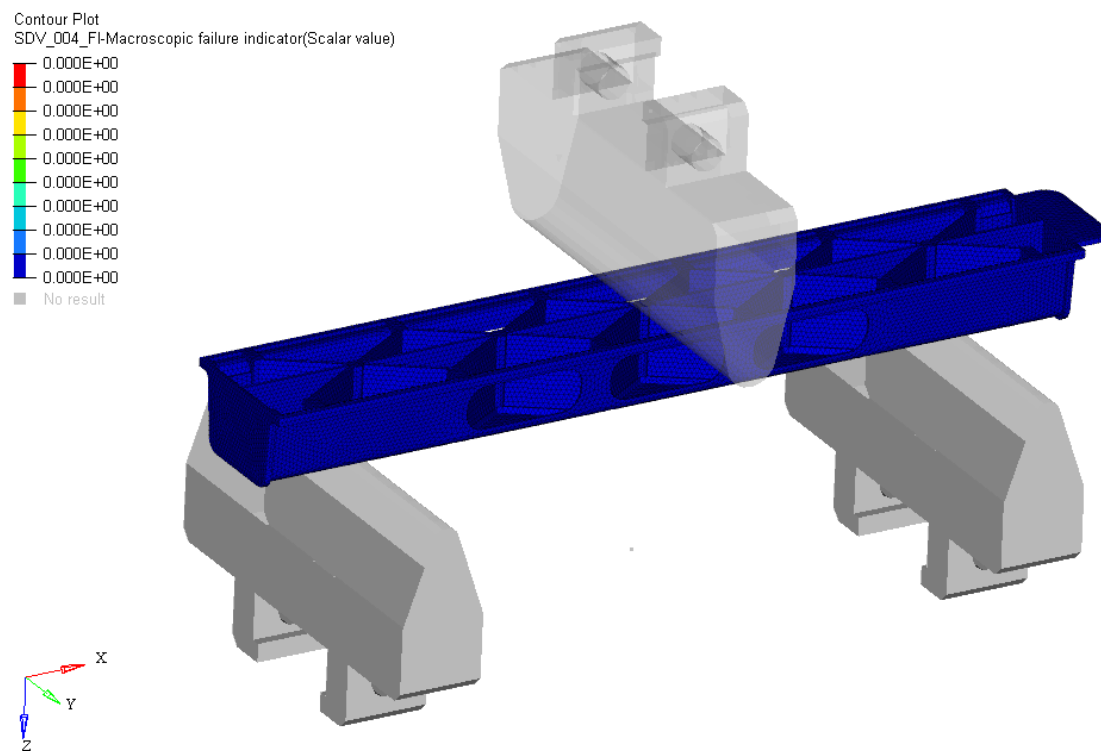
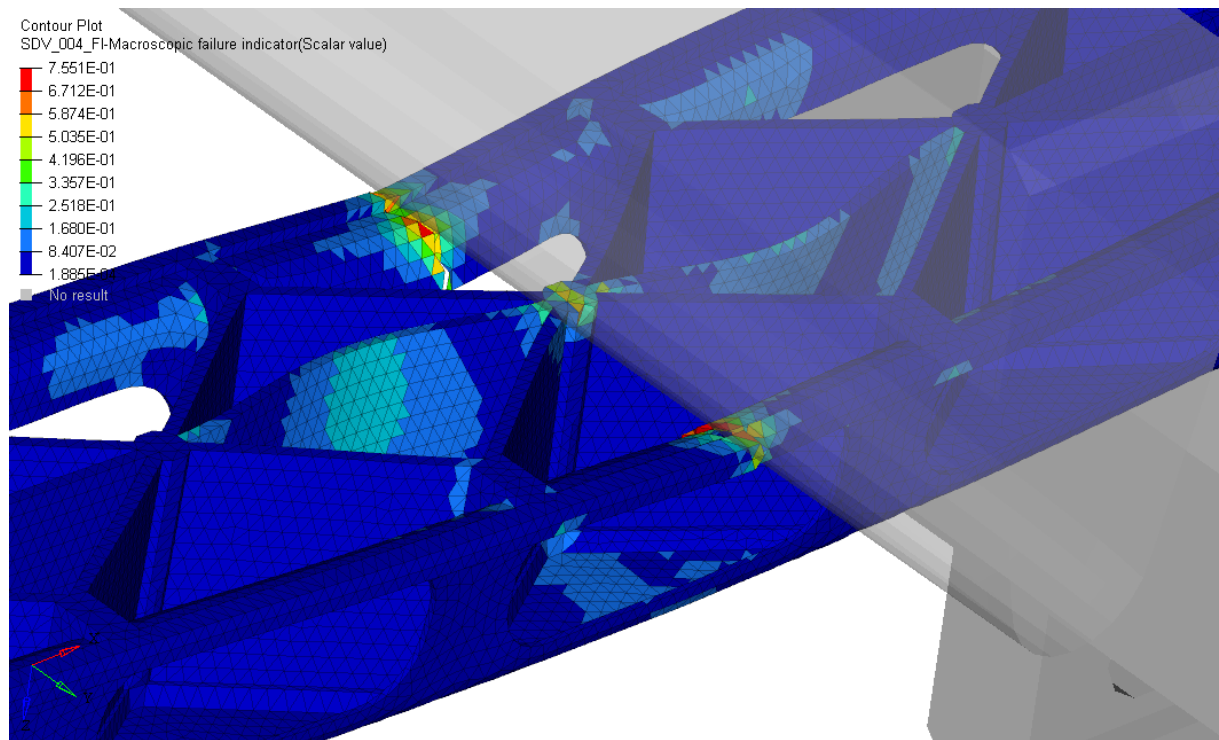**Fig. 5.14 Progression of the virtual test: beginning**
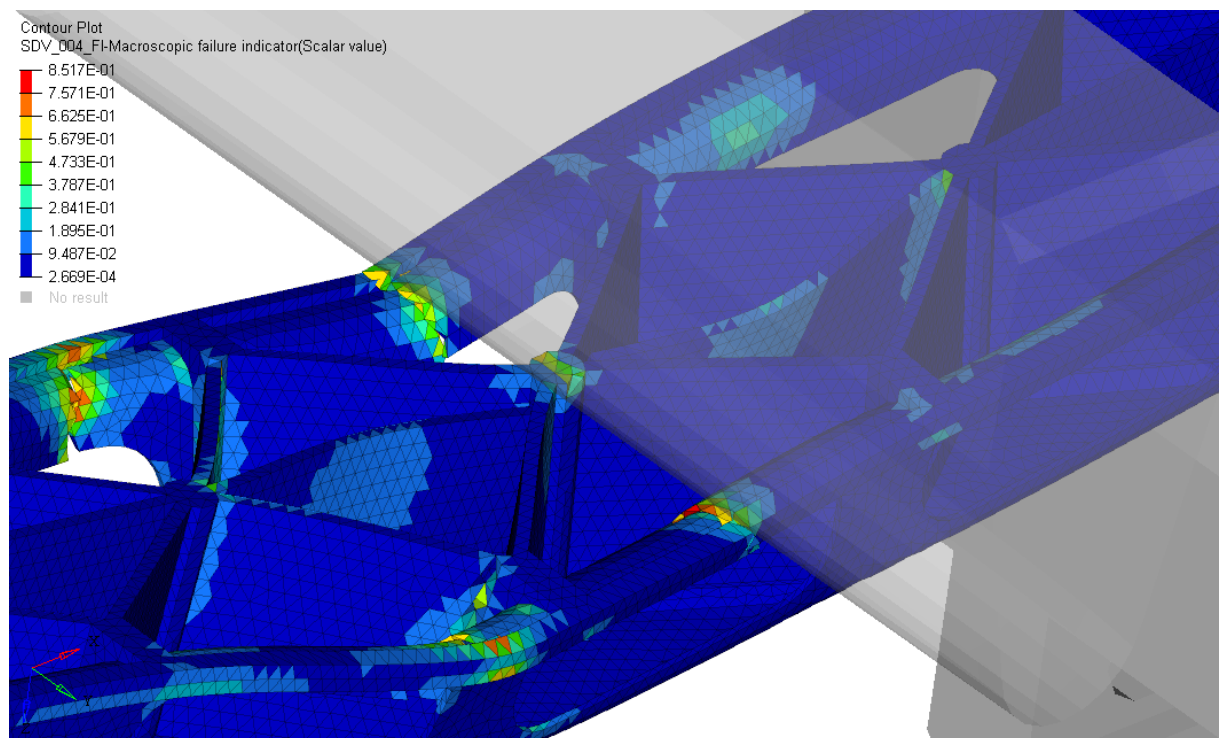
Fig. 5.15 Progression of the virtual test: peak force

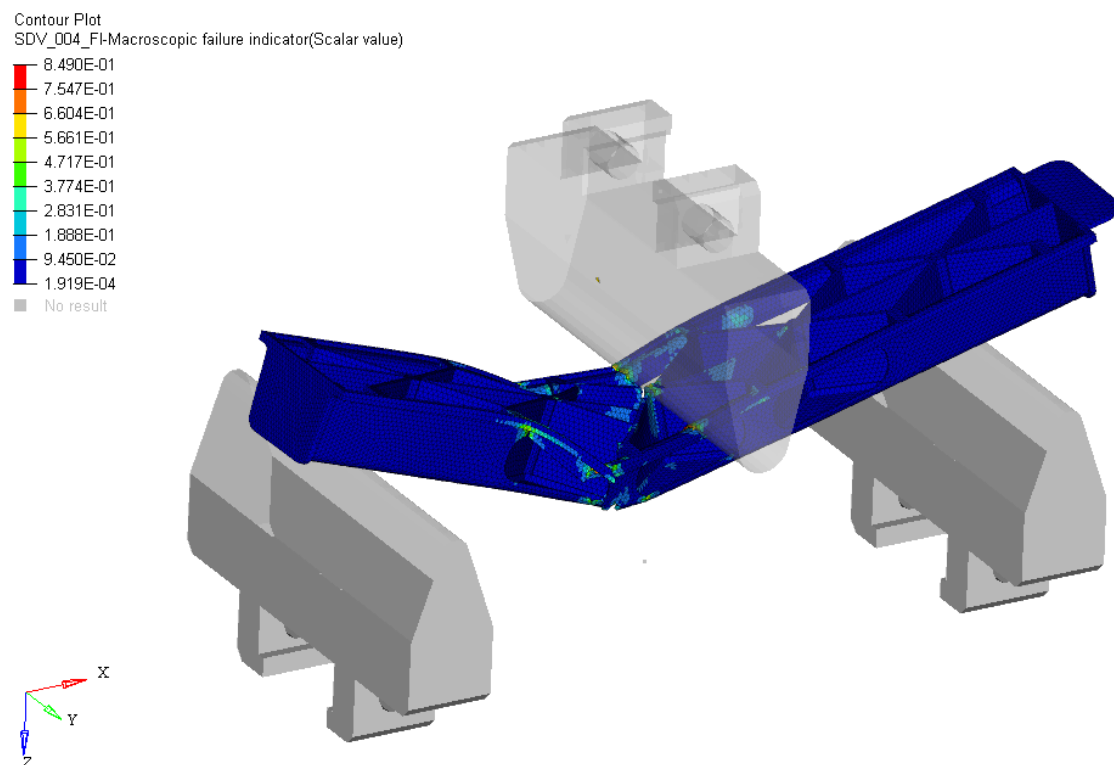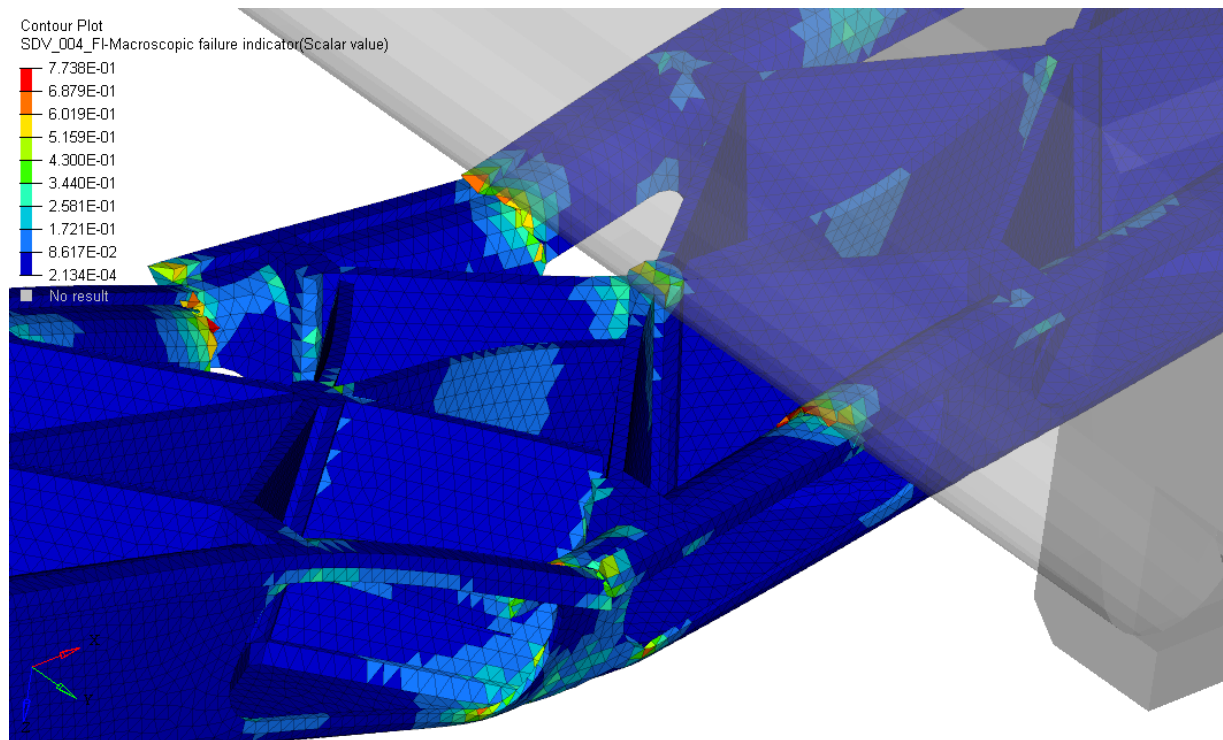**Fig. 5.16 Progression of the virtual test: considerable buckling**

Fig. 5.17 Progression of the virtual test: macro-failure of the component

Chapter 6

CONCLUSIONS

During my stay at Fiat Research Center (CRF) as graduate student a new methodological approach was investigated in order to meet company's expectations in advancing the accuracy of virtual simulation analysis of composite material structures.

The methodology proposed in Fig 4.1 proved to be effective on test specimens, achieving experimental correlation and possible suggestions for the testing material department.

Results obtained applying the methodology on the omega beam highlight that the multi-scale approach is able to improve the accuracy and the realism of the virtual simulation of composite materials giving the designer the possibility to push the performance of the component by managing in a different and better way the shape and material distribution on the final design. Moreover, first pseudo-grain failure is able to progressively reduce the composite stiffness following the evolution of the failure within pseudo-grains up to the final failure of the composite when a critical fraction of pseudo-grains has failed, giving precious insights to the designer.

Regarding failure and future developments it would be interesting to investigate the improvements in modeling weld lines with this methodology. In addition, it would be desirable to further test this approach on more complex components and research experimental correlation and integration with vast-scale virtual assemblies.

BIBLIOGRAPHY

[1]   Y. A. A. J. Stepan V. Lomov, Mori-Tanaka methods for micromechanics of random fibre, Copenhagen: 20th International Conference on Composite Materials, 2015.

[2]   B. B. L. &. C. K. Agarwal, Analysis and performance of fiber composites, III ed., New Delhi: John Wiley & Sons, 2006.

[3]   K. K. Chawla, Composite Materials Science and Engineering, IV ed., Birmingham, , AL: Springer, 2019.

[4]   R. G. Larson, The Structure and Rheology of Complex Fluids, New York: Oxford University Press, 1999.

[5]   Ex-Stream, Digimat User's Manual, 2018.

[6]   Nemat-Nasser and M. Hori, Micromechanics: overall properties of heterogeneous solids, Elsevier Science, 1993.

[7]   R. Christensen, Mechanics of Composite Materials, New York: Wiley, 1979.

[8]   J. Halpin, Primer on Composite Materials, Lancaster PA: Technornic, 1984.

[9]   S. Tsai and H. Hahn, Introduction to Composite Materials, Westport: Technomic, 1980.

[10] G. Belingardi, Il Metodo Degli Elementi Finiti Nella Progettazione Meccanica, Torino: Levrotto & Bella, 1995.

[11] Autodesk Moldlow Insight user's guide, 2018.

[12] EN ISO 527-1, *Plastics- Determination of tensile properties,* 1996.

[13] Simulia, Dassault systemès -Abaqus theory guide, 2016.